The Integration of Electric Vehicle Chargers Into a Trolleygrid Network

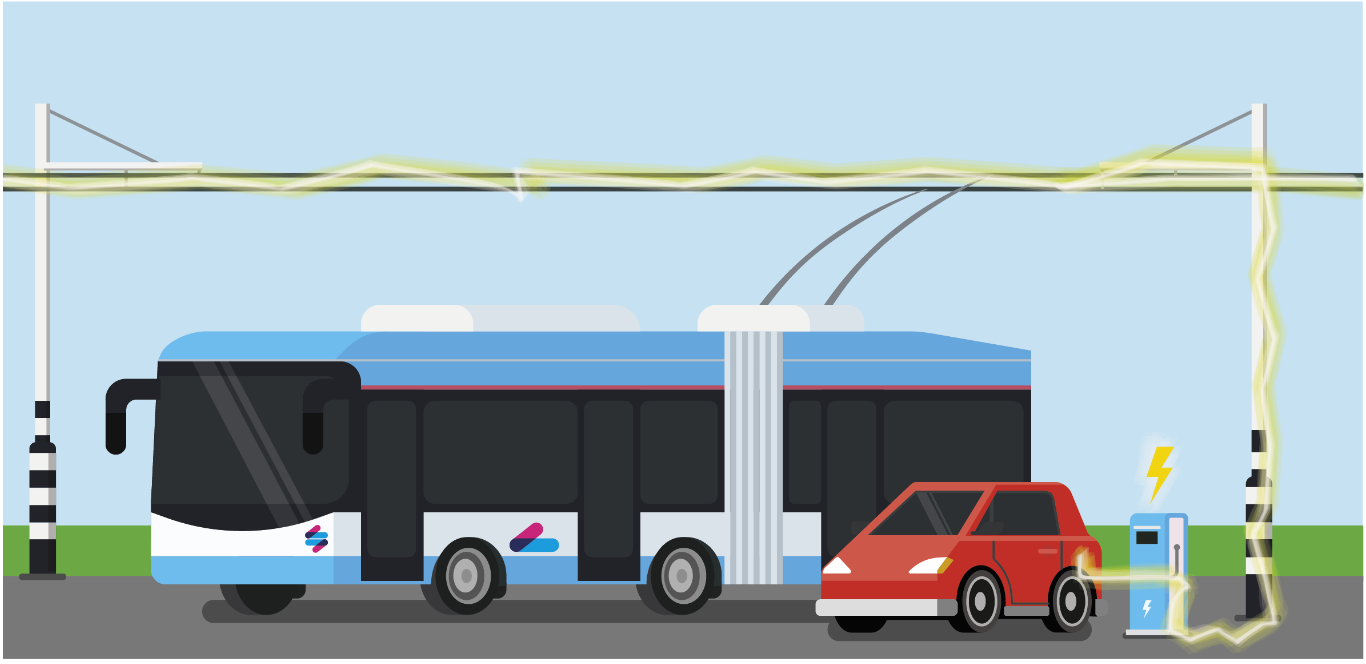

by

Koen van der Horst (4546520)

September 2022, Delft

Thesis supervisor: Dr.Ir. G.R. Chandra Mouli

Weekly supervisor: Ir. I. Diab

Promotor: Prof.Dr.Ir P. Bauer

Part of the Master of Science in Sustainable Energy Technology (SET)

Department of DCE&S, Electrical Engineering

TU Delft

ABSTRACT

Battery electric vehicles have gained a substantial market share in the last few years. The call for good charging infrastructure is urgent with the rapid shift from carbon-based cars toward battery electric vehicles. However, the present electrical distribution networks are not designed for large additional loads. Many cities have traction networks such as trams, metros, or trolleybuses for public transport purposes. This thesis explores the potential for charging electric vehicles directly from these traction networks. A case study uses public charging behavior to simulate EV charging on the trolleygrid network of Arnhem. Moreover, six smart grid methods are evaluated to increase a traction network's electric vehicle charging potential. Various trolleygrid parameters such as the trolleybus intensity, section length, and the charger's location on the trolleygrid play a role in the charging potential. An individual area can fully charge up to 111 electric vehicles daily. This study shows that increasing the substation capacity and introducing smart charging are the two smart grid methods that increase the potential up to 201 EVs/day. Adding an extra overhead line has a minor effect on the charging potential (+12 EVs/day). Increasing the substation nominal voltage has the same impact as the last mentioned method but is cheaper to implement. At the connection point of two isolated sections, the best smart grid methods are introducing a bilateral connection and using a multi-port converter. Charging battery electric vehicles from traction networks could be a suitable alternative to increase the charging possibilities in cities.

ACKNOWLEDGEMENTS

First, I would like to thank Ibrahim Diab for his assistance during my thesis. With the work he has done in previous years, I was able to integrate the electric vehicles on the trolleygrid. During the weekly meetings, Ibrahim could shared creative ideas and gave helpful feedback. Next, I would like to thank Gautham Ram Chandra Mouli, who allowed me to graduate from the electric mobility track of Sustainable Energy Technology. He showed interest in my thesis and gave support during our monthly meetings. Lastly, I could not have obtained my university degree without the help of my friends, family, and my girlfriend Anne, who supported me throughout the whole journey. Enjoy reading.

With warm regards,

Koen

CONTENTS

ABBREVIATIONS

LIST OF VARIABLES

1 INTRODUCTION

With the fast-growing adaptation of electric vehicles (EV) in the Netherlands, the need for new charging stations is high. In 2020, 20.5% of the new passenger cars sold in the Netherlands were battery electric vehicles (BEV), compared to 2.0% in 2017. To reach 100% zero-emission new car sales in 2030 [1]. To meet the increasing charging demand in the coming years, charging facilities need to find a way into the already heavily-loaded electrical network [2]. Expanding the electrical network requires high investment costs and time for the required permits. However, effectively utilizing existing electrical networks could reduce the need for expansion [3]. This thesis investigates the potential of integrating EV-charging points into the existing trolleybus grid of Arnhem. Unique in this situation is that the EV chargers are powered via the traction network. This Chapter gives background information on the basic principles of trolleygrid networks. Next, EV charging via a trolleygrid network will be introduced. Lastly, the problem statement and research questions are defined.

1.1 COMPONENTS IN A TROLLEYGRID NETWORK

A trolleygrid network is a grid of connected overhead wires that powers a trolleybus, similar to a tram network. Figure 1.1 shows a schematic overview of a typical trolleygrid. In this grid, the overhead wires, also known as the catenary, are powered via the feeder cables by the substation(s) (SS). The substations are then connected with the low voltage alternating current (LVAC) grid. The overhead wires are isolated from each other into different sections with a typical length of 0.5-2.5 km. A bilateral connection is possible in some cases, as discussed in Chapter 1.1.2. The unidirectional substation can power one or more sections at the same time with the use of a substation busbar. However, (recuperated) energy transfer from the trolleygrid to the LVAC grid is impossible due to the blocking diode.

1.1.1 The trolleybus

Trolleybuses are overhead powered electric buses used in public transportation systems in urban environments. In Figure 1.2a, a trolleybus is shown. The trolleybus has two operating modes: traction mode and braking mode. In the first mode, the bus consumes power from the trolleygrid for traction and auxiliary purposes. In the braking mode, the electric motor recuperates kinetic energy and sends it a) to other loads on the same supply zone, b) to the auxiliaries on the bus itself, and/or c) to the braking resistor. Figure 1.2b, displays an overview of the two operating modes with the associated power flows.

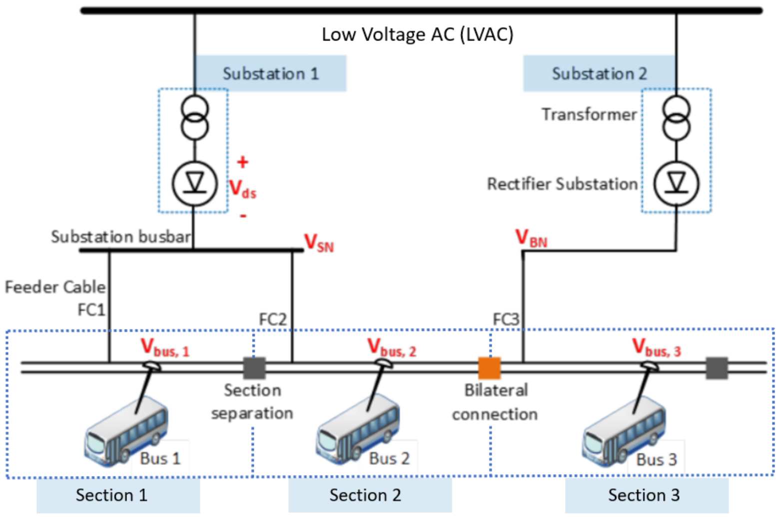

Figure 1.1: Schematic overview of the components in a trolleygrid [4].

(a) Picture of a trolleybus, powered by overhead wires [5].

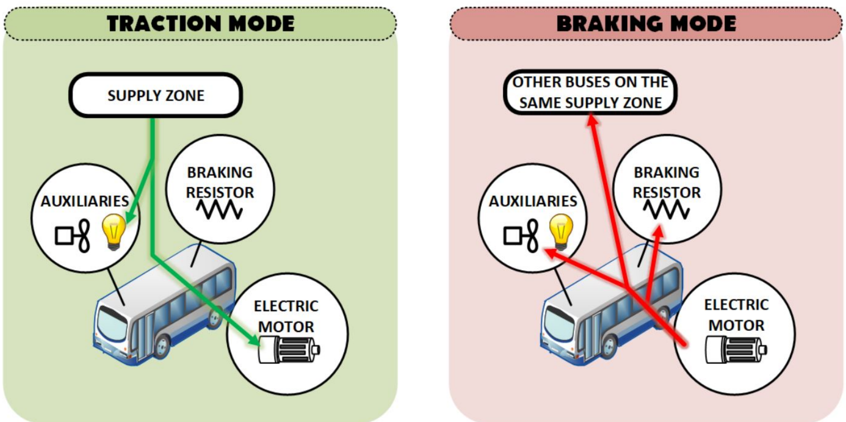

(b) The two operating modes for a trolleybus are traction mode and braking mode [4].

Figure 1.2: Picture of trolleybus and its operating modes.

Trolleybuses operate in urban environments where traffic and other circumstances can play a significant role in bus behavior. In Figure 1.3a, a typical speed profile of two trolleybuses is shown. The total power required for operating a trolleybus can be split into two categories: traction power and heating, ventilation, and air conditioning (HVAC). The traction power for the trolleybus is the sum of all the powers to accelerate and to overcome the forces (air resistance, rolling resistance, and gradient force) acting on a moving bus (Appendix A.2). Note that the traction power can be negative, i.e., the bus is decelerating or going downhill. The HVAC power is a collective name for the power required for the auxiliary services such as heating, ventilation, and air conditioning on the bus. Figure 1.3b shows, a typical load profile for two trolleybuses during the same period. Hereby, HVAC is included in the power demand of the buses. A trolleybus typically operates between -200 kW and 300 kW, with a voltage of around 600-700V [4, 6, 7, 8].

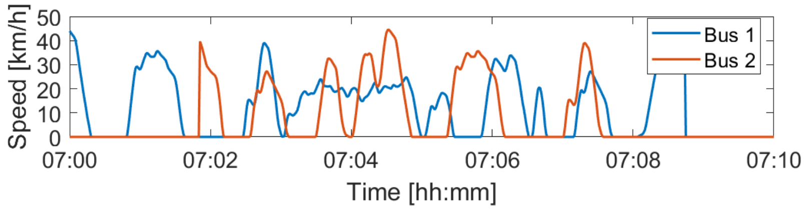

(a) Speed profile.

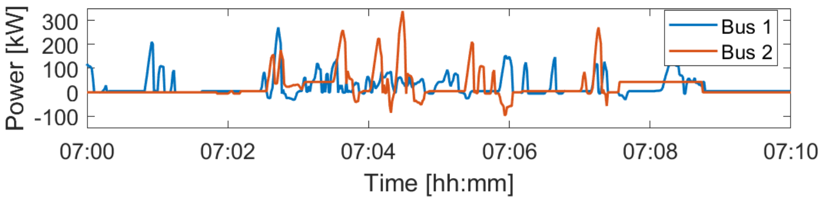

(b) Power demand.

Figure 1.3: Simulated bus behavior of two trolleybuses from 7:00 am to 7:10 am on a section.

Bus behavior and limitations

Most trolleybuses have an operating window between 400 V and 800 V [6, 7]. When the minimum line voltage is too low, the bus will reduce its power consumption with the aim of increasing the voltage level. On the other side, when the bus is braking, the voltage increases, and the power could be sent to other loads on the section or to the braking resistor, as shown in Figure 1.2b. For this thesis, the Swiss III trolleybus was used as a reference [9], and the main voltage parameters are summarized in Figure 1.4. The bus' safety mechanism reduces its power consumption when the voltage drops below 500 V. As a result, the bus cannot follow the drivers' input. If the voltage is below 400 V, the trolleybus is not able to draw any power from the traction grid due to its control mechanism. When the bus is in recuperation mode, the voltage at the braking bus rises and power is able tois able to power other loads on the trolleygrid. When the braking energy cannot be used by other loads, the braking resistor activates when the voltage is above 720 V ($V_{\text{braking,bus}}$) and will be fully engaged at a voltage of 740 to prevent an overvoltage on the trolleygrid [4].

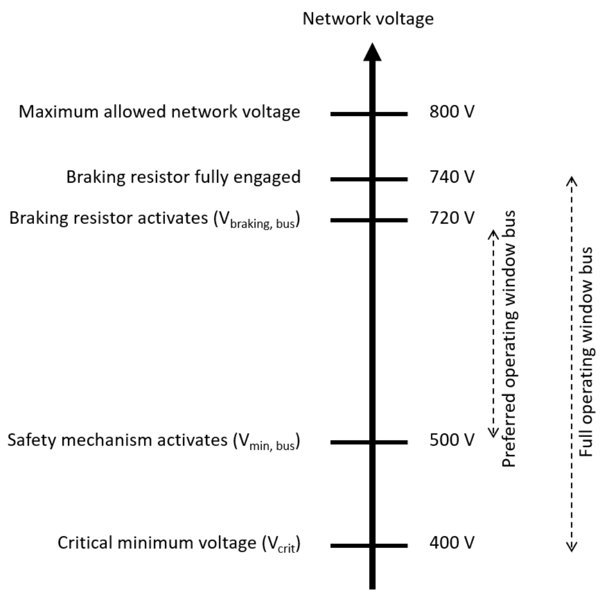

Figure 1.4: Operating window Swiss III trolleybus based on [7].

1.1.2 Catenary grid

The overhead wires, also called the catenary grid, is built up with parallel electrical lines. One is the feed side of the electrical circuit, and the other is for the return path. In many trolleygrids, buses operate in both directions in one section. Therefore, the parallel lines are doubled, see Figure 1.5a. For energy savings the overhead parallel lines are connected roughly every 100 meters, see Figure 1.5b. The trolleybus differs from the tram in that two wires are required to close the electrical circuit, whereas the tram uses the railway track as the return path for the electrical circuit.

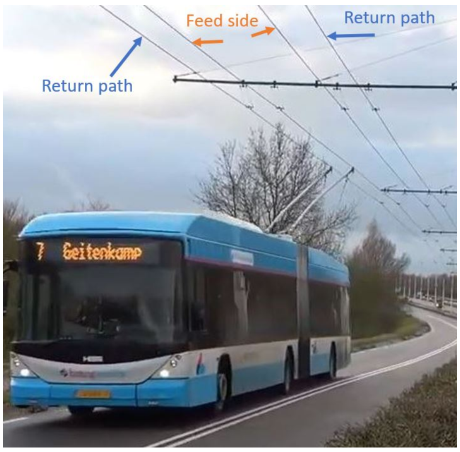

(a) Picture of a trolleybus with a double parallel cable [10].

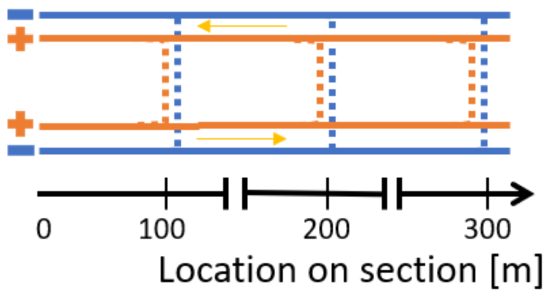

(b) Schematic overview of the catenary grid whereby the dotted lines indicate the connection between the parallel lines roughly every 100 meters. The yellow arrow indicates the bus direction.

Figure 1.5: Double parallel lines in the catenary grid.

In Figure 1.1, the overhead lines are isolated between two sections. In other words, powerflow from one section to the other via the section separation point is impossible when the sections are unilaterally connected. Powerflow between two sections, powered from the same substation, is possible via the shared substation busbar.

In some cases, individual sections can be connected with each other; a bilateral connection. In this case, a bus on a particular section could be powered by two different substations. For example, section 2 in Figure 1.1 can be bilaterally connected with section 3. In this case, both substations can power the bus on section 2.

1.2 INFLUENCE OF TROLLEYBUSES ON THE TROLLEYGRIDS' STATE PARAMETERS

Power profile substation
As mentioned, the trolleybuses are powered by an AC/DC unidirectional converting substation. With the highly fluctuating power demand of the trolleybus (Figure 1.3b), the power delivered by the substation is also very volatile. The power output of the substation is shown in Figure 1.6a.

Voltage on the section
The voltage levels on the trolleygrid is the second parameter that the loads will influence. Figure 1.6b shows the minimum voltage on the section for the same 10 minute time-interval. Due to the fluctuating loads, the minimum line voltage is also highly fluctuating.

Currents on the section
The third parameter that is influenced by the loads on the traction grid, are the currents in the overhead wires. In Figure 1.6c, the maximum line current on the simulated section during the interval is plotted.

Losses in section
There is a power loss in the cables due to the resistance in the feeding cables and overhead wires. As shown in Figure 1.6d, the power losses in the cables of the 10 minutes interval could reach up to 10%, therefore it could play a major role in the power consumption of the traction grid. The magnitude of the losses in the overhead wires depends on cable resistance, the feed-in cable length, the relative distance of the loads to the substation, and the amount of current through the cables.

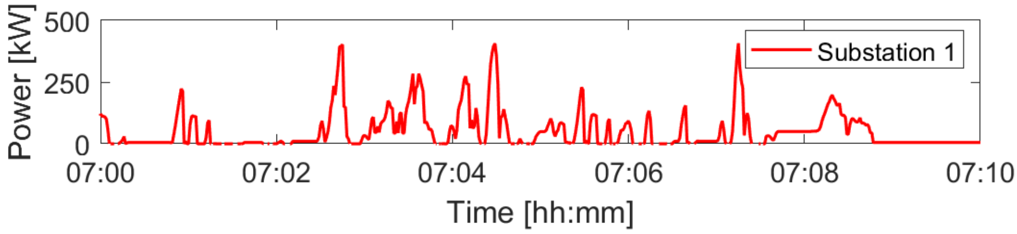

(a) Power delivered by the substation.

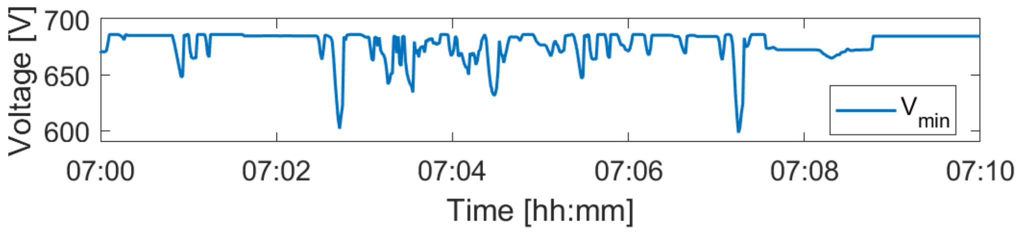

(b) Minimum voltage on the section.

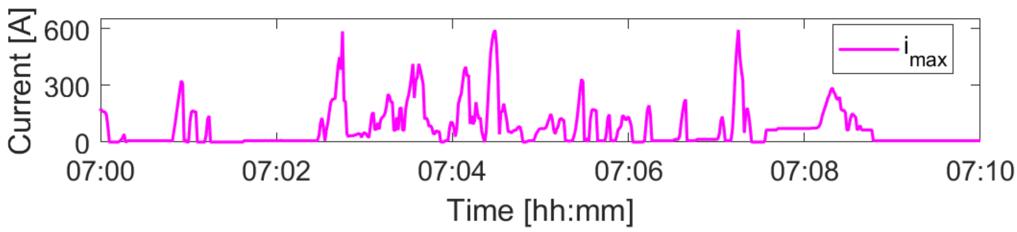

(c) Maximum current in overhead wires on the section.

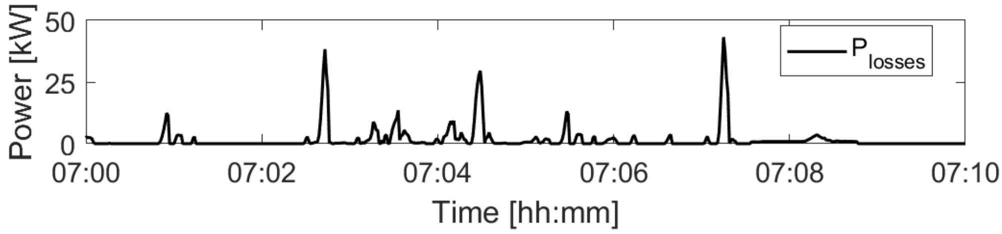

(d) Transmission losses in the feed-in cable and overhead wires.

Figure 1.6: Simulated trolleygrid behavior based on measurement from the trolleygrid of Arnhem from 7:00 am to 7:10 am [11].

1.3 INTEGRATING EV CHARGERS ON THE TROLLEYGRID NETWORK

As shown in the previous section, trolleybuses greatly affect the substations' power, line voltage, and current. At moments of low bus traffic, Figure 1.6 suggest that the substation could power additional loads such as EV chargers on the traction grid. In this section, an introduction to EV charging via a traction grid is given.

Batteries for an EV can only be charged by direct current (DC), but the EV cannot be directly coupled to the DC traction network due to the different and fluctuating voltage on the trolleygrid. Therefore, additional wiring and a DC/DC converter are needed. A schematic overview of the connection of an EV charger to the overhead wires is given in Figure 1.7a. Figure 1.7b shows a picture of an integrated EV charger into the traction network. The DC/DC converter is located in the EV charger pole and there are two connection plugs for two different EVs. The specifications of the DC/DC converter used in this thesis as a reference converter are described in Appendix A.5.

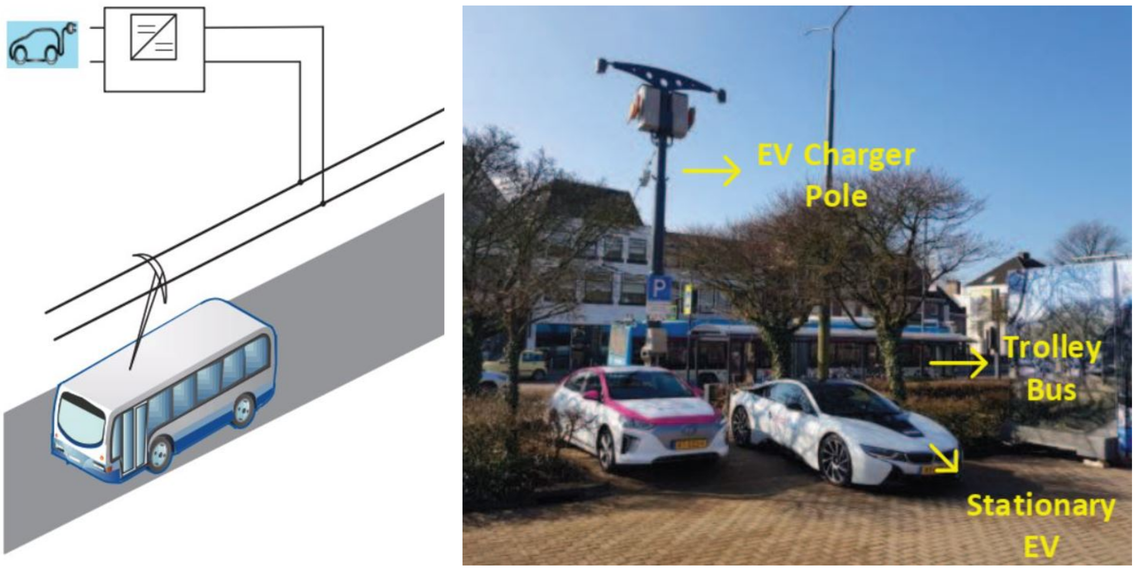

(a) Schematic overview of an EV charger connected to the overhead wires of a traction grid [12].

(b) Integrated EV charger to the traction grid in Arnhem. In the background, the trolleybus is shown. The electric cars are plugged into the EV charging pole. [12].

Figure 1.7: Integration of EV chargers in the trolleygrid of Arnhem.

1.4 PROBLEM STATEMENT

The need for EV charging demand will increase in the upcoming years. However, integrating charging facilities within the already heavily loaded electrical distribution networks could reach the design limits. On the other hand, electric urban transport networks are oversized and underutilized. Renewable energy sources (RES) must find a way into transport networks to transform traction grids into sustainable grid for the future. However, as shown in Figure 1.8, the substation is subjected to fluctuating power demands. Additionally, there is a mismatch between the photovoltaics (PV) generation and the load demand. Present solutions are curtailing the PV energy, exchanging with the electrical distribution network, or the need for expensive energy storage solutions.

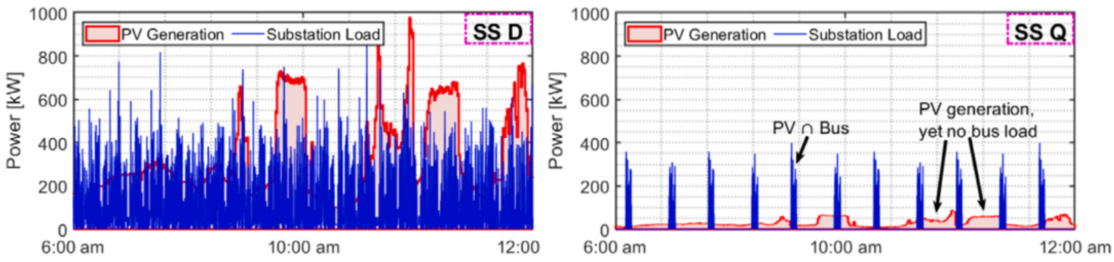

(a) Substation D (high traffic substation) (b) Substation Q (low traffic substation)

Figure 1.8: Mismatch of solar production and bus loads on two different substations in the trolleygrid of Arnhem [8].

Integrating a combination of EV chargers and PV systems into an electrical transport network grid could be another solution. Adding EV chargers to the traction grid can use the generated solar energy and, in the meantime, serve the EV charging demand. However, with the addition of extra loads to a traction grid, the substations' power, minimum line voltage, and maximum line current need to stay within the operating window of the traction grid. To determine the maximum available charging capacity at different locations, the trolleygrid is simulated using a multi-node computational model.

1.5 RESEARCH QUESTIONS

To effectively determine the maximum EV charging potential on a trolleygrid network, the following research questions were formulated:

RQ1: What is the EV charging potential in a trolleygrid network without violating the grids' substations' power, line voltage, and line current limitations?

RQ2: What is the effect of smart grid methods (Table 1.1) on increasing the EV charging potential on a trolleygrid within the substation power, line voltage, and line current limitations?

Table 1.1: The six smart grid methods are evaluated in this report.

Substation level	Grid infrastructural level	EV charging level
1.1 Increasing substation's voltage	2.1 Extra parallel line	3.1 Smart charging
1.2 Increasing substation power tolerance	2.2 Bilateral connection	3.2 Multi-port converter

RQ3: Case study: What is the available capacity for EV charging on the present trolleygrid network of Arnhem without violating the grids' substations' power, line voltage, and line current limitations?

1.6 THESIS LAYOUT

The structure for this thesis is as follows:

- **Chapter 1**
  Introduction on a trolleygrid and EV chargers. We are defining the problem statement and the research questions.

- **Chapter 2**
  Literature review on the present work on integrating EV chargers into a traction network.

- **Chapter 3**
  Methodology including a general approach for the integration of EV chargers into a trolleygrid and an explanation of the six smart grid methods.

- **Chapter 4**
  Results of the integration of EV chargers during the theoretical study, including the six smart grid methods.

- **Chapter 5**
  Results of the integration of EV chargers during the case study, including the six smart grid methods. Also, energy analysis is performed for the integration of EV chargers.

- **Chapter 6**
  Discussion, conclusions, and recommendations

2 LITERATURE REVIEW

This Chapter discusses the relevant literature on the integration of EV chargers into traction networks. The first section analyses the present studies on integrating EV chargers into a traction network. They are followed by review methods to determine charging profiles based on customer demand in urban environments. The possibility of charging EVs with dynamic power levels is considered in the third section. The final section defines the research gap.

2.1 INTEGRATION OF EV CHARGERS IN DC TRACTION SYSTEMS

The integration of EV chargers into traction networks is not a new concept. This section describes projects where EV chargers are integrated into a DC traction network. The traction networks are defined into two groups: the trolleybus/tram networks and the metro/train networks. In Table 2.1, the major characteristics of the two groups are highlighted. This thesis's literature review is limited to the trolleybus/tram category. Table 2.2 overviews the projects where EV chargers are integrated into low voltage DC traction networks.

Table 2.1: Main differences between tram/trolley and train/metro traction networks.

	Tram/Trolley	**Train/Metro**
Power (order of magnitude)	kW [13]	MW [14]
Nominal voltage	500 V – 750 V DC [13]	$>$ 750 V DC/AC [15]
Length of section	$<$ 3 km [16, 17]	1-40 km [18, 19]
Velocity and power profile	Unpredictable/ traffic dependant	Predictable/own track
Frequency of occurrences of accelerations/deceleration	High	Low

Table 2.2: Overview of the projects with the integration of EV chargers into traction networks powering trolleybuses and trams.

Location	*Traction network*	*Description/objective*
Solingen, Germany [20, 21, 22, 23, 24, 25]	Trolleybus	Investigating the potential of integrating decentralized renewable power generation (e.g., photovoltaics), charging stations for EVs, and stationary battery storage into the existing DC trolleybus infrastructure.
Gdynia, Poland [16, 26, 27, 7, 28]	Trolleybus	Analyzing the available capacity of the traction grid of Gdynia to charge electric cars. Furthermore, Smart Grids solutions for urban traction supply systems are introduced to improve the efficiency and stability of the traction network.
Edinburgh, Scotland [17, 29, 30]	Tram	Electrical capacity for EV charging systems based on four different charging control strategies are assessed and tested on the public tram system. The various connection topology, earthing methods, and stability criteria are considered.
Lisbon, Portugal [31]	Tram	Integration of bidirectional EV chargers into a DC catenary grid for trams. The authors looked into the concept V4G with an associated fuzzy control method. Furthermore, the benefits of an energy storage system in a catenary grid are demonstrated.
Sheffield, UK [32, 33]	Tram	Method to improve the energy efficiency of trams with the use of static energy storage systems and EV batteries in the public tram network. Current flow measurements and tram GPS data were used to simulate the energy flow in the catenary grid using a MATLAB/Simulink model.

2.1.1 Battery Overhead Line Buses (BOB), Solingen (Germany)

In Solingen, Germany, the project Battery Overhead Line Buses (BOB) (German: Batterie-Oberleitungs-Bus) aims to advance the existing DC trolleybus infrastructure into a Smart Trolley System (STS) [23]. Hereby, decentralized renewable power generation (e.g., PV systems), stationary battery storage, and charging stations for EVs are integrated into the catenary 660 V DC grid, see Figure 2.1.

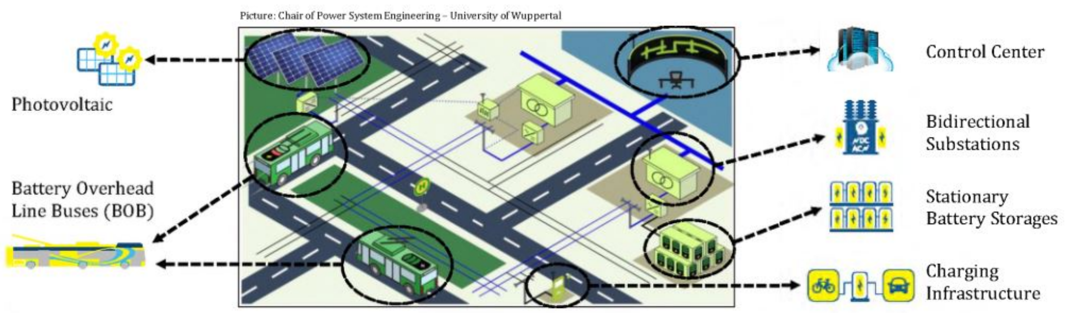

Figure 2.1: Schematic overview of the Smart Trolley Bus System of Solingen, Germany [23].

One of the sub-project integrates PV systems and EV charging stations in the BOB project [22]. The authors demonstrate a method for determining the location for both systems into the trolleygrid of Solingen. The method for PV system integration is not further discussed in this thesis. To analyze the impact of EV chargers on the catenary grids' voltage and current, the writers use a predetermined power profile of a bus as described in [21], see Figure 2.2a.

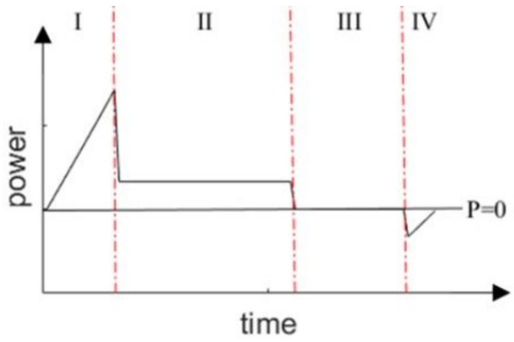

(a) The power profile of the bus used to locate and size the EV chargers in the BOB traction grid of Solingen, Germany (I = acceleration; II = constant speed; III = Coasting; IV = braking) [21].

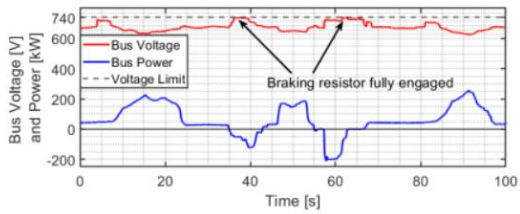

(b) Power and voltage measurement from the trolleygrid in Arnhem, the Netherlands. At 740 V the braking resistor is fully engaged to prevent overvoltages in the trolleygrid [4].

Figure 2.2: Comparison between a predetermined power profile (left) and an accurate power profile (right) of a trolleybus.

As shown in Figure 2.2b, the actual load profile differs significantly. Furthermore, a test-grid environment with four substations and five busses is used, where the timetable describes the positions of the busses. The EV chargers are placed at fixed nodes in the test grid. An iterative process does the sizing of the EV chargers with intervals of 22 kW (size of a public charging station) up to a maximum of 132 kW. This article's limiting factor is that only the minimum voltage criteria are considered. Furthermore, the branch current limitations of 600 A for feed-in cables and 400 A for overhead lines and the maximum power limitation of the substation (1 MW) are not analyzed as limiting factors for the size and location of EV chargers. In this thesis, the current and substation limitations will be considered, as well as a more realistic power profile of the trolleybus to determine a suitable location and size for EV chargers.

As part of the same sub-project, Weisbach et al. [23] opt for a flexible charging and pricing algorithm, considering the trolleybus behavior. They do this by looking at the available power with four vehicle access points at a charging area. The charging algorithm is based on two external factors: grid utilization forecast and user-selected charging request. The charging plan for the connected EVs is made by combining the external factors with the information from the other connected vehicles at the charging point. If the charging station cannot provide the 50 kW of rated power, the DC/DC-inverter can reduce the power by steps of 12.5 kW. As shown in Figure 2.3, the available charging power can drop to almost zero due to the loads on the grid. EV charging without dynamic charging suggests that the maximum installed capacity is limited by the minimum power available for EV charging. However, with dynamic charging, the paper demonstrates that EV charging is still possible at moments with low grid loads. In the research, the dynamic charging algorithm is based on the power limitations of the substation. Unlike the test-bed environment mentioned earlier, Weisbach et al. do not address grids' minimum voltage. Also, current limits are not considered. Furthermore, this research does not address current losses and additional voltage drop on the grid associated with the dynamic charging of EVs.

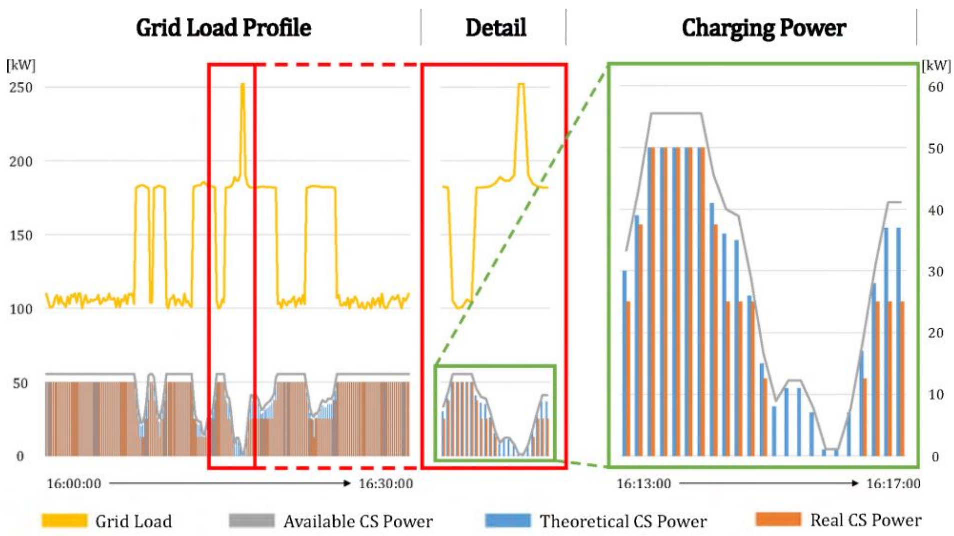

Figure 2.3: Results of dynamic charging possibility for the trolleygrid in Solingen [23]. Yellow: trolleybus power loads, grey: the available EV charging power, blue: theoretical EV charging power with steps of 12.5 kW charging, orange: the real EV charging with the opted charging algorithm. The minimum available power between 16:13:00 and 16:17:00 is 2 kW.

The effect of dynamic charging on the EV charging utilization with and without dynamic charging is not compared by Weisbach et al. However, dynamic charging of EVs with the associated control strategy can be one method to increase the charging utilization of the grid. The limitations of dynamic charging are further discussed in section 2.3.

2.1.2 Trolley:2.0 project, Gdynia (Poland)

Bartlomiejczyk et al. [26] discuss the integration of EV chargers in the trolleygrid of Gdynia. This article presents four possible connection methods of EV chargers to the trolleygrid. The authors suggest a connection of the EV chargers directly to the overhead supply lines. This type of connection has the possibility of using the regenerative braking energy from the trolleybuses. On top of that, the EV chargers can be placed over a large spatial area. The main downsides of this type of connection are the limitations in the traction network, voltage fluctuations, and a relatively expensive DC/DC converter.

Bartlomiejczyk et al. use voltage and load level recordings from the traction supply network for their analysis. The supply lines are limited by three main criteria, see Table 2.3.

Table 2.3: Criteria for the trolleygrid overhead lines to verify the possibility of EV integration [26].

Criterion	Conclusion
(I) Maximal load current	Continuous load: 840 A
(II) Maximum voltage drop	A) Minimum voltage in overhead lines is 400 V B) Allowed mean voltage drop at the trolleybus current collector is 99 V
(III) Acceptable power loses	Should not exceed 10% of the total energy consumption of the trolleygrid network

The authors use a linearization for the electric circuit to calculate the voltage drop with the addition of EV chargers. They assume the most unfavorable condition for the EV chargers, i.e., at the end of the power section, where the resistance of the supply wires is the highest. With superposition, the calculated voltage drop of the EV charger and the measured voltage due to the trolleybuses is added together. This is not correct due to the non-linear behavior of the electrical system (the voltage drop is higher due to the larger current required in the supply wires). Furthermore, a constant charging power of 44 kW is assumed.

As the paper concludes, in most cases, the voltage criteria (II) is critical if the EV chargers are located at the end of the power supply. This thesis will also look into the placement of EV chargers closer to the substation, so all the criteria mentioned in this paper will be analyzed. This paper demonstrates that the integration of EV charging in a trolleygrid is possible; however, the utilization is limited.

As part of the same project, [7, 27] studies the recovery of braking energy with five different methods, as shown in Table 2.4. The various techniques were implemented in the trolleybus network of Gdynia. The researchers use data measurements from the traction substation and the trolleybuses taken from December 2011 to November 2012. The associated energy savings for the method is determined based on the measurements. These methods aim to use recuperation energy again for new purposes. Interestingly, methods 1, 2, and 5 could also be implemented to increase the EV charging utilization in the trolleygrid.

In the fifth method, the use of a supercapacitor (SC) located at the substation is investigated. As shown in Figure 2.4, there is a relation between the number of buses on the section and the flow of braking energy into the SC or the other buses. At areas with a low bus density, the energy storage system (ESS) utilization is higher than busy sections, where the braking energy is absorbed by other buses. In ideal circumstances, the SC could save up to 30% of the energy used in the grid. As mentioned in [7], introducing a SC in the grid could have high investment costs. However, using the recuperation energy for EV charging could be an exciting solution without the high investment costs for supercapacitors. As mentioned before, the bus density needs to be considered when investigating this method.

Table 2.4: Comparison of five different methods used to recover braking energy in the trolleygrid network of Gdynia, Poland [27].

Use of recuperation energy	Method of increasing recuperation	Total energy savings
Recovered energy consumption in a vehicle	1. Implementation of an "intelligent" heating	3 – 10%
Transfer of recovered energy between vehicles	2. Implementation of bilateral supply of traction network	5 – 15%
	3. Splitting the neighboring supply sections	1 – 5%
	4. Reducing no-load substation voltage	1 – 5%
Accumulation of recovered energy	5. The use of energy storage systems	5 – 30%

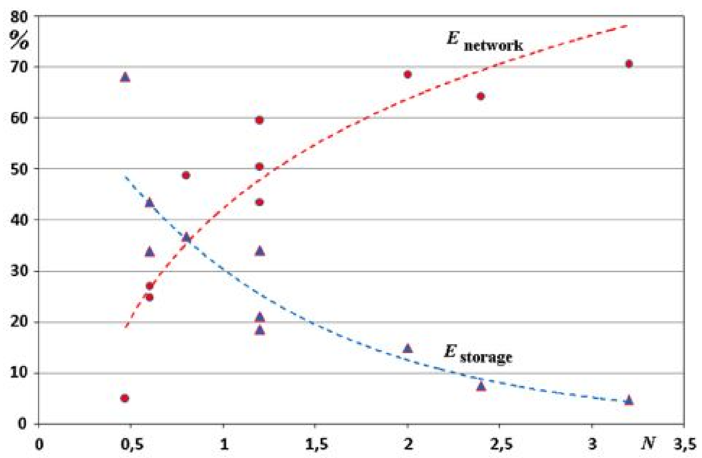

Figure 2.4: Relation between the bus density and the energy flow into the ESS or other buses. [27].

2.1.3 EV integration into the tram network of Edinburgh (Scotland)

Smith et al. [29] describe the integration of EV chargers into Edinburgh's DC tram grid. The authors looked into the aggregated energy consumption from each substation for half-hourly time intervals over an entire year. For sizing the EV chargers, they looked into the available power (contracted power capacity at the substations minus the tram power demand at any moment) with a certain probability. P90, for example, indicates that for 90% of the time, the power capacity is available for other power applications (e.g., overnight electric bus charging). The paper only looks into charging stations located at the substations, they introduce three different methods for connecting the charging stations, see Figure 2.5. As mentioned in the paper, topology 2.5c is the most flexible connection.

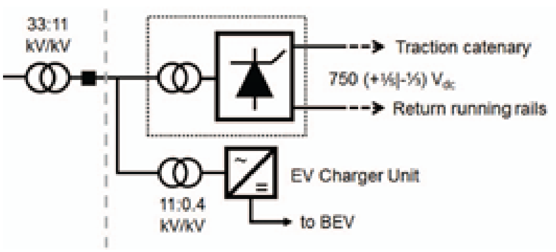

(a) EV charger interfaced via ac connected step down transformer and EV charging inverter.

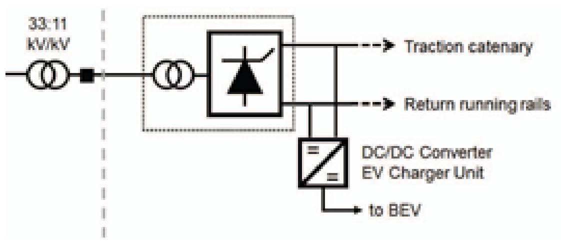

(b) EV charger interfaced via dc/dc converter connected to dc bus bar of the traction supply.

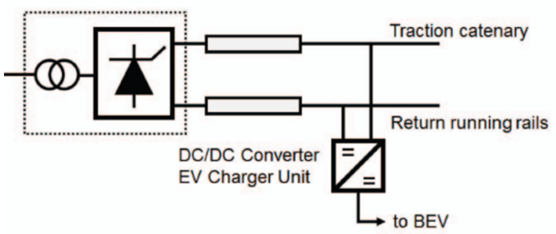

(c) EV charger interfaced via dc/dc converter connected to dc catenary and returning rail.

Figure 2.5: Different typologies were used in [29] for the integration of charging points in the tram catenary grid.

In the case study of Edinburgh, the authors use three different load profiles, namely for electric buses with onboard storage, electric taxis, and residential EV owners. For the demand profile of the electric buses, they assume a constant overnight charging profile of 75 kW to recharge a 300 kWh onboard battery. The demand profile for taxis and residential charging is based on data obtained from various projects and the Edinburgh grid. In Figure 2.6, a graphical representation of the different charging profiles is shown. This graph shows that the taxi and residential EV owners show the opposite pattern with regard to the available capacity of the trolleygrid. Using a combination of various EVs (i.e., an electric bus with onboard storage, electric taxis, and private electric cars) could increase the total EV charging utilization of the trolleygrid. The authors do not investigate the optimal combination of EV charging in their work. In section 2.2, charging profiles for EVs are discussed in more detail.

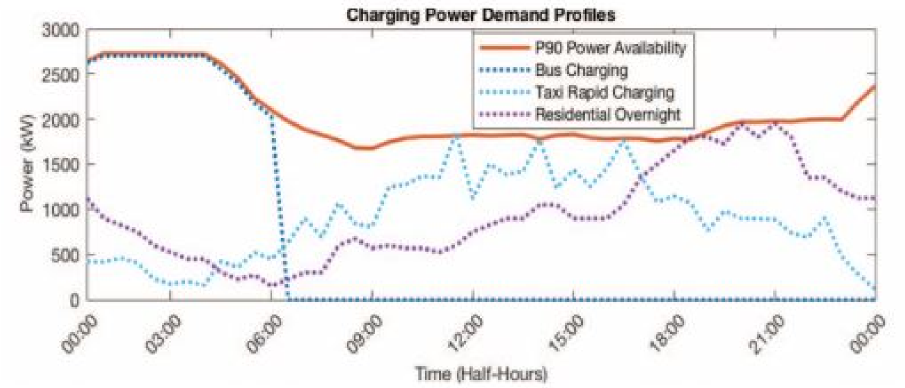

Figure 2.6: Three different load profiles were used to demonstrate the charging potential for EVs in Edinburgh. P90 refers to the power available for 90% of the time. In this case, 56 buses (dark blue), 3118 electric taxis (light blue), or 1500 residential EV users (purple) could be added to the trolleygrid network [29].

2.1.4 EV charging from tram network in Lisbon (Portugal)

A study by Santos et al. [31] shows a method for integrating bidirectional EV chargers into a DC catenary grid for trams. The authors looked into a concept called vehicle-for-grid (V4G). In this situation, the vehicle is not only providing energy to the grid but is also able to improve the voltage regulation, as well as the efficiency of the traction network. The MATLAB/Simulink-based model includes 12 non-regenerative trams equally distributed along the 24 km tram line. All the trams follow the same predefined driving cycles. The variable resistance in the overhead lines depends on the tram's position, and the associated voltage drop is included in the simulation. Also, seven fast charging stations (50 kW each) were modeled on the network.

The authors introduce a fuzzy controller for the dynamic charging of the EV battery. The controller is integrated into each EV charging station with two input variables, local grid voltage (u_k) and the state-of-charge (SOC) of the battery. At moments where the SOC of the battery is low, and the voltage is medium or high, the battery will be charged. When the SOC is medium or high, and the voltage is low, the fuzzy controller will discharge the battery and increase the network voltage. The fuzzy rules are summarized in Table 2.5. The voltage set-points are determined for each charging station individually by looking into the voltage at the predetermined node on the traction grid when no EV charger is integrated. A summary of set points is shown in Table 2.6.

Table 2.5: Fuzzy rules are used in the power flow control of EV chargers. u_k represents the voltage at each EV charging location and state-of-charge (SOC) of the EV battery. [31].

		u_k		
		Low	**Medium**	**High**
SOC	**Low (20%)**	Neutral	Charge	Charge
	Medium (50%)	Discharge	Charge	Charge
	High (80%)	Discharge	Neutral	Neutral

Table 2.6: Voltage levels on DC tram network without EV chargers integrated. Measured on the connection point of the EV chargers. Considering a DC traction network with a rated voltage of 600 V (European Standard EN 50163) [31].

u_k	**Medium** $\bar{u}_k$(V)	**High** max (u_k) (V)	**Low** min (u_k) (V)
u_1	609.0	625.3	575.3
u_2	590.3	620.0	530.1
u_3	574.8	616.6	486.2
u_4	562.6	613.7	443.5
u_5	553.9	613.4	403.4
u_6	548.8	613.4	378.4
u_7	547.1	613.4	368.6

As shown in the paper, the voltage regulation is improved with the integration of bidirectional EV chargers in the DC tram grid. As a result, introducing vehicle-for-grid systems on the tram network could increase the average current drawn from the substation by 60% compared to only grid-to-vehicle charging stations. However, due to the repetitive and simple method for the tram modeling (not taking into account delays, HVAC, drivers behavior etc.), the effect of V4G on the charging utilization needs to be investigated in more detail. Furthermore, the authors do not include the ramp-up or ramp-down speed of the EV charger, which limits the flexibility of V4G.

2.1.5 Integration of energy storage systems in Sheffield's (UK) tram network

Improving the energy efficiency of trams with the use of static ESS and EVs in Sheffield is discussed in [32] and [33]. For the case study, real-time GPS data from the trams are collected with a resolution of one second. A MATLAB/Simulink model is used to simulate the traction power and the energy flows for the unidirectional substation braking resistors and regenerated energy use. For sizing the ESS, the research looked into the maximum current demand for the trams in the network. The case study looks into the effect of changing the location of the 1000 Ah ESS along the tram line between the stops 'Halfway' and 'Crystal Peaks'. Two substations power this segment. Initially, the ESS was placed next to the tram stops due to the easy track access and future EV parking locations. However, the authors found that the highest braking energy recovery could be obtained at the mid-point between two substations, see Table 2.7.

An ESS that is dedicated to storing the braking energy of the trams is used by the authors. The authors have used in their simulation an ESS that is dedicated to storing the braking energy of the trams. However, as they conclude [33], this type of ESS is not economically viable in most cases. As a solution, the authors suggest that by replacing the ESS with an EV battery, the economic feasibility could improve substantially. As

Table 2.7: Energy use from the substations during a single trip from stops 'Halfway' to 'Crystal Peaks' with six different locations for the 1000 Ah ESS [32]. Scenario (4) gives the best energy savings and is located between the two substations.

Location of ESS	Energy lost in a resistor (kWh)	Total energy from substations (kWh)
(1) without ESS	7.954	14.454
(2) Halfway	3.375	13.89
(3) Westfield	2.451	10.905
(4) Waterthorpe	1.975	10.598
(5) Beighton	2.157	11.196
(6) Crystal Peak	3.914	14.223

demonstrated in the case study, the correct placement of the ESS on a traction network could increase the whole system's efficiency by 16%. In this thesis, various locations for the EV chargers will be taken into account, and the behavior on the energy savings for substations will be evaluated.

2.2 LOAD PROFILES OF EV-CHARGERS FOR ELECTRIC CARS IN AN URBAN ENVIRONMENT

This section describes two methods to determine a realistic load profile for a set of EV chargers. Load profiles for electric vehicles simulate the EV load during a period on an electrical network. Actual data or synthetically generated data form the basis for the two methods. An example of such a load profile based on accurate data is given in Figure 2.7 [34]. In this article, data obtained during the EV project [35] was used. The authors derive a typical one-day charging profile based on weekday and weekend charging behavior. The optimal location for EV chargers for maximum profit is found with the use of a mixed-integer linear model.

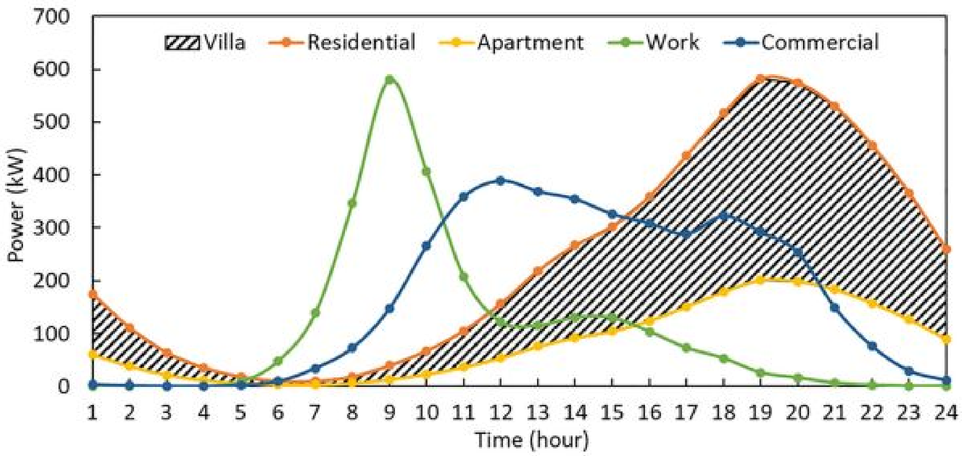

Figure 2.7: Typical EV charging demand profiles at the different land uses [34].

In [36], the load profile is modeled for a whole week, see Figure 2.8. Based on empirical data from EVs in Germany, the authors determined a synthetic EV load profile and validated it with the data used [37]. Furthermore, three different types of EV charging profiles in the Edinburgh network are used, as shown in Figure 2.6. Both methods give realistic load profiles; however, the choice between the two methods depends on the available representative input data.

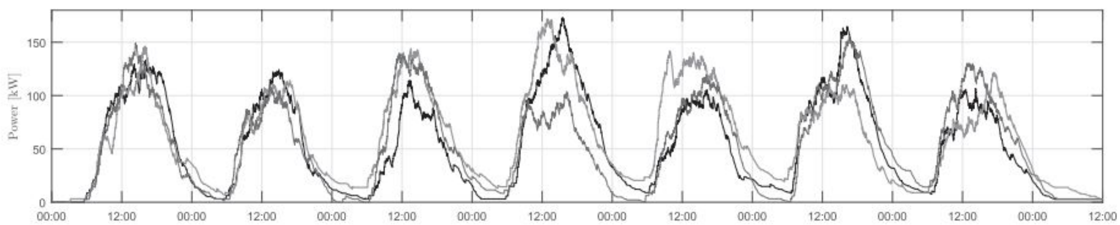

Figure 2.8: Three simulated load profiles for electric cars over a week, starting on Monday [36].

2.3 DYNAMIC CHARGING

As the available power in the DC trolleygrid will fluctuate, dynamic charging (i.e., charging with variable power; called smart charging in this thesis) could improve the utilization of EV chargers on the traction grid. Mouli et al. [38, 39] looked into the dynamic charging of EVs powered by fluctuating renewable energy sources (e.g., PV and wind). As CCS/Combo and Chademo are used in DC networks without additional inverters, only these types of charging methods will be discussed.

With Chademo v1.0, the charger cannot change the maximum current going into the battery. In this protocol, dynamic charging is not possible. However, this is changed in Chademo v2.0. Here the minimum and the maximum current are set every 200 ms based on the SOC, temperature, etc. For the experimental verification, the researchers found that 20 A/s ($\approx 5 - 10$ kW/s) ramp up and ramp down speed can be assumed with Chademo v2.0 charging [38].

The paper shows that CCS/Combo charging is less flexible than Chademo charging. This is mainly because the response time depends on the EVs' manufacturer [40]. This could take up to 60 seconds where the need for changes is around 2 seconds in the applications with renewable energy sources. The authors' experimentally verified the CCS/Combo charging method with two different EVs. They concluded that CCS/Combo charging can be used for dynamic charging, but the performance varies between the EVs.

The Chademo protocol is further investigated and tested by Casaleiro et al. [41]. In their test-bed, they use the Nissan Leaf 2015 model with a 24 kWh Li-ion battery and a method described in [42]. As shown in Figure 2.9, the charger is connected to an LVAC grid. During the experiment, the response time and the power accuracy are measured for various power requests. In Figure 2.10, an example of the change in power output is shown with the associated response time. The authors come up with a general formula for the total response time, as shown in equation 2.1.

$$\text{Total response time} = 0.26 \times \left|\Delta P_{\text{request}}\right| + 4.04[\text{s}], \tag{2.1}$$

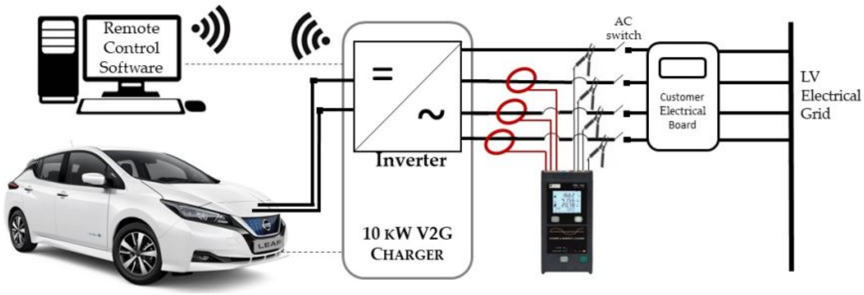

Figure 2.9: Experimental setup for validation of charging and discharging of Nissan Leaf 2015 for grid support [41].

Moreover, in [43], charging three different EVs with 3.7 kW AC power is evaluated. This paper uses the IEC 61851 standard and an experimental validation setup. As shown in the article, the response time of each vehicle is different, but all the tested vehicles can respond within 3 seconds to the reference current.

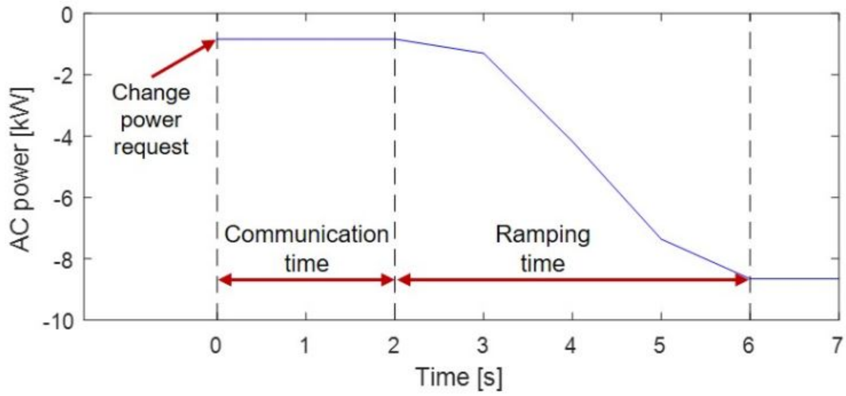

Figure 2.10: Response time of charger measured at the alternating current (AC) side of the converter [41].

2.4 RESEARCH GAP

Earlier work suggests that EV chargers can be integrated into an existing traction network. However, none of the research combines the most critical grid parameters with the placement of various-sized EVs at different locations on a representative traction grid. In Table 2.8, the projects are summarized.

Weisbach et al. [23] (Solingen) introduced an intelligent charging strategy to increase charging utilization with dynamic charging. In this research, the grid is represented by a predetermined power profile, and only power limitations are considered in the control scheme of the charger. In the same sub-project, a method to determine the optimal placement is suggested in [22]. This study considers voltage limitations, but the research is limited to a test-bed environment. Combining smart EV charging with the trolleybus behavior under variable circumstances within the traction grid's power, voltage, and current limitations is still undiscovered.

In the research performed on the trolleygrid of Gdynia, the authors use real-time load level recordings from the grid to represent the traction grid behavior. This is the only work that looks into the most critical grid limitations, as shown in Table 2.3. The downside of this research is that they use a linearized approach to simulate the electric circuit with EV chargers connected to it. Furthermore, the work does not include determining the size and location of EV chargers. The authors show that with the use of an ESS on the traction grid, energy consumption from the substation could be reduced by up to 30%.

The effect of ESS is further demonstrated in the traction networks of Lisbon and Sheffield. The researchers show a reduction in energy consumption and an improvement in voltage regulation. The size and location size of the ESS are fixed to the tram stops in these articles. Additionally, in this research, not all the grid limitations are considered.

To give a good representation, the dynamic charging parameters discussed in Chapter 2.3 will be used as limits for the charging infrastructure.

As mentioned earlier, non of the research shown in Table 2.8 gives a complete study of the integration of EV chargers into a traction network. This thesis investigates the potential of EV charging in a trolleygrid using expected traction grid behavior. The case study determines the location and maximum size of EV chargers in combination with representative charging profiles of public EV chargers directly connected to the traction grid. The most important traction grid limitations will be considered. Furthermore, this thesis will compare different smart grid methods (Table 1.1) to increase the charging utilization in a traction grid. In the case study, multiple supply zones of the trolleygrid of Arnhem will be simulated in a MATLAB environment.

Table 2.8: Overview of the projects and the methods used in their study.

	Solingen [20, 21, 22, 23, 24, 25]	**Gdynia** [16, 26, 27, 7, 28]	**Edinburgh** [17, 29, 30]	**Lisbon** [31]	**Sheffield** [32, 33]	**Arnhem** [4, 8, 12] (This thesis)
Traction network	Trolleybus	Trolleybus	Tram	Tram	Tram	Trolleybus
Traction grid representation	Predetermined power profile	Real-time load level recordings	Average over 30 min	Predefined driving cycle	Real-time GPS data	Real-time GPS data
EV Charging profile representation	Charging, based on available power	Constant power	Three different power profiles	Constant power	Constant power	Public charging profile
Size of EV chargers	Intervals of 12.5 kW, up to 50 kW	22 kW or 44 kW	Based on available power	7x 50 kW EV Chargers	-	Intervals of 25 kW, up to 500 kW
Locations of EV chargers	Fixed nodes in test-bed environment	Furthest point from substation	At substation	At tram stops	At tram stops	Every 100 m, End-of-Line Feed-in SS
Grid limitations considered	Power	Power, Voltage, Current, Ohmic losses	Power	Voltage	Current	Power, Voltage, Current
Connection with traction grid	Directly from overhead lines	Directly from overhead lines	Directly from overhead lines	Directly from overhead lines	Directly from overhead lines	Directly from overhead lines
Method used	Simulation	Simulation, implementation	Simulation	Simulation	Simulation	Simulation
Comments	Dynamic charging	Linear model, bilateral connections	Charging profiles	V4G, Fuzzy rules	Economic aspects	Smart grid methods

3 METHODOLOGY

For this thesis, two studies were performed firstly, a theoretical study to illustrate the effect of adding EV chargers to an artificial traction grid. Predetermined trolleybus speed profiles are used to simulate trolleybus behavior. Secondly, a more in-depth analysis of the integration of EV charging was done in the case study. Actual bus behavior was used for two different supply zones in the trolleygrid of Arnhem.

The first part of this Chapter describes the limitations of a trolleygrid network. Secondly, an introduction to the computational trolleygrid model is given. This will be followed by how EV charging profiles are created based on measured charging behavior in the Netherlands. In section 3.4, the six smart grid methods are described. Next, the method of determining the EV charging potential is given. Lastly, an overview of the theoretical and case study is presented.

3.1 LIMITATION OF THE TROLLEYGRID

Due to variable power demand, the trolleybuses are subjecting the trolleygrid to highly volatile loads. As a result, the trolleygrid parameters can change in a short period. Three main trolleygrid parameters were analyzed to determine if the traction grid can supply energy to the EV chargers.

1. **Substations power rating.** Most substations in Arnhem are designed for a power rating of 800 kW. According to standards, allowable traction substation overload rates are 120% for 60 minutes, 150% for 5 minutes, and 300% for 1 minute [44, 45]. Stressing the power beyond these limits could increase the temperature beyond the components' specifications, resulting in failures. Currently, in the trolleygrid of Arnhem, a substation overload up to 120% for 10-15 seconds is not uncommon. Based on the IEEE standard, the substations' limitations can be stressed beyond the present situation. However, for this thesis, the temperature of the components in the substation is not modeled. Hence this research will use a very conservative approach based on the current situation of the trolleygrid. In other words, the substations' power (P_{ss}) level cannot be above 100% of the rated capacity for 10 or more consecutive seconds and can never be above 120% of the rated capacity. In the smart grid method, increasing the substation power tolerance, the effect of this conservative approach is demonstrated.

2. **Minimum voltage in the overhead lines.** With a nominal voltage (V_{nom}) of 600 V and the standard EN 50163 [46], the voltage can range from 400 V (-33%) to 720 V (+20%) on the trolleygrid. On top of that, the trolleybuses operating in Arnhem have an additional safety mechanism (Chap 1.1.1). Below 500 V, the trolleybus reduces the power automatically to recover the grids' voltage [9]. As a result,

the trolleybus cannot follow the driver's input. The low voltage on the section is undesired but not critical. Therefore, the minimum line voltage ($V_{\text{min,line}}$) on the trolleygrid can be between the minimum trolleybus voltage ($V_{\text{min,bus}}$) of 500 V and critical grid voltage (V_{crit}) of 400 V for 120 seconds. The voltage can never be below V_{crit} (400 V).

3. **Maximum current overhead lines.** The standard EN 50119 stated that the long-term current in a single 100 mm^2 copper cable could be between 400 and 460 A [22, 26, 47]. Above this current, the temperature in the overhead wires can exceed the limit of 80°C. The overhead wires consist of N parallel lines (Chap. 1.1); hence the maximum continuous current (I_{max}) in the overhead cables is set to 880 A for 50 minutes ($N \cdot 440$ [A], where N the number of parallel lines is) and 1200 A for 30 minutes.

As the typical feed-in cables have a much larger cross-sectional area (630 mm^2) compared to the overhead lines, the long-term load current in the feed-in cable was not considered a limiting factor [26]. Table 3.1 summarizes the most critical parameters of the trolleygrid with the associated limitation.

Table 3.1: Limitations on the trolleygrid parameters

Limiting factor	Limitation	Allowable duration
Substation Power	$100\% < P_{SS} \leq 120\%$	10 consecutive seconds
	$P_{SS} > 120\%$	Never
Minimum voltage	$400 < V_{\text{min,line}} < 500$	Average over the previous 120 seconds [9]
	$V_{\text{min,line}} \leq 400$ V	Never [46]
Maximum current	$I_{\text{max,1}} < 880$ A	Average over the previous 50 minutes [26, 22]
	$I_{\text{max,2}} < 1200$ A	Average over the previous 30 minutes [47]

Maximum voltage on the trolleygrid

In the real world, during periods where the braking resistor is activated ($P_{\text{bus init}} > P_{\text{loads}}$), the voltage at the braking bus must be above 720 V (1.1.1). However, due to the way of simulating, the calculated voltage at the braking bus is just high enough to overcome the voltage drop associated with the Ohmic resistance to feed the other loads. In the simulation, the power sent to the braking resistor was calculated in the following way:

$$P_{\text{braking}} = P_{\text{bus init}} - P_{\text{bus calculated}} \tag{3.1}$$

In other words, the braking resistor is fully engaged at V_{braking}, which can be below 720 V in the simulation environment. Consequently, equation 3.1, is only valid for that particular scenario if the maximum voltage on the section is below 720 V during a whole day.

3.2 HOW THE MODEL WORKS

For this thesis, the existing model as described in [4, 8] was used. With the help of MATLAB, the model can represent accurate bus behavior on a traction grid based on measured data from the Arnhem trolleygrid [11]. The model (Figure 3.1) starts by creating a bus load profile with a resolution of 1 second. The bus loads include traffic data, various bus schedules etc. In the next step, the location of the buses is determined. The addition of realistic EV charging profiles and the introduction of smart grid methods to increase the charging potential is added to the existing model in this thesis. With a backward-forward sweep method [48], the voltage and current at each node are calculated for each second of the day. Based on these results, the branch currents were determined with their associated transmission losses.

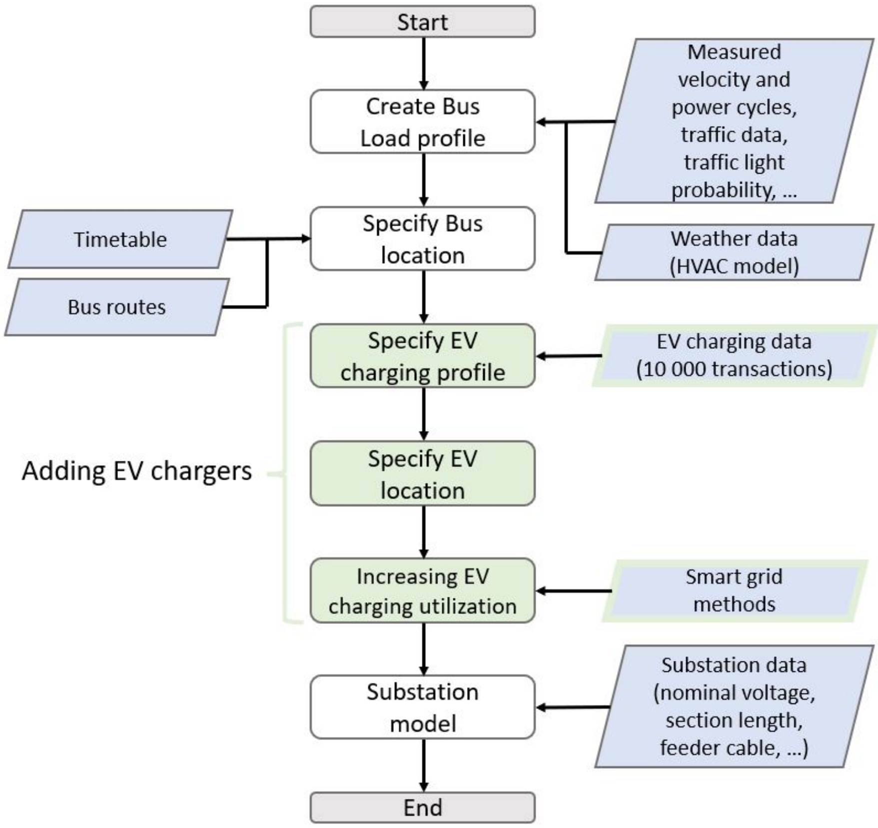

Figure 3.1: Flowchart of the extended trolleybus grid model. The white and blue blocks were present in the existing model [4]. The green blocks represent the EV charging parts that will be added to the MATLAB model for this thesis.

In the model, each bus/load is represented as a node with two input variables for each time-step, 1. load profile demand, and 2. location on the section. In Appendix A.1, a more detailed explanation with an example is given. In the next section, the addition of EV chargers to the model (green blocks) are explained in more detail.

3.3 ADDING EV CHARGERS TO THE MODEL

EV chargers can be modeled as an additional load on the section with the same two input variables for each time-step: load profile demand and positions on the trolleygrid. In this thesis, only stationary EV charging is considered (the EV chargers' location is not changing over time). Note: the positions of EV chargers can change in various simulated scenarios, but within the scenario, the location of the EV charger is fixed.

3.3.1 Creating realistic charging profile

To give an accurate EV charging power demand, real public EV charging behavior will be used. Two charging profiles are created based on a dataset of 10 000 public charging transactions in The Netherlands during 2019 [49]. One for weekdays and one for the weekends. Figure 3.2 shows the different stages of how the raw data was processed.

Figure 3.2: Stages for the creation of EV charging profiles for weekends and weekdays.

1. Each transaction contains two-time indicators, the connection time with the EV charger and the actual charging time. For simplification reasons, a constant charging power during the charging time of one transaction is assumed, as shown in Figure 3.3a.

2. The data is time-shifted to match the local time and the bus schedules. Daylight savings are also considered during this time shift.

3. A distinction is made between weekdays (7235 transactions) and weekends (2765 transactions). The two charging profiles are used for various simulated bus schedules; see Chapter 3.7.2.

4. Based on the two datasets, a probability mass function (PMF) is created with a resolution of one second for the weekdays and weekends. In this case, the PMF is a measure for the relative EV charging power for every second of the day.

5. In the last stage, the PMF is scaled to a maximum value with the scaling factor α. During the simulations, variable-sized EV chargers are added to the trolleygrid. For a fair comparison, each different-sized EV charger follows the same profile were only the magnitude difference. For example, the power demand of a 100 kW EV charger connected to the trolleygrid follows the profile described in Figure 3.3b. Depending on the type of day, this 100 kW EV charger reaches its maximum value of 100 kW around 9 am during the weekdays and 3:30 pm during the weekends.

The outcome of stage 5 is two scaled probability mass functions with an interval of one second. The magnitude of the scaling factor is based on the scenario input described in Chapter 3.5.

The so-called idle time, the difference between connection time and the charging time shows the duration that the EV charger is not charging but is connected to the EV

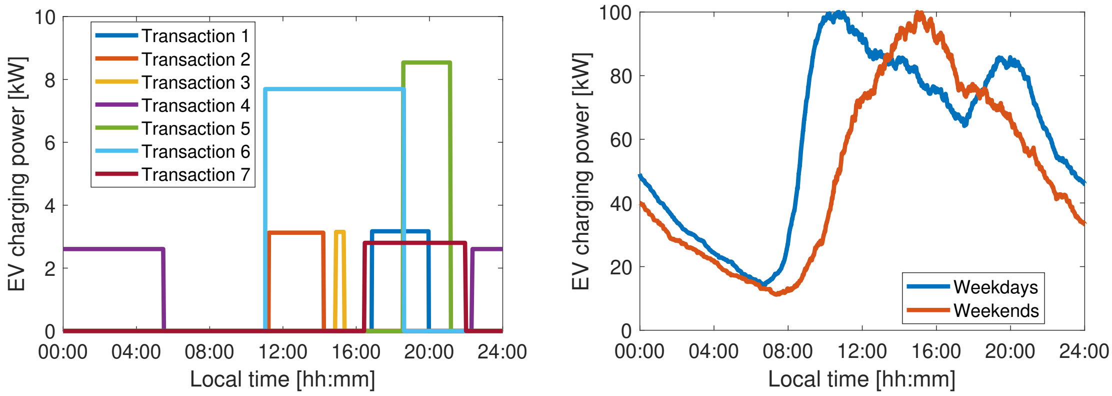

(a) Various charging transactions.

(b) EV power profile distribution over a day.

Figure 3.3: Creating EV charging demand. Own work, raw data obtained from [49].

charger. Figure 3.4 shows the distribution and duration of the idle time for the public charging transactions studied. 54.5% of the transactions have an idle time of less than 30 minutes. With 27.5% of the EVs having an idle time of more than 180 minutes, vehicle-to-grid (V2G) could be an interesting option for the trolleygrid. V2G is a technology whereby the vehicle's battery can deliver energy back to the power grid. In this case, the EVs could act as a distributed power source, reducing the overhead wires' voltage drops and increasing the EV charging potential.

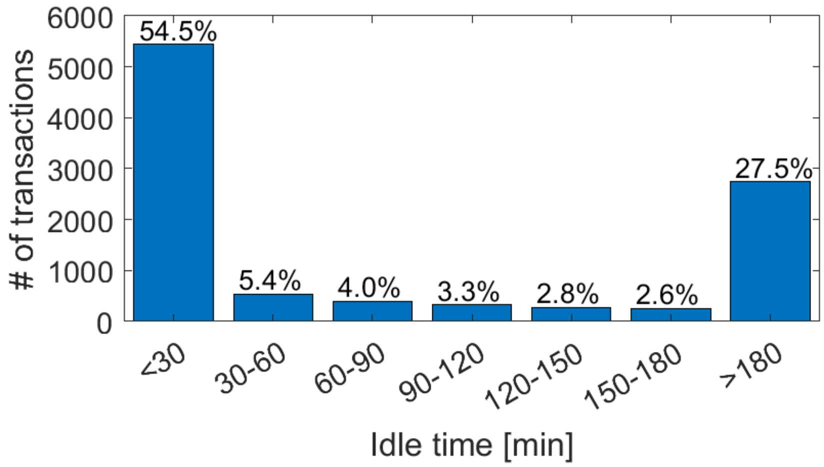

Figure 3.4: Distribution of the idle time of EVs at public EV chargers for all the transactions. Own work, data obtained from [49].

But, the possibility for V2G also depends on the amount of EVs available during different times on the day. Figure 3.5 shows the amount of EVs in idle modes (idle for more than 30 minutes) relative to the amount of EVs in charging modes. At night time, there are more EVs in idle modes than EVs charging. However, during the majority of the operation hours of the trolleybus and especially during EV charging peak moments, there are more EVs charging than in idle modes. Therefore, V2G is not considered in this study.

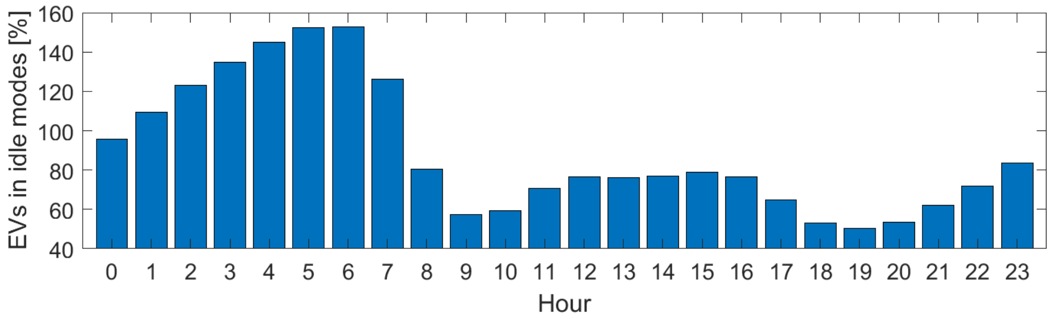

Figure 3.5: The amount of EVs in idle mode relative to the amount of EVs in charging mode at various hours on the day. An EV is considered in idle modes if the charging has stopped for more than 30 minutes and is still connected to the charger. Own work, data obtained from [49].

3.3.2 EV charger hardware

As shown in Figure 1.7b, the EV charger pole can be installed very close to the overhead wires. Considering this, the assumption was made that there are no transmission losses from the overhead cables to the DC/DC converter as described in Appendix A.5. A converter efficiency of 98% and constant battery charging efficiency of 95% was assumed [50]. The EV charging potential is expressed with two different units, the size of the EV charger in kW and the number of EVs that can be fully charged with a battery size of 60 kWh.

The ramp-up/down speed of the EV charger is one of the input variable used in the smart charging simulation. This parameters is based on multiple inputs such as converter type, battery pack, and type of EV [38, 39, 40]. As the EV chargers in the trolleygrid needs to serve multiple types of EVs not a single value can be chosen. Therefore, the ramp-up/down speed can vary between 3 kW/s and 9 kW/s with intervals of 3 kW/s.

3.3.3 EV charging location

For the simulations, an interval based approach for the placement of EV charger is chosen. Hereby, the EV chargers' geographic capabilities and spatial planning are not considered. In the computational model, there is a trade-off between simulation time and accuracy. Reducing the interval for the placement of the EV chargers increases the accuracy but also the number of simulations. For the case study, an interval of 100 meters was used to determine the location of the EV chargers.

As mentioned in Chapter 1.1, the double parallel overhead wires are connected roughly every 100 meters with each other. The same interval is chosen for the placement of the EV chargers to be inline with the assumption that the resistance can be divided by two. The EV chargers are also placed at key locations of the section, such as the section's start and end points and the substation's feed-in location.

3.4 THE SIX SMART GRID METHODS

The six analyzed methods are described below.

1. **Substation level**

   1.1 *Increasing substation nominal voltage*
   This method has two main goals:

   - Reducing the chance that the minimum voltage on the section will be lower than the threshold levels of $V_{\text{bus, min}}$ and V_{crit}.
   - Reducing the current in the overhead wires for the same power demand.

   Additional benefits of reducing the current are: less voltage drop in the overhead wires, and less transmission losses in the feed-in and overhead lines. A downside could be that the braking resistor could be activated more frequently, beceause the trolleybuses are operating closer $V_{\text{braking, bus}}$ (Chap. 1.1.1). As a result, the total power consumption could be increased by this method (Table 2.4).

   1.2 *Increasing allowable substation's power tolerance or additional converting capacity*
   By improving the substation capacity, the power limitation could be less often violated. Especially in areas where the substation is powering multiple sections, the substations' power rating could be a limiting factor for increasing the EV charging potential. The voltage and current limitations are not affected by this method. The downside of this method is that the components could operate closer to their limit with the associated risks involved.

2. **Grid infrastructure level**

   2.1 *Adding extra parallel line*
   The impedance in the overhead wires is reduced by adding an extra parallel line to the catenary grid. The main goals are to increase the maximum current rating in the overhead wires by 50% and to reduce the voltage drop in the overhead lines. The downsides of this method are the costs, spacial availability above the road, and the additional horizon pollution.

   2.2 *Introduction of bilateral connection*
   The introduction of a bilateral connection has the benefit of powering loads by two different substations. As a result the current in the overhead lines is reduced with a higher minimum voltage and lower transmission loses as a result. On the other hand, due to the larger feeding section, faults in the system could occur more often and influence a larger area.

3. **EV charging level**

   3.1 *Introduction of smart charging*
   With smart charging, the EV charging load could be reduced at moments when the bus loads are high. In this thesis, the assumption is made that the substations, buses, and EV chargers can communicate with each other. Based

on this information, the power output of the EV charger was determined. The complexity of this smart grid method makes it hard to implement.

3.2 *Introduction of multi-port converter*
The multi-port converter can charge an EV from two separate power sources [12]. At the intersection point, two cables from each section could be connected to the EV charger. This method aims to reduce the load on the individual isolated sections. It is assumed that there is no power transfer from one section to the other via the multi-port converter. This method has the downside of being limited to the connection point.

In Table 3.2, the goal of the smart grid methods are summarized.

Table 3.2: Summary of the six methods addressed in this thesis and their positive (+), negative (-), or neutral (o) effects on reducing the grid violations in power, voltage, and current, as well as their effect on the transmission losses (RI^2) and the braking energy recuperation (BR). *Unless both substations are heavily loaded. Courtesy of I. Diab.

	Reduces violations			Effect on	
	P	V	I	RI^2	BR
1.1 Higher SS Voltage	+	++	+	+	-
1.2 Higher SS Power tolerance	++	o	o	o	o
2.1 Smart Charging	++	++	++	+	++
2.2 Third paralleled Line	+	++	++	++	+
3.1 Bilateral Connection*	++	++	++	++	++
3.2 Multi-port Converter	-	-	-	+	+

3.5 METHOD OF DETERMINING EV CHARGING POTENTIAL

To determine the EV charging potential in a trolleygrid, the work flow as shown in Figure 3.6, was used.

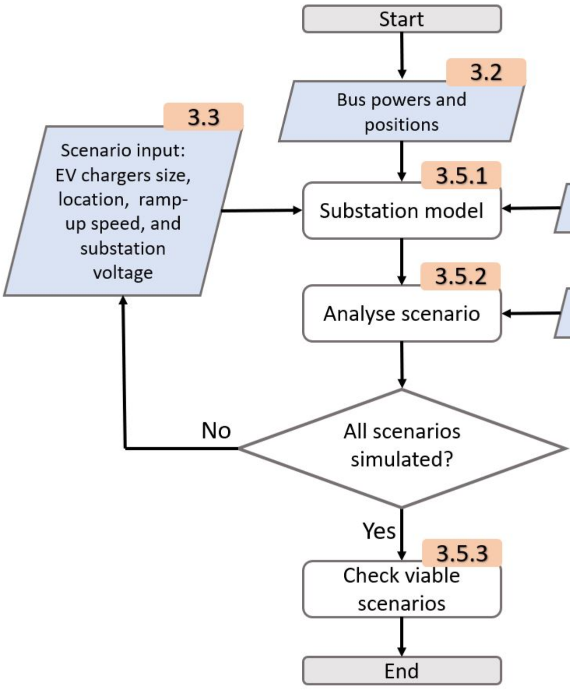

Figure 3.6: Flow chart of determining the EV charging potential.

3.5.1 Substation model

The first step, substation model, corresponds to the substation model described in Figure 3.1 and has three input variables. Firstly, the simulation starts by loading the realistic bus powers and locations for the simulated day and section, as mentioned in Chapter 3.2. The second input variable is the smart grid method used in the simulation (Chap. 3.4). In total, six smart grid methods will be evaluated to reduce the chance that one or more of the limitations (Chap 3.1) will be violated using these methods. The third input for the substation model is based on the smart grid method used and the associated input parameters such as the EV charging size, substation voltage, etc, see Table 3.3.

Table 3.3: The input characteristics for the EV charger for the various scenarios. *In the bilateral connection, the maximum size of EV chargers is 700 kW (only one EV charger added to both sections). **Theoretical study: interval is set to 150 meters.

Scenario variable	Minimum	Interval	Maximum
Size EV charger [kW]	0	25	500*
Location EV charger [m]	0	100**	section length
Ramping speed EV charger [kW/s]	0	3	9/inf.
Substation nominal voltage [V]	650	10	730
Number of parallel lines	1	1	3
Tolerance substation power	100%	20%	200%
Base current smart charging [A]	0	88	880

3.5.2 Analyze scenario

As described in Chapter 3.1, the addition of EV chargers cannot lead to a failure of the trolleybus operations. In this step, each simulated scenario is tested and evaluated for viability. In the case when a scenario is not possible, the limiting factor will also be determined.

3.5.3 Check viable scenarios

For every smart grid method a certain number of unique scenarios was simulated. In the last step, the maximum EV charging potential for each location based on the simulated scenarios will be determined. The maximum EV charging potential is expressed into two variables; 1. the maximum EV charging potential in kW, and 2. the number of EVs charged per day. The two variables have the following relation:

$$\text{\# of EVs/day} = \frac{\eta_{\text{con}}\eta_{\text{bat}}}{E_{\text{bat}}} \sum_{t=1}^{86400} P_{\text{EV}}[t] \tag{3.2}$$

Whereby:
η_{con}; the DC/DC converter efficiency (98%) (Chap. 3.3.2),
η_{bat}; the constant battery charging efficiency (95%) (Chap. 3.3.2),
E_{bat}; EV battery size (60 kWh) (Chap. 3.3.2),
$P_{\text{EV}}[t]$; EV charging power profile (Chap. 3.3.1).

3.5.4 Logic smart charging

Based on the trolleygrid parameters, the EV charger decides the EV charging demand. In this thesis, the assumption is made that the substations, buses, and EV chargers can communicate. Figure 3.7 shows the logic used during the simulations. The initial EV charging demand at time-step t, P_{EV}, equals the charging demand from the previous second. If one of the grid parameters, as listed in Table 3.1, is violated, the EV charger reduces its output up to a maximum of the ramp-down speed. If the grid limits are not violated, the EV charger increases its power demand up to the maximum ramp-up speed. An example is given in Chapter 4.3.5.

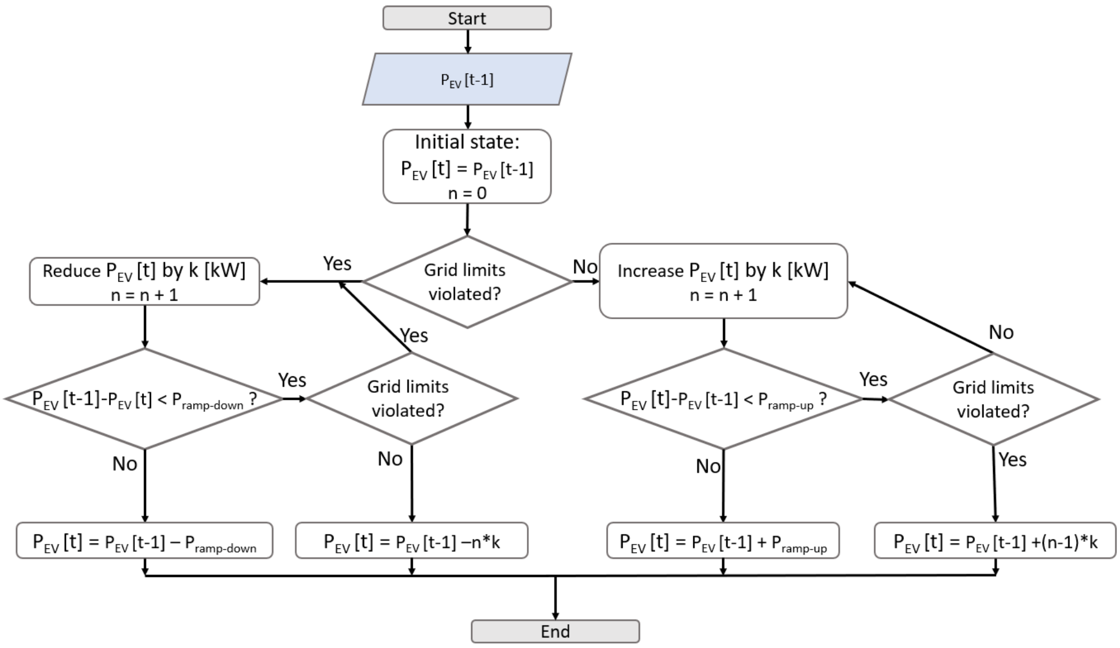

Figure 3.7: Logic used for the power demand of the smart charger. Whereby: the ramp-up/down speed is charger dependant and varies in every simulation, k the resolution of every iteration (0.2 kW is used), n the number of iterations.

3.6 OVERVIEW THEORETICAL STUDY

3.6.1 Trolleygrid layout used in the theoretical study

The theoretical study shows the effect of a long section (1500 meters) and, in literature, commonly used trapezoidal driving cycle on the EV charging potential in a trolleygrid. Unlike in the case study, seasonal variations or bus schedules will not be considered in the theoretical study.

In Figure 3.8, the trolleygrid layout for the theoretical study is shown. Substation 1 is powering section 111. Whereas substation 2 is powering both sections 112 and 113. The section length, substations nominal voltage, and feed-in cable characteristics are based on typical trolleygrid parameters [4, 8, 26] and summarized in Table 3.4. Furthermore, the limitations described in Chapter 3.1, are used in the theoretical study. In the theoretical study, EV chargers can be placed at various locations on section 111 and 112. Placing EV chargers on section 113 is out of the scope of the theoretical study. In Tables 3.6 & 3.7, the characteristics of supply zone T of the theoretical study are summarized.

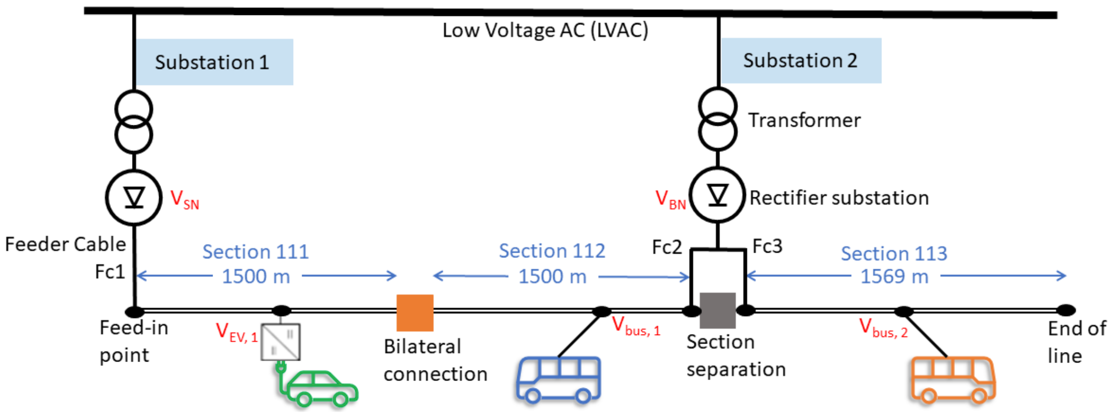

Figure 3.8: Layout theoretical section based on [4, 8].

Table 3.4: Grid parameters were used for the theoretical study [4, 8, 26].

Theoretical Grid Parameters	Quantity	Unit
Total track length	4569	$[m]$
Section lengths	[1500; 1500; 1569]	$[m]$
Overhead line impedance	0.172	$[\Omega/km]$
Overhead line max current	840	$[A]$
$P_{\text{SS, rated}}$	800	$[kW]$
$V_{\text{nom, SS1}}$	650	$[V]$
$V_{\text{nom, SS2}}$	650	$[V]$
$V_{\text{min,bus}}$	500	$[V]$
V_{crit}	400	$[V]$
Feed-in point of substation	[0; 1500; 0]	$[m]$
Feed-in cable length	[100; 100; 100]	$[m]$
Feed-in cable impedance	0.0566	$[\Omega/km]$

3.6.2 Bus behavior used in the theoretical study

For the theoretical study, the SORT 2 driving cycle will be used [51, 52]. This driving cycle represents bus behavior in easy urban environmental areas. The maximum speed in the driving cycle is 50 km/h, with an average speed of 18.6 km/h. The base cycle is around 180 seconds and is built up out of three trapezoids. Each trapezoid has various acceleration, maximum speed, and duration. Figure 3.9 presents the SORT 2 driving cycle. After each trapezoid, the bus stops for 20 seconds, representing a traffic light or a bus stop. The base cycle repeats 10 times (5 times on the outward journey and 5 times on the return journey). Table 3.5 summarizes the specifications of the SORT 2 driving cycle.

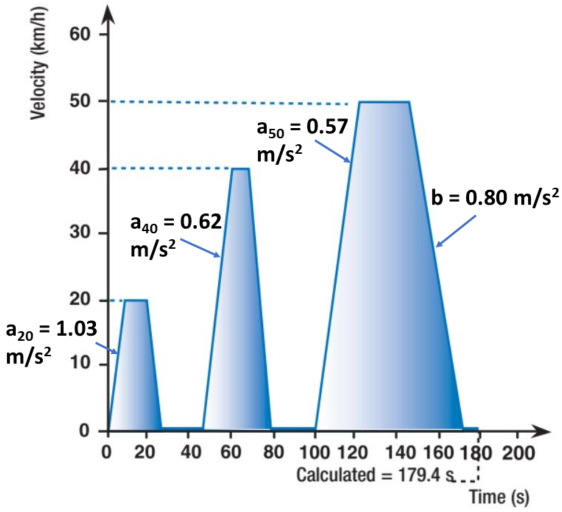

Figure 3.9: SORT 2 driving cycle [52].

Table 3.5: SORT 2 driving cycle specifications [52].

SORT 2 Parameters	Quantity	Unit
Number of traffic light stops	2	-
Number of bus stops	1	-
Rated average speed	18.6	$[km/h]$
Maximum bus speed	[20; 40; 50]	$[km/h]$
Acceleration	[1.03; 0.62; 0.57];	$[m/s^2]$
Deceleration	[0.8; 0.8; 0.8];	$[m/s^2]$
Length of trapeze (inc. acc. and dec.)	[100; 220; 600]	$[m]$
Duration of stops	[20; 20; 20]	$[s]$
Gradient	0	$[\%]$
Length base cycle	920	$[m]$
Total length full cycle	4569	$[m]$
Bus frequency	4	$[Buses/hour]$
Delay bus 2	15	$[s]$

Repeating the base cycles 10 times results in a total duration of one entire trip of 30 minutes with a total length of 4569 meters, as shown in Figure 3.10. The whole trip of the bus repeats during the time interval between 5 am to 0:30 am. In this theoretical study, a delay of 15 seconds for bus 2 was taken into consideration. The time shift avoids an exact overlap of the maximum peaks of the two busses. The power demand of the bus is calculated with the forces acting on the moving bus as described in Appendix A.2 [51]. An additional 40 kW auxiliary power is added to the power demand to represent HVAC and other electrical services. The total power demand of the buses is shown in Figure 3.11.

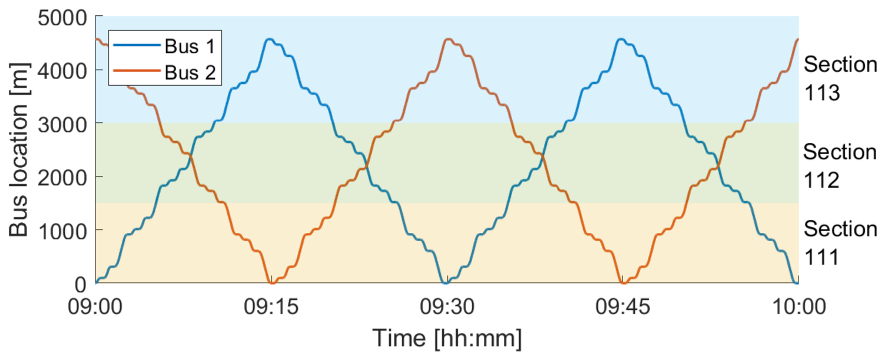

Figure 3.10: Location of the two buses.

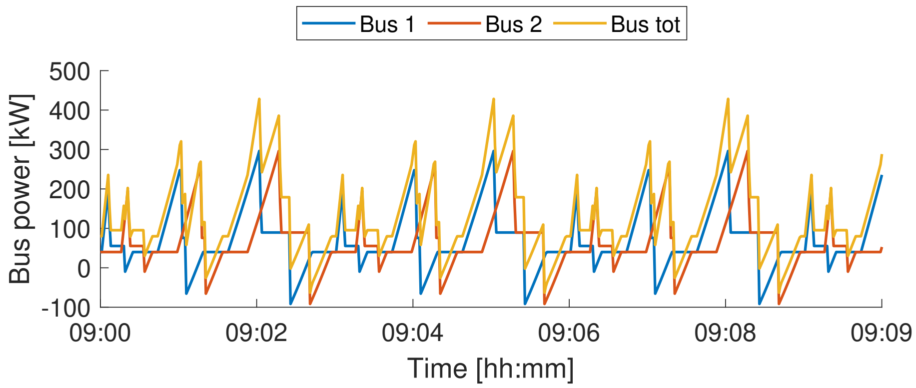

Figure 3.11: The power demand of both buses and the sum of them. Based on the acting forces on the bus. There is a time shift of 15 seconds between bus 1 and bus 2.

The number of buses in sections 111 and 112 is shown in Figure 3.12.

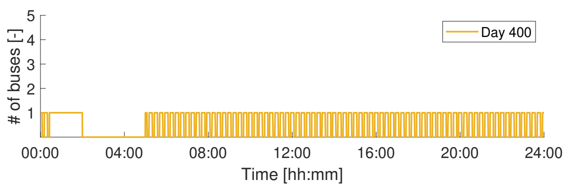

(a) Section 111.

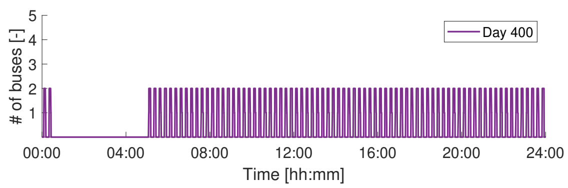

(b) Section 112.

Figure 3.12: Number of buses on section 111 and section 112.

3.7 OVERVIEW CASE STUDY

3.7.1 Simulated supply zones in the case study

The case study investigates two different energy supply zones, zones A and B, with their characteristics summarized in Table 3.6. The EV chargers are placed in supply zone A on sections 23 and 2, and in supply zone B, on sections 25 and 26. The main difference between these sections is the bus intensity. Section 23 has one trolleybus line operating on the section, and section 25 has four trolleybus lines. As listed in Table 3.7, the other characteristics are very comparable to each other.

Table 3.6: The characteristics of the two different supply zones investigated in the case study.

Supply zone	Substation & powering section(s)	Trolleybus intensity	$V_{\mathrm{nom,SS}}$	Bilateral between sections
T	$SS_1 = 111$	Medium	$SS_1 = 650$ V	111 & 112
	$SS_2 = 112$ & 113		$SS_2 = 650$ V	
A	$SS_{12} = 23$ & 24	Low	$SS_{12} = 686$ V	23 & 2
	$SS_{13} = 2$ & 3		$SS_{13} = 698$ V	
B	$SS_9 = 25$	High	$SS_9 = 677$ V	25 & 26
	$SS_{14} = 26$ & 27 & 41		$SS_{14} = 628$ V	

Table 3.7: The characteristics of the sections where the EV chargers are placed for the case study.

Supply zone	Section	Length [m]	Feed-in point SS relative to section start [m]	Feed-in cable length [m]
T	111	1500	0	100
	112	1500	1500	100
A	23	850	80	98
	2	1300	1210	300
B	25	860	100	180
	26	650	550	70

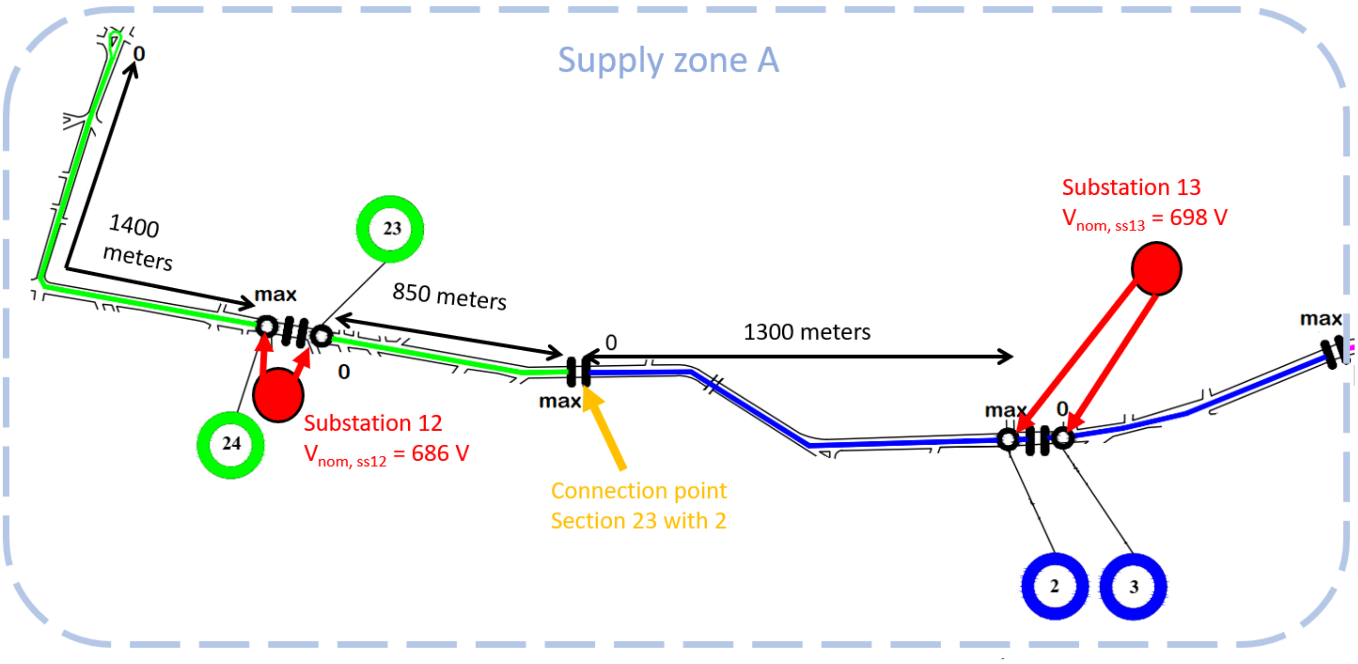

(a) Supply zone A.

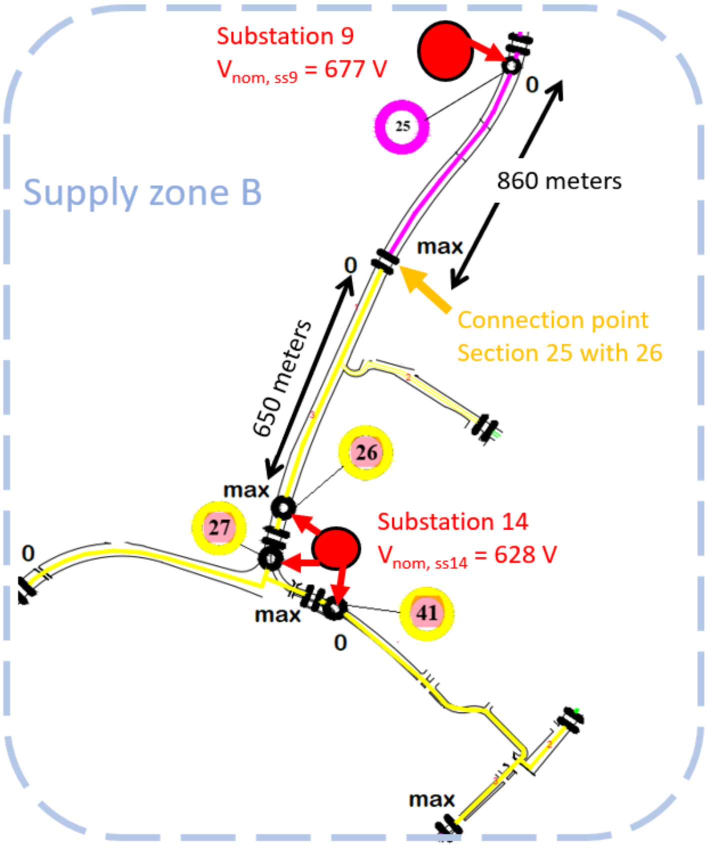

(b) Supply zone B.

Figure 3.13: The case study investigated two supply zones in Arnhem's trolleygrid.

3.7.2 Days simulated in case study

The literature [4, 8] describes that bus power demands can vary due to seasonal effects and scheduling. Therefore, six different days are chosen for this case study to get expected trolleybus behavior for an entire year. The characteristics of the days are listed in Table 3.8. On top of that, the different EV charging profiles (Chap. 3.3.1) will simulate various EV charging demands for weekdays and weekends.

Table 3.8: The characteristics of the six days used in the case study to represent various trolleybus scheduling and HVAC conditions [4].

Day	Schedule Category	Bus intensity	Auxiliaries (HVAC)
1	School holiday	High	High (winter)
117	Sunday & special holiday	Low	Low (spring)
197	Summer weekday	Low	Medium (summer)
200	Summer Saturday	Low	Medium (summer)
268	Regular weekday	High	High (winter)
305	Regular Saturday	Low	High (winter)

For the two different investigated sections, the bus intensity is shown in Figure 3.14. On section 23, the maximum number of buses is 2. Whereas, on section 25, there could be four buses simultaneously.

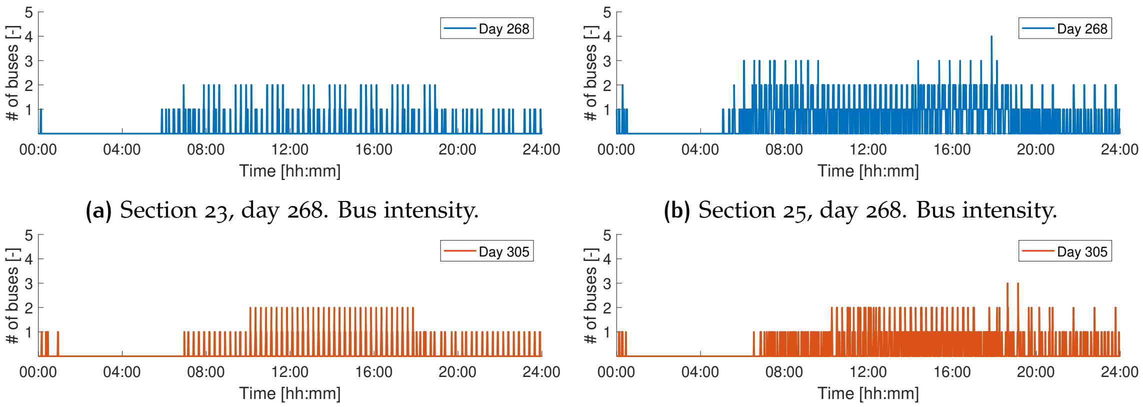

(a) Section 23, day 268. Bus intensity.

(b) Section 25, day 268. Bus intensity.

(c) Section 23, day 305. Bus intensity.

(d) Section 25, day 305. Bus intensity.

Figure 3.14: Number of buses on two different days.

3.8 ENERGY FLOW IN THE TROLLEYGRID

The energy flow through traction systems is described by [53]. In this thesis, the simplified model for the energy analysis, as shown in Figure 3.15, will be used. Two substations ($E_{\text{ss,n}}$) convert energy from AC to DC. In this process, it is assumed that there are no conversion losses. The substations will power all the loads on the sections whereby transmission losses are included as $E_{\text{loss,trans}}$. The total energy going into the EVs' battery is defined as E_{bat}. Hereby energy charging losses ($E_{\text{loss,charging}}$) (Chap. 3.3.2) will be considered. The bus uses energy for traction and HVAC purposes (combined into E_{traction}). Furthermore, when the bus's recuperated power is larger than the loads on the sections, the bus sends power toward the braking resistor (E_{brak}) (Chap. 1.1.1).

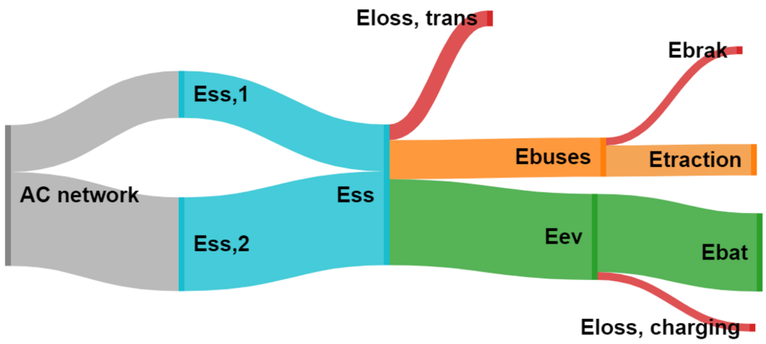

Figure 3.15: Simplified energy flow of the trolleygrid, not on scale [53].

4 THEORETICAL STUDY

This Chapter discusses the impact of the integration of EV chargers on the substations' power, minimum overhead line voltage, and maximum overhead line current on the theoretical supply zone. The computation model (Chap. 3.2) and theoretical supply zone (Chap. 3.6), will be used. Firstly, no smart grid methods are implemented in the baseline simulation. Later on, the six smart grid methods were analyzed.

4.1 EFFECT OF ADDING EV CHARGERS – THEORETICAL STUDY

An EV charger of 100 kW at a location of 750 meters on section 111 was simulated to illustrate the effect of the EV charger on the grid parameters.

4.1.1 Substation power

Figure 4.1 present the effect of integrating EV chargers on the power delivered by substation 1. In the left graph, no EV charger was integrated into the section. On the right chart, an EV charger of 100 kW was placed at a location of 750 meters. In both cases, the substation's power level is always below the rated power of 800 kW. The outcome suggests that the power rating of the substation is not the limiting factor with the integration of EV chargers on section 111.

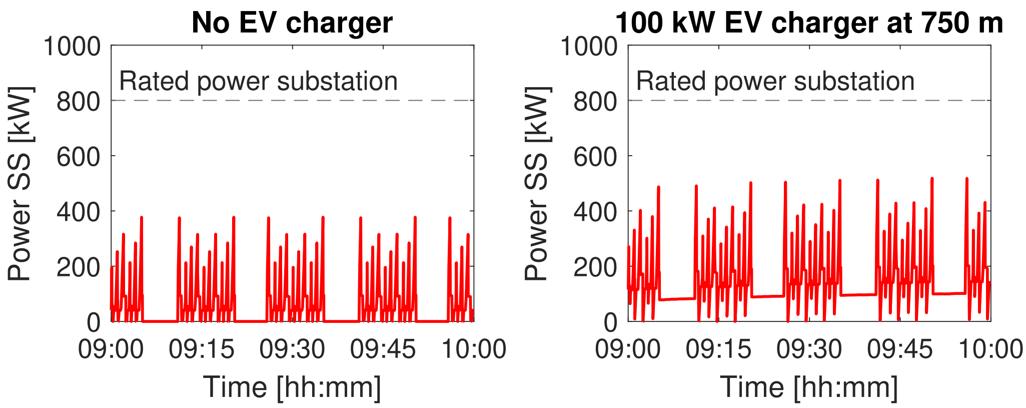

Figure 4.1: Power delivered by substation 1 from 9 am till 10 am. The power limitation is not violated during this period in both cases.

4.1.2 Minimum voltage in the overhead wires

Figure 4.2 shows the effect of integrating EV chargers on the minimum overhead line voltage on section 111. In the theoretical study $V_{\text{nom, SS1}}$ is set to 650 V. In the case where the EV charger is not integrated into the section, the minimum voltage stays above $V_{\text{bus,min}}$ (500 V). However, with the integration of a 100 kW EV charger at 750 meters (right graph), there are moments where the voltage is below 500 V. This indicates that the minimum overhead line voltage could be a limiting factor for the integration of EV chargers on the trolleygrid. In the right graph of Figure 4.2, the voltage is only at short instances below the threshold with a maximum duration of 4 seconds.

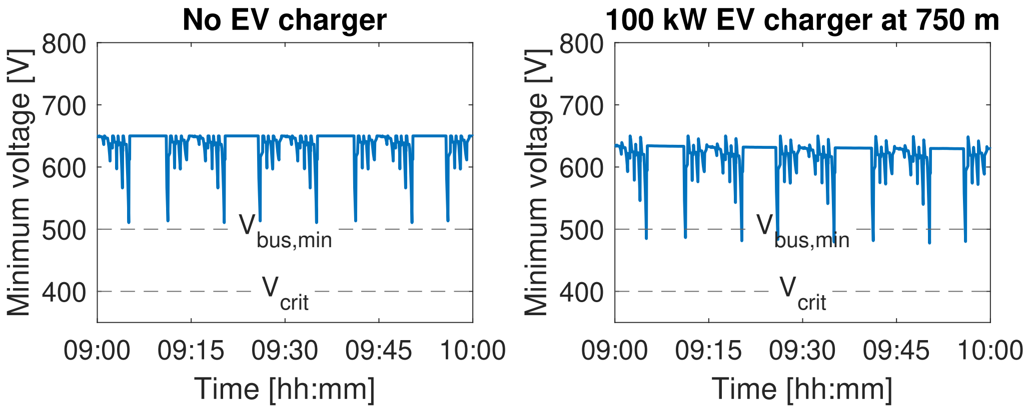

Figure 4.2: Minimum overhead line voltage on section 111 from 9 am till 10 am. In the left graph, no EV charging is integrated. On the right chart, an EV charger of 100 kW is placed at a location of 750 meters.

4.1.3 Maximum current in the overhead wires

The maximum current in the overhead lines for both cases are displayed in Figure 4.3. With the integration of a 100 kW EV charger, the maximum long-term current in the overhead wires of 880 A is not violated. This graph indicates that the EV maximum current in the overhead cables should not be the limiting factor for the integration of EV chargers.

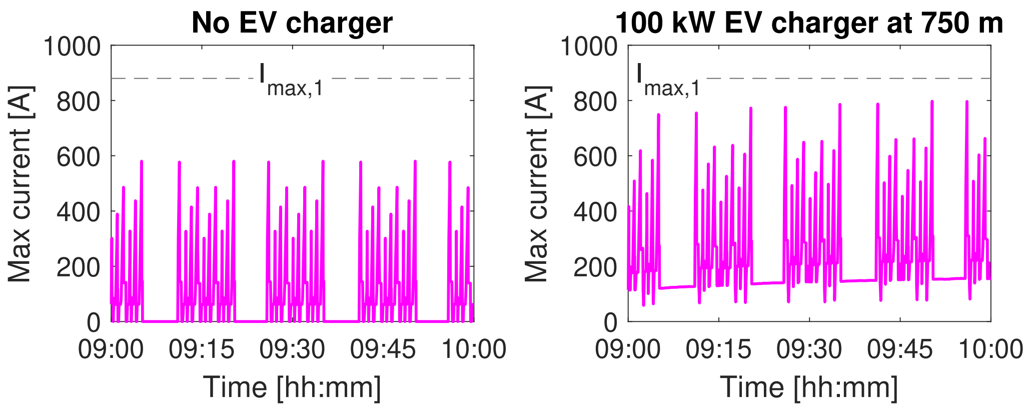

Figure 4.3: The maximum current in the overhead lines from 9 am till 10 am. In the left graph, no EV charging is integrated. On the right graph, an EV charger of 100 kW is placed at a location of 750 meters.

4.2 BASELINE SIMULATION

In the baseline simulation, EV chargers varying from 0 kW to 500 kW with intervals of 25 kW are placed at different locations (150 meters intervals) on section 111. In Figure 4.4, the potential for EV charging is shown. The potential for EV charging depends on the EV charger's location relative to the feed-in point. This is the consequence of the limitations discussed in Chapter 3.1. Close to the feed-in point of the substation (0 meters), the potential for EV charging is 500 kW. When the EV charger is placed further away from the feed-in point, the potential is reduced to a minimum of 100 kW (22 EVs/day).

The colored areas in the graph represent the limiting factors for a particular size of EV charger installed at that location. The minimum voltage on the section is often the limiting factor for the further increase of EV charging. Furthermore, the maximum substation is violated if a large EV charger is placed between 0 and 450 meters. As shown with the pink dashed area in Figure 4.4, the current limitation of the overhead line is never the only violated criteria. In the next Chapter, six smart grid methods will be evaluated to increase the charging potential on the grid further.

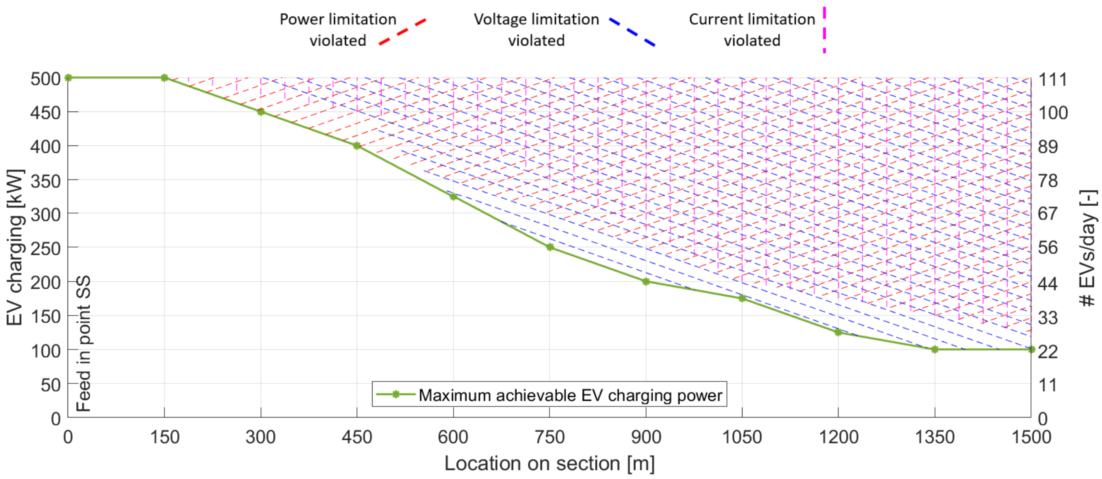

Figure 4.4: Maximum achievable EV charging power on the theoretical section without any smart grid methods implemented. The colored area indicates the limiting factor which reduces the EV charging utilization.

4.3 EFFECT OF SMART GRID METHODS ON THE EV CHARGING POTENTIAL

This Chapter discusses the impact of the six smart grid methods on the EV charging potential on section 111. For the theoretical study, each method will be handled separately. For the case study, a combination of smart grid methods is presented.

4.3.1 Substation level - Changing substations' nominal voltage

Increasing substations' nominal voltage has two main goals; 1. reducing the chance that the minimum voltage on the section drops below V_{crit}, and 2. a reduction in the overhead line current and the associated voltage drop for the same power demand. On top of that, transmission losses are reduced with higher efficiency due to the lower overhead line current. In the simulation, the nominal voltage of the substation varies between 650 V and 730 V with an interval of 10 V.

Figure 4.5 shows the maximum achievable EV charging potential for three different $V_{\text{nom, SS1}}$. Increasing the substations' nominal voltage reduces the chance that the $V_{\text{min,line}}$ is below V_{crit}. Consequently, the EV charging potential at most locations increases.

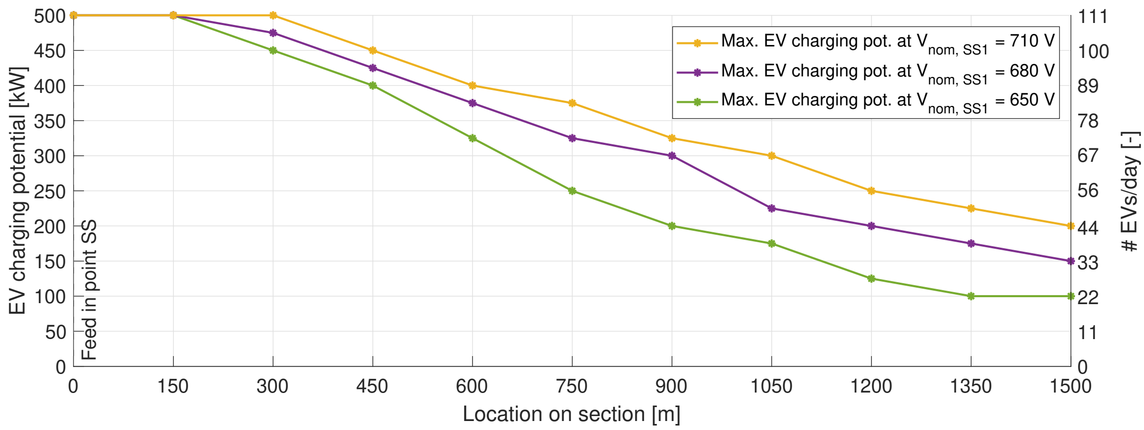

Figure 4.5: Maximum achievable EV charging potential with three various levels of $V_{\text{nom, SS1}}$ on the theoretical section.

Figure 4.6 shows the minimum nominal voltage of the substation to facilitate a specific EV charger size. One can see that if the nominal voltage is higher, the EV charging potential increases. For example, placing a 250 kW EV charger (middle right graph) at 1200 meters requires a substation nominal voltage of 710 V. If the voltage is below this value, the voltage and the current limitations are violated, as shown with the blue and magenta dashed areas. Placing a 300 kW EV charger or higher (bottom two graphs) is not possible at a location further than 1050 meters.

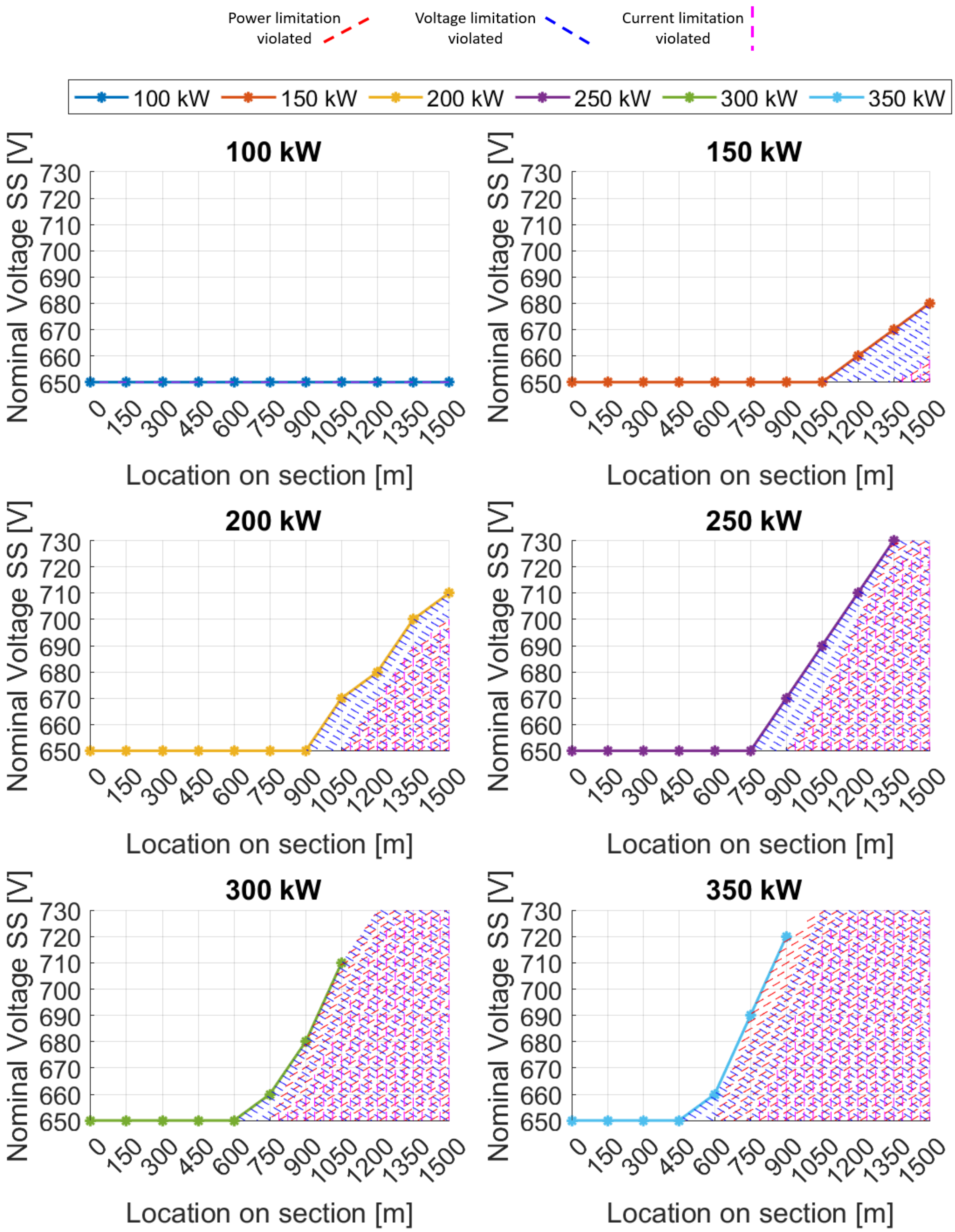

Figure 4.6: The minimum voltage required to facilitate a different sized EV chargers (title subplot). The colored area indicates where the nominal voltage of the substation is too low to enable the size of the EV charger for that specific location.

4.3.2 Substation level - Increasing allowable substation's power tolerance

This part discusses, the effect of increasing the substations power tolerance on the EV charging potential for the theoretical study. As mentioned in Chapter 3.1, the substation power limitation is chosen very conservatively. Therefore, accepting a higher power through the substation could increase the EV charging potential. The substation maximum power tolerance will be varied between 120% and 200% for 10 or 60 seconds. Figure 4.7 shows the EV charging potential with various substation tolerances. For example, the yellow bar scenario accepts a $P_{SS,1}$ between 100% and 150% of the substation power rating for 10 consecutive seconds. The power cannot be above 150% of the rated substation power. As shown in the Figure, only at the location between 300 and 450 meters, there is slight increase in EV charging potential (+25-50 kW). Increasing the substation power rating for the other locations does not influence the EV charging potential.

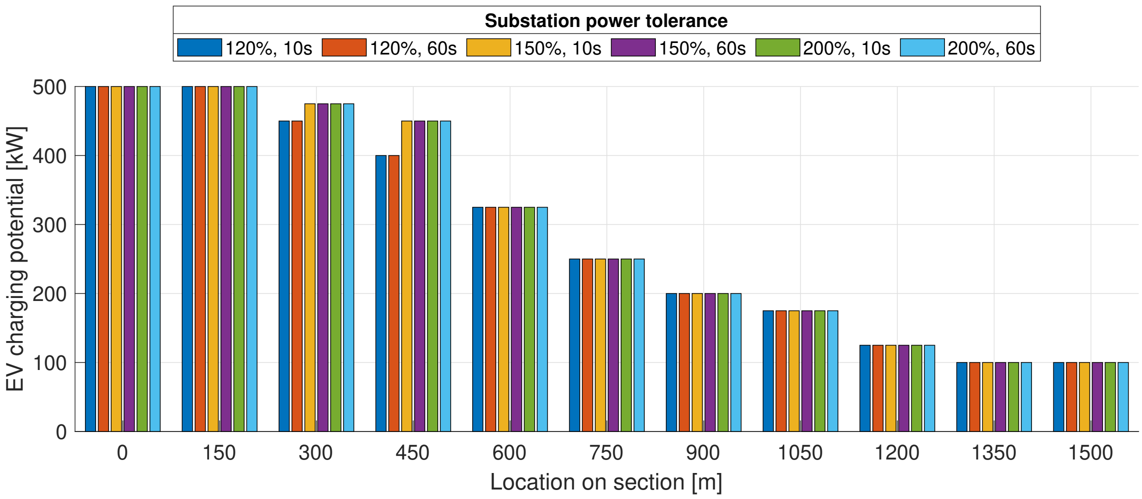

Figure 4.7: Effect of various substation power tolerances on the maximum EV charging potential on section 111 for different locations. The first number gives the threshold value relative to the substation power rating. The second number is the consecutive duration between 100% and the threshold. The substation cannot be above the threshold for all the scenarios.

Increasing the substation power tolerance has little to no effect on the EV charging potential. However, in supply zones where the substation is powering multiple sections (i.e., substation 2 for example (Fig. 3.8)), the substations' power tolerance could be the limiting factor for a further increase of EV charging potential. For this reason, the smart grid method 'increasing the substation power tolerance' will be discussed in the case study.

4.3.3 Grid infrastructure level - Extra parallel line

As shown in the baseline simulation, the voltage is predominately the limiting factor for a higher EV charging utilization on section 111. With an extra parallel line the impedance reduces by 33.3% and therefore reduces the voltage drop in the cables. As a result, the EV charging potential could increase significantly. Furthermore, adding an extra cable increases the maximum continuous current (Table 3.1) to $I_{max,1}$ and $I_{max,2}$ to 1320 A and 1830 A, respectively. An additional parallel line over the whole section is assumed for the simulation.

Figure 4.8 shows the maximum EV charging potential with and without an extra cable. At a location of 900 meters, the EV charging potential increases from 200 kW to 400 kW (+100%). The colored area above the graph shows the limiting factor for the 3 parallel line scenario. In most cases, the substation power rating is the new limiting factor.

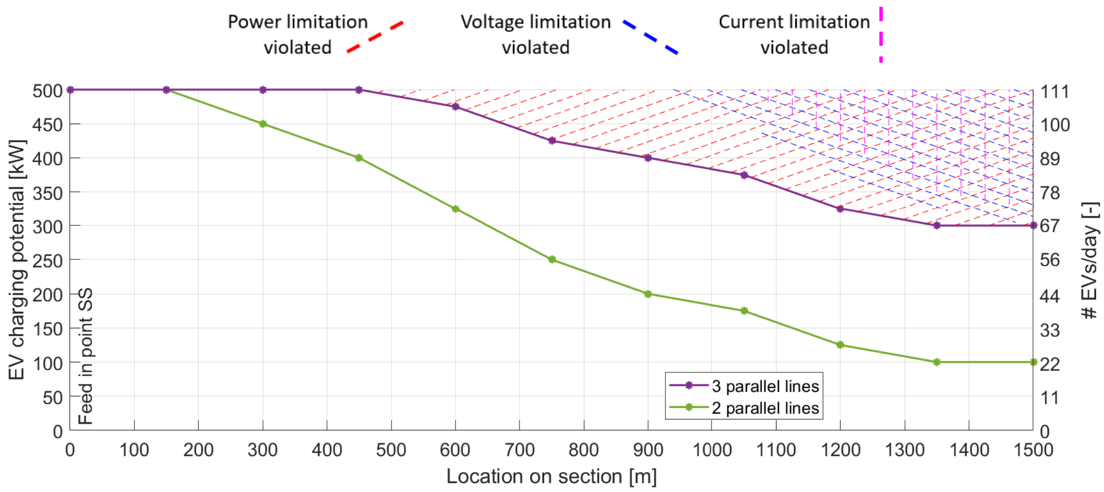

Figure 4.8: Comparison of the maximum achievable EV charging potential on section 111 with the addition of an extra overhead parallel line over the whole section. The colored area indicates the limiting factor for the 3 parallel lines case.

In Table 4.1, a comparison is made for the energy consumption of the substation and the transmission losses for adding an extra parallel line. The transmission losses are reduced up to 37.7%, whereas the substations' energy consumption decreases up to 3.13%, based on the location of the EV charger.

Table 4.1: Comparison of energy consumption substation and transmissions loses with an extra parallel line.

Location [m]	EV charger [kW]	E_{SS} [kWh/day] 2 lines	E_{SS} [kWh/day] 3 lines	$E_{loss,trans}$ [%] 2 lines	$E_{loss,trans}$ [%] 3 lines
0	500	8134	8112 (-0.27%)	0.97	0.70 (-27.8%)
300	450	7779	7623 (-2.01%)	5.65	3.72 (-34.2%)
600	325	6044	5856 (-3.11%)	8.18	5.23 (-36.1%)
900	200	4092	3964 (-3.13%)	8.11	5.12 (-36.9%)
1200	125	2905	2820 (-2.93%)	7.45	4.67 (-37.3%)
1500	100	2521	2447 (-2.94%)	7.46	4.65 (-37.7%)

4.3.4 Grid infrastructure level – Introducing bilateral connection

In the baseline simulation, section 111 and section 112 are isolated, and power transfer between the two sections is impossible. With the introduction of bilateral connection, energy transfer between the sections is possible. Both $V_{\text{nom, SS}}$ are set to 650 V for the bilateral connection analysis. As shown in Figure 3.8, substation 2 is also connected to section 113. This section is included in the power consumption of substation 2.

The maximum EV charging potential for both unilateral and bilateral connections is shown in Figure 4.9. In the bilateral case, the EV charging potential increases in the middle of the two sections, with its peak on the left of the connection point where the traffic on section 111 is less heavy. The colored areas in the graph indicate the limiting factor for the bilateral connection case.

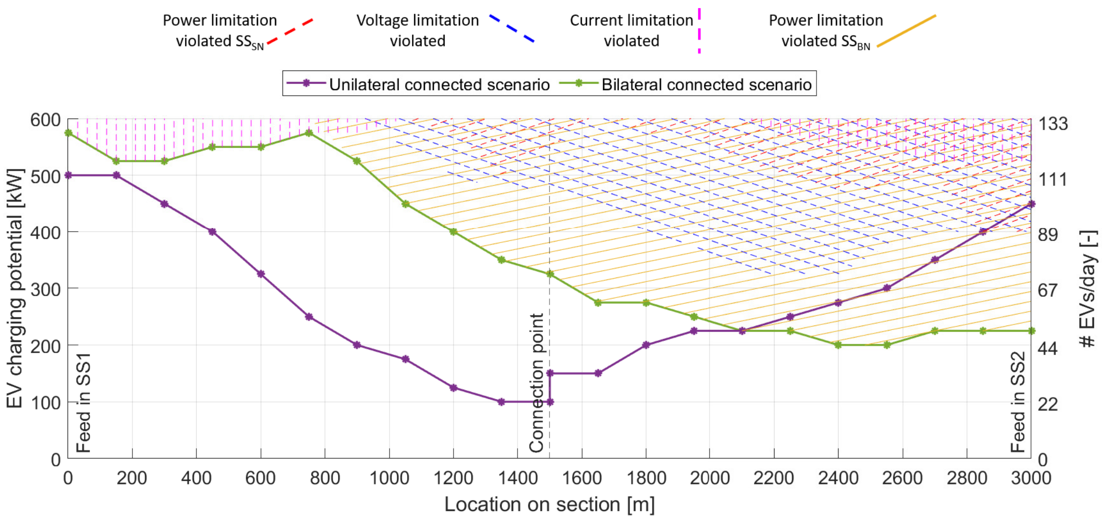

Figure 4.9: Maximum achievable EV charging potential with the introduction of a bilateral connections between sections 111 (0-1500m) and 112 (1500-3000m). Legend: substation connected with the main section (SS_{SN}); substation connected with the bilateral section (SS_{BN})

4.3.5 EV charging level - Introduction of smart charging

This Chapter discusses the increase of charging potential when smart charging for EVs is added. As mentioned in Chapter 3.3.2, the EV charger needs to be able to change the load demand. For the simulation, various maximum changing rates for the EV chargers are considered with intervals of 3 kW/s.

Figures 4.10a and 4.10b display, the different loads on the section when an EV charger is placed at 400 meters with a ramp-up/down speed of 3 kW/s and 9 kW/s respectively. With both converter specifications, the substation power level is below the rated power. As seen in the Figures, the higher ramp-up/down converter can respond faster to various bus loads, with better peak shaving as result.

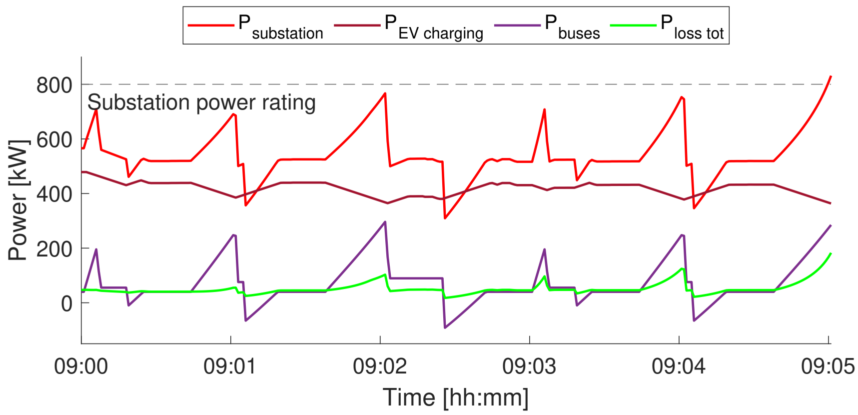

(a) Loads on section 111 with a ramp-up/down speed of 3 kW/s.

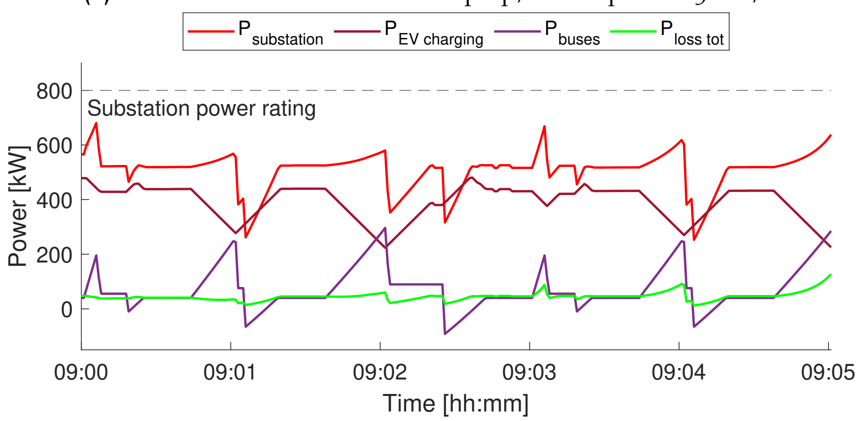

(b) Loads on section 111 with a ramp-up/down speed of 9 kW/s.

Figure 4.10: The substation power is presented here as a positive value for easy comparison.

Figure 4.11 displays the effect of two different ramp-up/down speeds of converters on the grids' minimum voltage and maximum current. For both the ramp-up/down speed converter types, the minimum line voltage (Fig. 4.11a) is below $V_{\text{min, bus}}$ for a short period. Looking at the maximum line current, the peaks for both the EV chargers are above $I_{\text{max},1}$. One can see that the duration of the peaks are limited. As a result, the average current in the last 50 minutes is still within the current limitation.

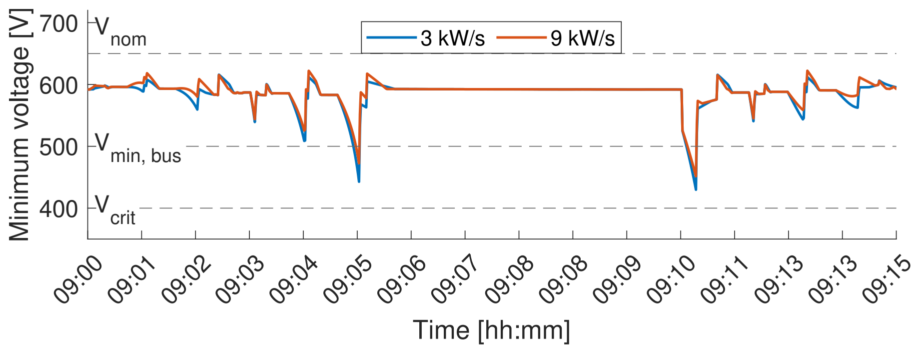

(a) Minimum voltage on the section.

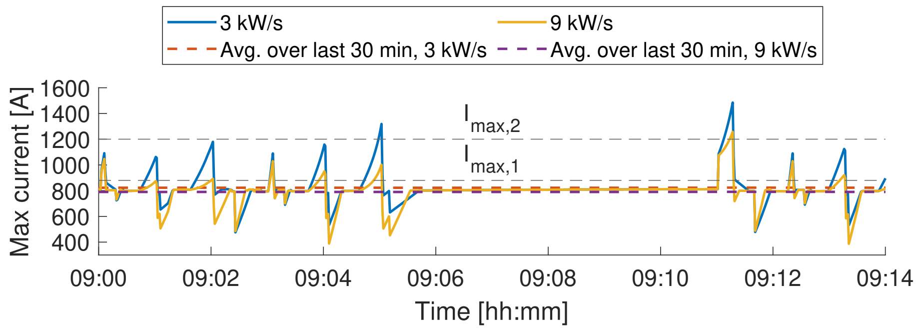

(b) Maximum current on the section.

Figure 4.11: Effect on the grid parameters with two different ramp-up/down speeds of EV chargers.

Figure 4.12 shows the average daily charging power potential with various converter specifications. The ramp-up/down speed of the EV chargers influences the EV charging potential at various locations. A faster EV charger can control the voltage drops in the overhead wires at places where the voltage limiting factor is (500 - 1500 meters). Consequently, the EV charging potential is higher with a higher ramp-up/down speed. Close to the feed-in point of the substation, the average EV charging capacity increases by 200 kW (+74 EVs/day). At the end of the line, with the best ramp-up/down speeds, 74 EVs can be charged daily (+54).

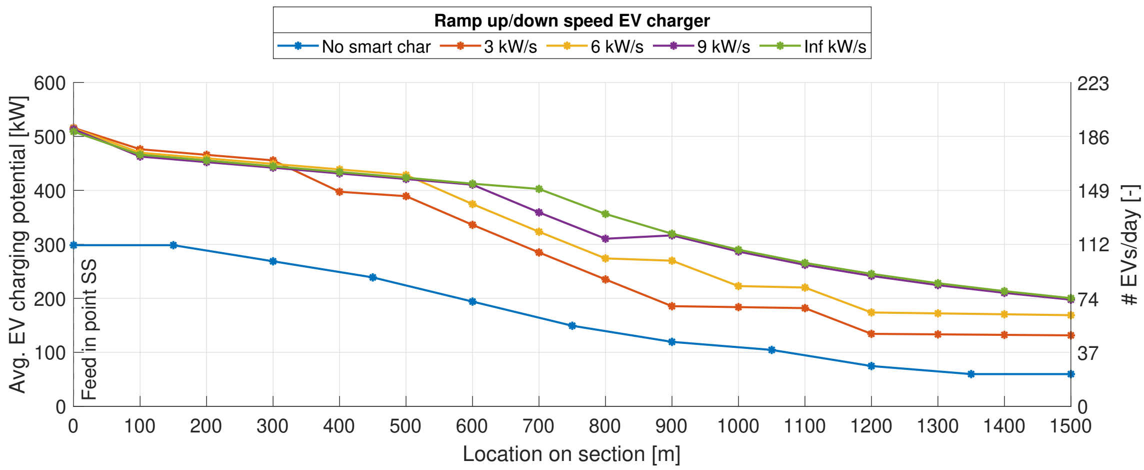

Figure 4.12: Maximum achievable EV charging potential with various converter specifications for the smart charging method.

4.3.6 EV charging level - A multi-port EV charger

As shown in the baseline simulation, the maximum EV charging potential at the end of section 111 is 100 kW. Looking at the EV charging potential of theoretical section 112 at the connection point with section 111 (0 meters), one can see in Figure 4.13 that there is an EV charging potential of 150 kW.

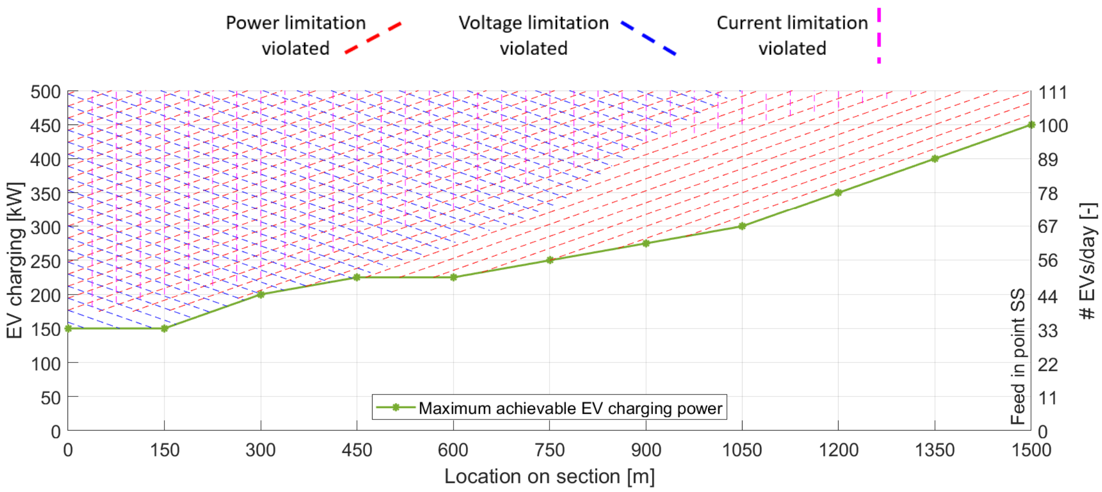

Figure 4.13: Maximum achievable EV charging potential on the theoretical section 112 with a $V_{\text{nom, SS2}}$ of 650 V. The colored area indicates the limiting factor which reduces the EV charging potential.

As a result, there are three suitable options for the EV charger at the connection point between the two sections:

1. A single-port converting EV charger connected to section 111 with a maximum power rating of 100 kW.
2. A single-port converting EV charger connected to section 112 with a maximum power rating of 150 kW.
3. A multi-port converting EV charger connected to section 111 (max. 100 kW) and 112 (max. 150 kW) with a maximum power of 250 kW (56 EVs/day).

Using a multi-port converter can increase the EV charging potential at the intersection point of the two sections. For the case study, an analysis of the energy use of the substation will be done.

4.4 OVERVIEW OF THE SMART GRID METHODS – THEORETICAL STUDY

As shown previously, various methods affect the EV charging potential. The results are summarized in Figure 4.14. As shown in the Figure, introducing smart charging is on of the best method to increase the number of EVs charged daily. The introduction of a bilateral connection improves the EV charging potential, especially around the connection point. Adding an extra parallel line to reduce the resistance in the overhead wires significantly influences the EV charging potential on all locations. The smart grid methods: increasing the substation power tolerance and adding a multi-port converter are not added to this graph as they are not affecting the EV charging potential at many locations on the section. Table 4.2 summarizes the numerical results for all the smart grid methods. One EV charger can be added to each section in the unilateral scenarios, resulting in two EV chargers on sections 111 and 112. In the bilateral connection and the multi-port converter, only one EV charger is added to sections 111 and 112.

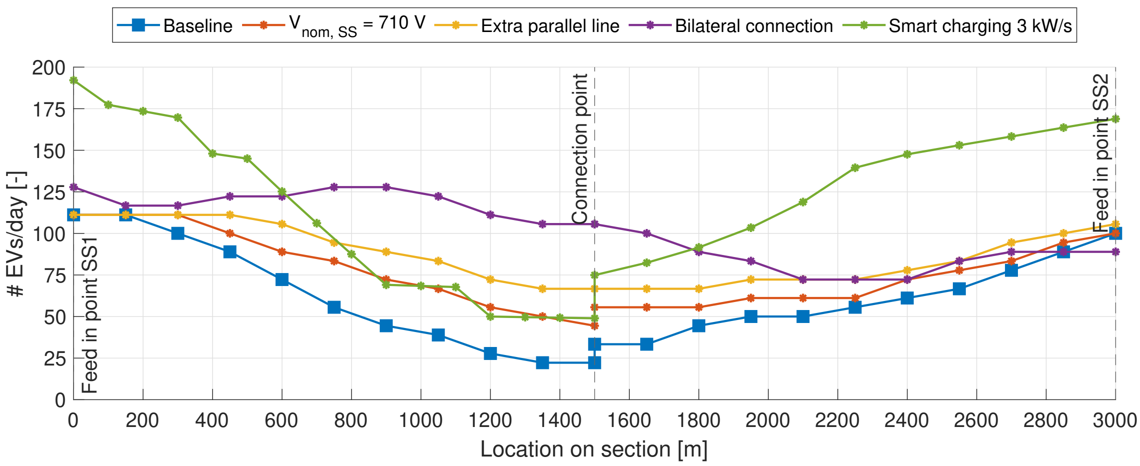

Figure 4.14: Summary of various smart grid methods on the maximum achievable EV charging potential on the theoretical sections 111 and 112. Smart grid methods: increasing substation power and the multi-port converter are excluded from this graph.

Table 4.2: Supply zone T: effect of smart grid methods on the maximum achievable EV charging potential in the theoretical study. *Achievable with one charging facility. **Achievable with one charging facility at the connection point of the sections.

Smart grid method	Section 111 [# of EV/day]		Section 112 [# of EV/day]		Sec. 111+112 [# of EV/day]
	Max.	Mean.	Max.	Mean.	Max.
0.1 Baseline	111	63	100	60	211
1.1 Increasing voltage	111 (0)	81 (+18)	100 (0)	71 (+11)	211 (0)
1.2 Substation power	111 (0)	65 (+2)	111 (+11)	74 (+14)	222 (+11)
2.1 Extra overhead line	111 (0)	93 (+30)	106 (+6)	80 (+20)	217 (+6)
2.2 Bilateral connection	128* (+17)	119* (+56)	106* (+6)	86* (+26)	128* (-83)
3.1 Smart charging	182 (+71)	110 (+47)	167 (+67)	126 (+66)	349 (+138)
3.2 Multi-port converter	22 (-89)	0	33 (-67)	0	56** (-155)

As discussed in this Chapter, the six smart grid methods affect the ability to charge EVs via a trolleygrid in various ways. The next Chapter describes the case study on the trolleygrid of Arnhem. The case study will also give a more in-depth analysis of the transmission losses and the energy consumption of the substations.

5 CASE STUDY

This Chapter evaluates the integration of EV chargers into two different supply zones in the trolleygrid of Arnhem (Fig. 3.13). With the use of the computational model described in Chapter 3.2, the number of EVs that can charge daily is determined on various days with different smart grid methods. The first section assesses the effect of adding EV chargers on the trolleygrid. This will be followed by determining the EV charging potential in each supply zone. Next, the six smart grid methods are discussed individually. Section 5.4 gives an overview of all the smart grid methods. Lastly, the effect of EV chargers on the PV utilization is discussed.

5.1 EFFECT OF ADDING EV CHARGERS - CASE STUDY

The section discusses the effect of the integration of EV chargers on the substations' power, minimum voltage, and maximum current in the trolleygrid of Arnhem. In the baseline simulation, no smart grid methods was implemented, and a regular weekday in winter (day 268) will be used as a reference.

5.1.1 Substation power

Figure 5.1 shows how adding EV chargers to the traction grid affects the substations' power output. As discussed previously, the bus intensity on section 25 is higher than in section 23. However, substation 12 is powering both sections 23 and 24. Therefore, the power output of substation 12 (Fig. 5.1a) is comparable with substation 9 (Fig. 5.1b). With the integration of a 75 kW EV charger at 500 meters on both sections, the power delivered by the substation increases. This increase in power is mainly due to the additional load on the section. On top of that, the extra transmission losses due to the higher current play a role. But also, due to the higher current in the overhead wires, the voltage drop is higher, resulting in a higher current with extra transmission losses. As shown, the substations' power is on both supply zones in the case with EV chargers still below the rated capacity of 800 kW.

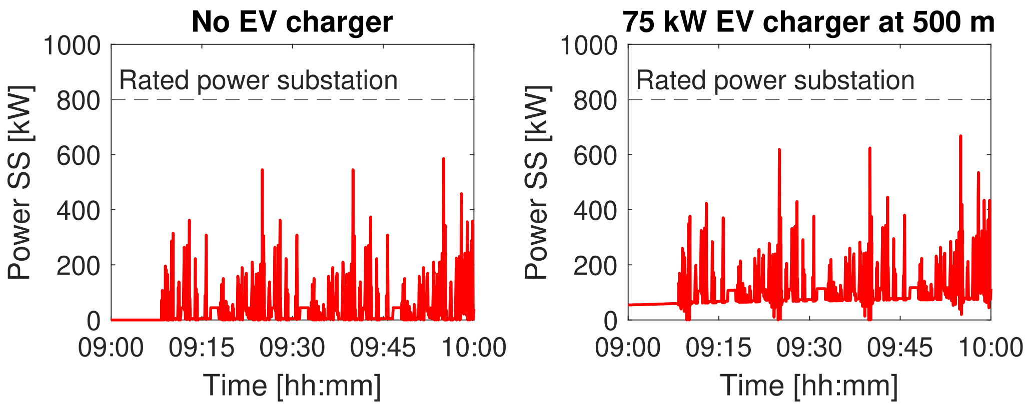

(a) Supply zone A, substation 12. A 75 kW EV charger is placed at 500 meters on section 23. The substations' power limitation is not violated during this period in both cases.

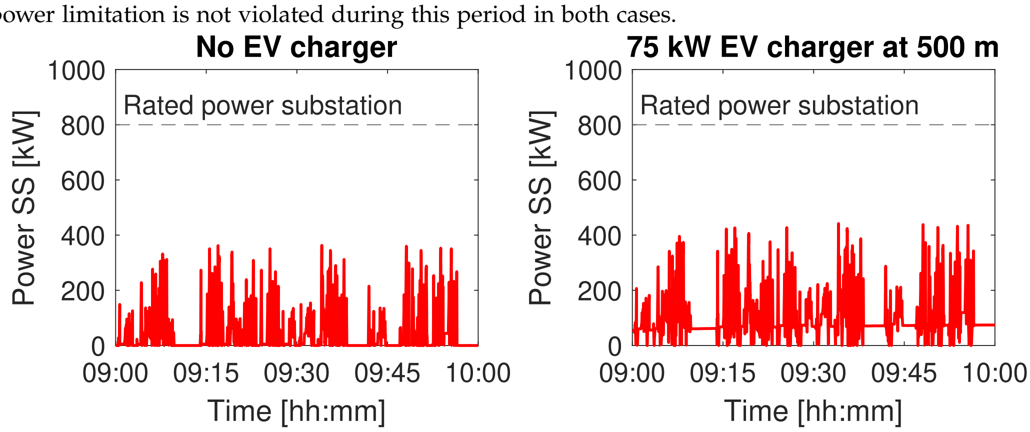

(b) Supply zone B, substation 14. A 75 kW EV charger is placed at 500 meters on section 25. The substations' power limitation is not violated during this period in both cases.

Figure 5.1: Power delivered by substation 12 in supply zone A (Fig. 5.1a) and substation 9 in supply zone B (Fig. 5.1b) from 9 am to 10 am.

5.1.2 Minimum voltage in the overhead wires

Figure 5.2a & 5.2b shows the effect of integrating EV chargers on the case study supply zones. As shown in the Figures, the voltage drops when a bus is on the section and recovers back to $V_{\text{nom, SS12}}$ when it leaves. With the addition of a 75 kW EV charger, the minimum voltage shifts slightly down (right graphs). The shift is due to the higher current and associated voltage drop. With the integration of the EV chargers, the minimum voltage is still above $V_{\text{bus,min}}$ (500 V) for both sections.

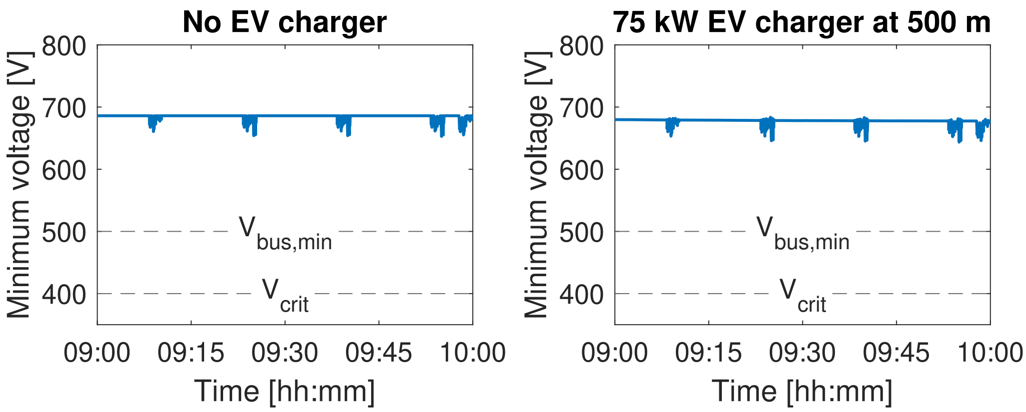

(a) Supply zone A. Minimum voltage on section 23 where a 75 kW EV charger is placed at 500 meters. The voltage limitation is not violated during this period.

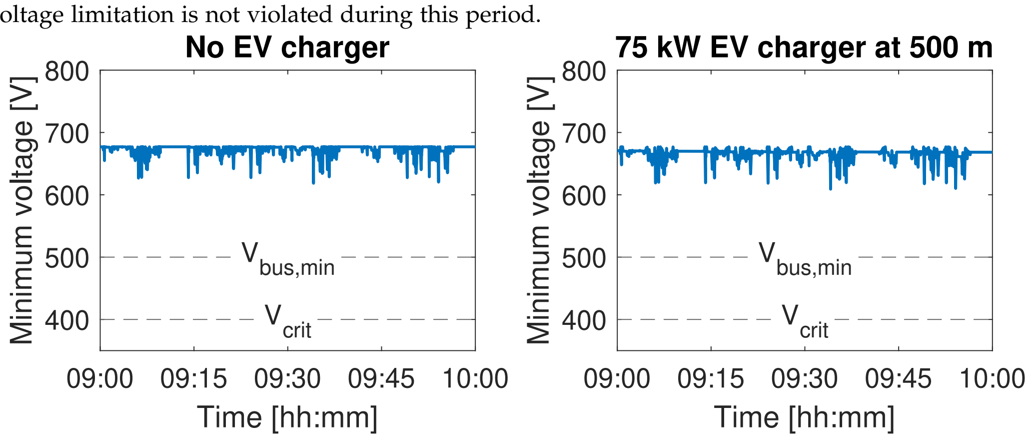

(b) Supply zone B. Minimum voltage on section 25 where a 75 kW EV charger is placed at 500 meters. The voltage limitation is not violated during this period.

Figure 5.2: The minimum voltage on the section where the EV charger is placed from 9 am to 10 am.

5.1.3 The maximum current in the overhead wires

The effect of adding EV chargers on the maximum current in the overhead lines is shown in Figure 5.3. In the left graph of Figure 5.3a, the maximum current is violated ones when there is no EV charger added. As mentioned before, the current increases due to the additional load and the lower voltage at the node. With the EV charger, the maximum current is above $I_{max,1}$ for a few seconds during this hour. However, the duration of the violation is only three consecutive seconds. Interestingly, on the busier section 25 (Fig 5.3b), the maximum current is not violated with and without the addition of the 75 kW EV during this time interval.

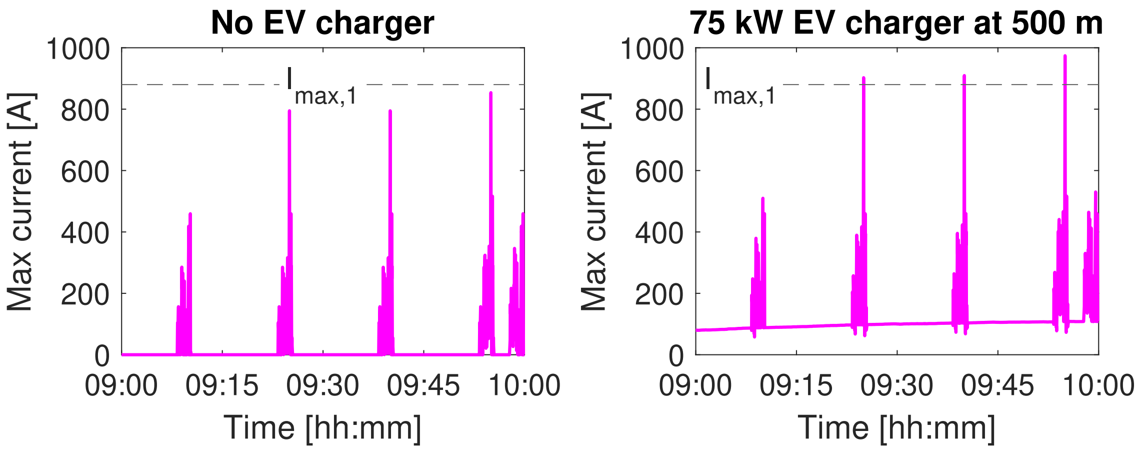

(a) Supply zone A. Maximum current in the overhead wires on section 23 with a 75 kW EV charger located at 500 m. During this hour, the current limitation in violated.

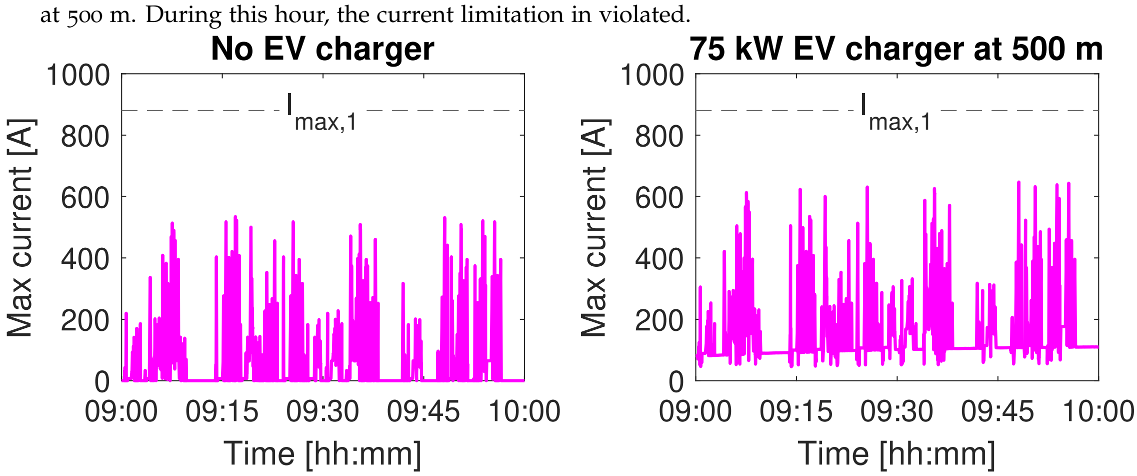

(b) Supply zone B. Maximum current in the overhead wires on section 25 with a 75 kW EV charger located at 500 m. The maximum current limit is not violated.

Figure 5.3: The maximum current in the overhead wires on the section where the EV charger is placed from 9 am till 10 am.

5.2 EV CHARGING POTENTIAL

This part will look into the potential of EV charging on the trolleygrid in the two supply zones mentioned in Chapter 3.7. For the baseline simulation, various size EV chargers with intervals of 25 kW are added at different locations on the section.

5.2.1 Supply zone A

Figure 5.5, shows the potential for EV charging on section 23 for various days. For all days, the maximum substation power is the limiting factor to further increasing the EV charger size. In section 23, the overhead wires' maximum current or minimum voltage never reduces the EV charging potential. On all days, the highest EV charging potential is close to the substation's feed-in point (80 meters). Due to the additional transmission losses (RI^2), the EV charging potential decreases when the EVs are placed further away from the feed-in point. With an EV charging potential between 250 kW and 300 kW, day 268 has the least EV charging potential. This could be explained by the high power demand of the buses in the winter season and the regular weekday bus scheduling. The size of the EV charger is limited by day 268 and, therefore will be used as a reference to analyze the effect of smart grid technologies on the EV charging potential.

Furthermore, Table 5.1 summarizes the substations' energy use and trolleygrid flow with a 100 kW EV charger placed at different locations on the trolleygrid. In the worst case, the transmission losses rise from 6 kWh/day to 40 kWh/day (+566%). Consequently, the substation uses up to 34 kWh/day more energy. In Figure 5.4 the energy flow and magnitude are visually represented for a 100 kW EV charger at 800 meters.

Table 5.1: Section 23: comparison of energy use and flow in the trolleygrid with a 100 kW EV charger at different locations on the section on day 268.

Location [m]	E_{SS} [kWh/day]	$E_{traction}$ [kWh/day]	$E_{EV,bat}$ [kWh/day]	$E_{loss,trans}$ [kWh/day]	$E_{loss,brak}$ [kWh/day]	$E_{loss,charg}$ [kWh/day]
80 (Feed-in)	1621	177	1334	6	4	99
200	1627 (+6)	177	1334	12 (+93%)	4 (0%)	99
400	1636 (+15)	177	1334	21 (+245%)	4 (0%)	99
600	1645 (+24)	177	1334	30 (+392%)	4 (-1%)	99
800	1653 (+32)	177	1334	38 (+532%)	4 (-1%)	99
850 (EOL)	1655 (+34)	177	1334	40 (+566%)	4 (-2%)	99

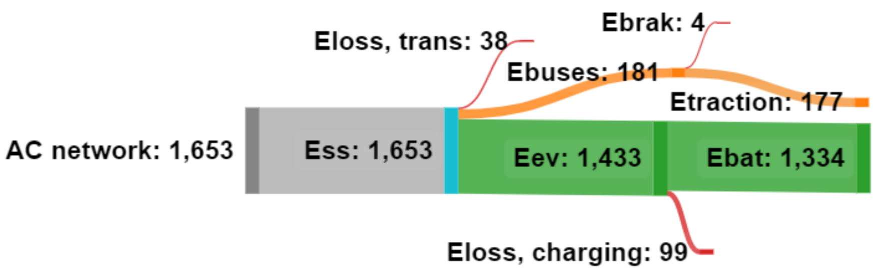

Figure 5.4: Section 23, energy flow in the trolleygrid with a 100 kW EV charger at 800 meters on day 268.

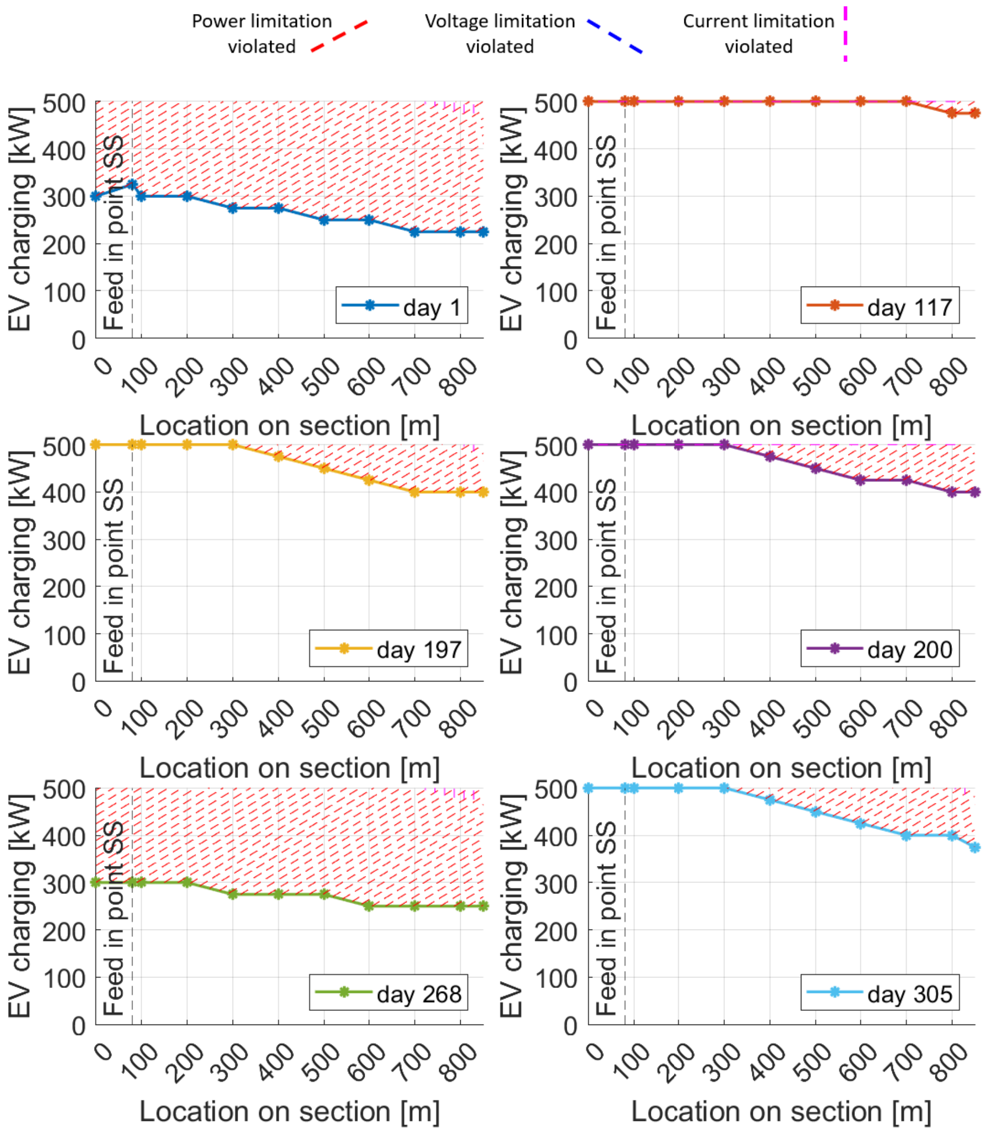

Figure 5.5: Supply zone A, section 23. EV charging potential in the baseline simulation for six different days. The colored area indicated the limiting factor for further increasing the EV charging potential.

5.2.2 Supply zone B

Figure 5.7, shows the potential for EV charging on section 25. On this section the substation power is also the limiting factor to further increase the EV charging potential on all days. Only with high EV charging powers (>450 kW) and at a location of 600 meters or more, the maximum current in the overhead lines plays a limiting factor. The minimum voltage in the overhead lines is not a limiting factor on this section. As shown in the Figure, day 268 also has the least potential for EV charging. On day 268, the EV charging potential close to the feed-in point of the substation is around 400 kW, whereas at the end of the line the potential is 325 kW. The difference in EV charging potential can be explained by the additional required substation power to overcome the transmission losses (RI^2).

Table 5.2 shows the substations' energy consumption for the trolleybuses and a 100 kW EV charger in section 25. One can see that the transmission losses are significantly higher (+240%) when the EV charger is placed further away from the feed-in point. The extra power required from the substation to compensate for the transmission losses reduces the EV charging potential further away. Figure 5.6 visualizes the energy flow in the trolleygrid for a 100 kW EV charger at 800 meters. The energy demand of the trolleybuses is the main difference between the two supply zones.

Table 5.2: Section 25: comparison of energy use and flow in the trolleygrid with a 100 kW EV charger at different locations on the section on day 268.

Location [m]	E_{SS} [kWh/day]	$E_{traction}$ [kWh/day]	$E_{EV,bat}$ [kWh/day]	$E_{loss,trans}$ [kWh/day]	$E_{loss,brak}$ [kWh/day]	$E_{loss,charg}$ [kWh/day]
100 (Feed-in)	1818	331	1334	16	37	99
200	1823 (+5)	331	1334	21 (+34%)	38 (0%)	99
400	1833 (+15)	331	1334	32 (+100%)	38 (0%)	99
600	1844 (+26)	331	1334	42 (+165%)	37 (0%)	99
800	1852 (+34)	331	1334	51 (+224%)	37 (-1%)	99
860 (EOL)	1855 (+37)	331	1334	54 (+240%)	37 (-1%)	99

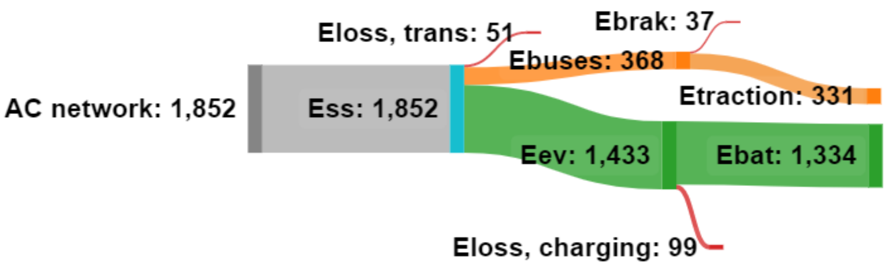

Figure 5.6: Section 25, energy flow in the trolleygrid with a 100 kW EV charger at 800 meters on day 268.

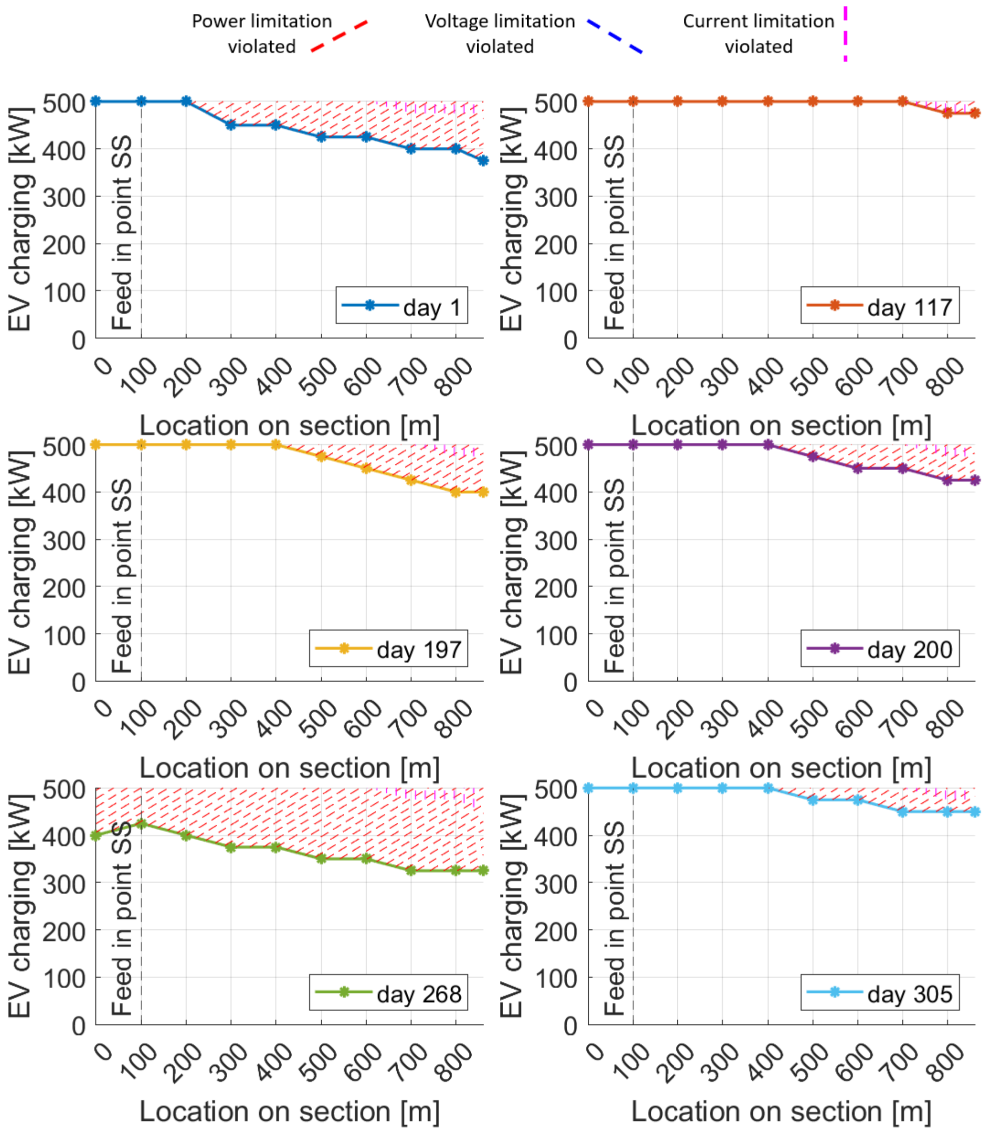

Figure 5.7: Supply zone B, section 25. Maximum achievable EV charging potential in the baseline simulation for six different days. The colored area indicated the limiting factor for further increasing the EV charging potential.

5.3 EFFECT OF SMART GRID METHODS ON EV CHARGING POTENTIAL

5.3.1 Substation level - Changing substations' nominal voltage

This section discusses the impact of varying the substations' nominal voltage ($V_{\text{nom, SS}}$) on the EV charging potential of the traction grid. The two supply zones and six days will be analyzed in the case study described in Chapter 3.7.

Supply zone A

For this study, multiple scenarios are simulated and evaluated. The size of the EV chargers varies from 250 kW to 500 kW and are placed at various locations on section 23 with intervals of 100 m. The substations' nominal voltage can vary between 650 V and 730 V with intervals of 10 V. The actual nominal voltage of substation 12 is set to 686 V and acts as a reference voltage to analyze the effect of the smart grid method.

Figure 5.8 displays the effect of various $V_{\text{nom, SS12}}$ on the EV charging potential on section 23. On average, the EV charging potential increases by 2 EVs/day with a substation nominal voltage increase from 686 V to 710 V. Increasing the substation voltage does not have the same effect as found in the theoretical study. The difference could be explained by the substation power being the limiting factor on this section instead of the minimum line voltage.

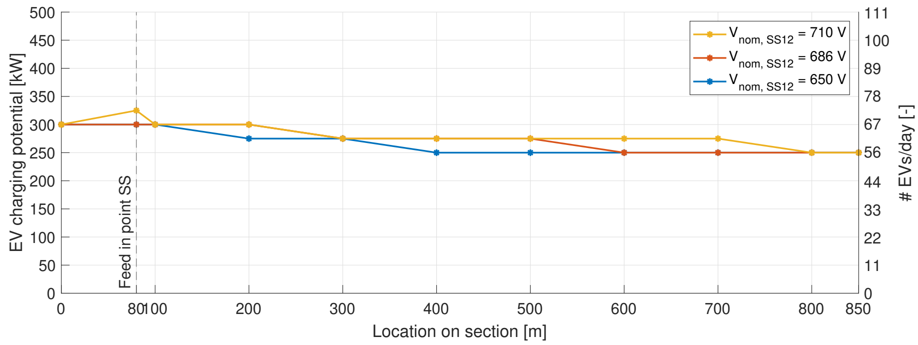

Figure 5.8: Section 23: Maximum achievable EV charging potential for various $V_{\text{nom, SS}}$ on, day 268. The EV charging potential increases when $V_{\text{nom, SS}}$ is higher.

Figure 5.9 shows the minimum voltage required to facilitate a specific size EV charger on day 268. With the colored areas, the limiting factors for the various-sized EV chargers are shown. As mentioned before, the substations' power limits the EV charging potential.

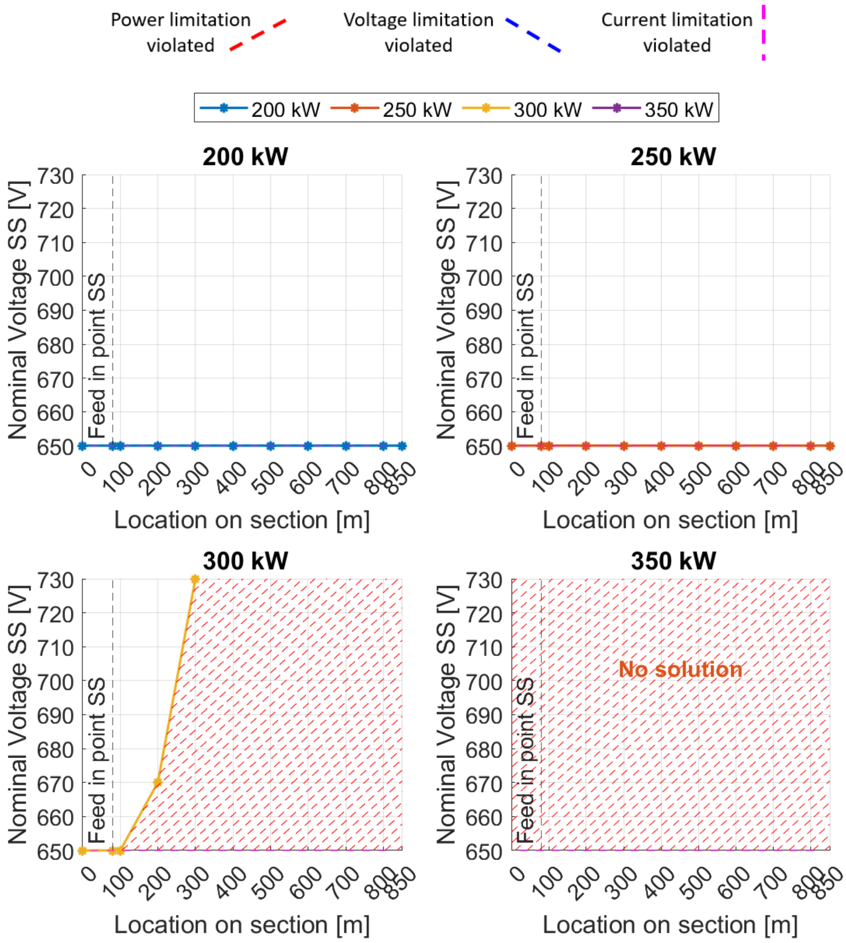

Figure 5.9: Section 23, the effect of varying substations nominal voltage on the EV charging potential on day 268. The colored area indicates the limiting factor for EV chargers' various sizes (title subplot). The minimum voltage and the maximum current are not violated with the addition of EVs up to 350 kW.

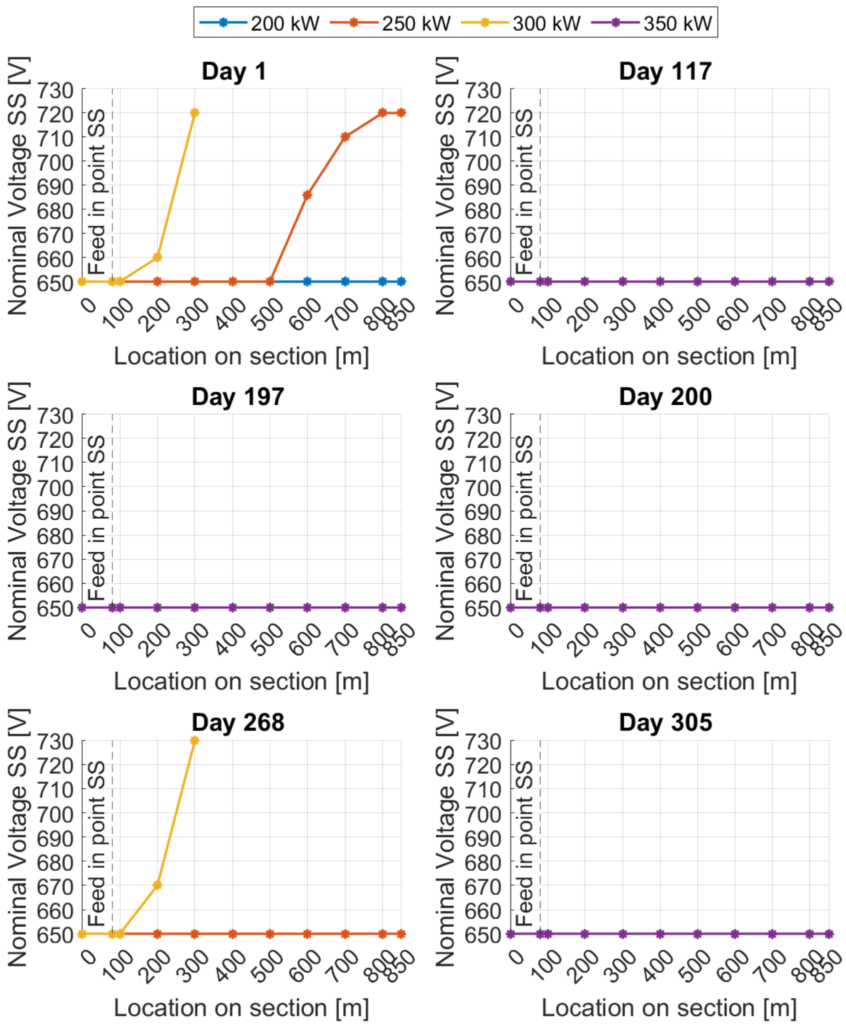

Figure 5.10: Effect of varying substations nominal voltage on the maximum achievable EV charging potential on section 23, for various days.

As previously shown (Chap. 5.2), bus scheduling influences the EV charging potential. Figure 5.10 shows the effect of varying the substations' nominal voltage on different days. On relatively quiet days (days 1, 197, 200, and 305), the minimum required nominal voltage is 650 for EV chargers up to 350 kW. The regular weekday in winter (day 268) and summer holiday requires the highest $V_{\mathrm{nom,\,SS12}}$, with the least charging potential possible.

Energy consumption with various $V_{nom, SS}$

This section analyzes the energy consumption of the substation with various $V_{\text{nom, SS12}}$. As mentioned earlier, the efficiency of the trolleygrid system could increase due to a reduction of transmission losses in the overhead wires. However, as mentioned in Chapter 1.1.1, the bus activates the braking resistor at 720 V. Consequently, with a higher nominal voltage of the substation, the braking resistor can be activated more frequently. Therefore, the increase of $V_{\text{nom, SS12}}$ could increase the power sent to the braking resistor and reduce the overall efficiency of the trolleygrid system.

In Figure 5.11, the maximum voltage at each second on the section is shown for various $V_{\text{nom, SS12}}$ on day 268. One can see that the results for $V_{\text{nom, SS12}}$ of 720 V, and 730 V are above V_{braking} and therefore invalid (Chapter 1.1.1). Consequently, only the results with a substation nominal voltage of 650 V to 710 V are analyzed for the energy consumption of the substation.

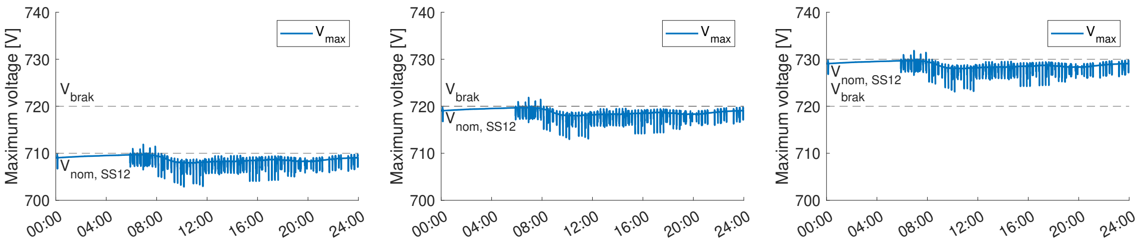

(a) $V_{\text{nom, SS12}} = 710$ V **(b)** $V_{\text{nom, SS12}} = 720$ V **(c)** $V_{\text{nom, SS12}} = 730$ V

Figure 5.11: Maximum voltage on section 23, day 268. If the maximum voltage during the whole day is below 720 V, equation 3.1, is valid. That is not the case with a $V_{\text{nom, SS12}}$ of 720 V (Figure 5.11b) and 730 V (Figure 5.11c).

In Figure 5.12, the effect of the energy consumption of the substation relative to the default nominal substation voltage (686 V) is shown. A 200 kW EV charger is placed at four locations on the section. Placing the EV charger close to the feed-in point (80 m) has little to no effect on the energy consumption of the substation. However, when the EV charger is placed further away from the feed-in point, increasing the voltage can save up to 0.31% (11 kWh/day) of the substations' energy use on day 268. The energy savings from the transmission losses are higher than the increase of energy sent to the braking resistor. Increasing the voltage with a base load in the supply zone can increase the total efficiency.

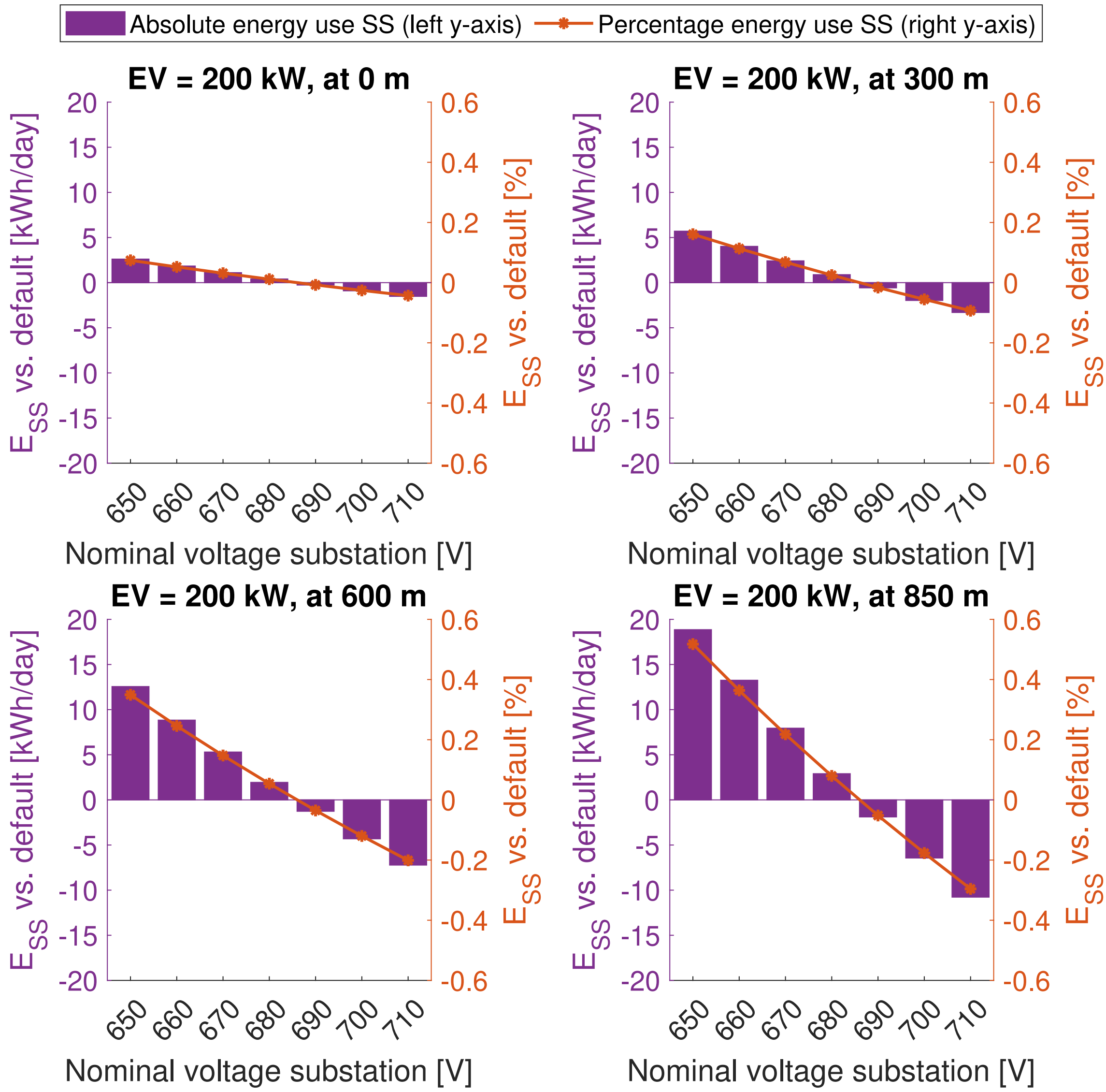

Figure 5.12: The energy use of the substation for various size EV chargers at different locations on the section compared to the default voltage. The left axis shows the absolute energy use, whereas the right axis shows the percentage of energy savings. Only the scenarios where the maximum voltage on the section stays below 720 V are used.

Supply zone B

The existing substations' nominal voltage on substation 9 in supply zone B is set to 677 V and acts as a reference voltage to analyze the effect of the smart grid method. Figure 5.13, shows the impact of various $V_{\text{nom, SS9}}$ on the EV charging potential on section 25. Increasing the substation voltage from 677 V to 710 V increases EV charging potential by 25 kW (+6 EVs/day) in some locations. The increase is slight because the minimum voltage in the overhead line is not the limiting factor on this section. Therefore, only the energy savings due to the higher voltage reduces the power required from the substation with a limited result.

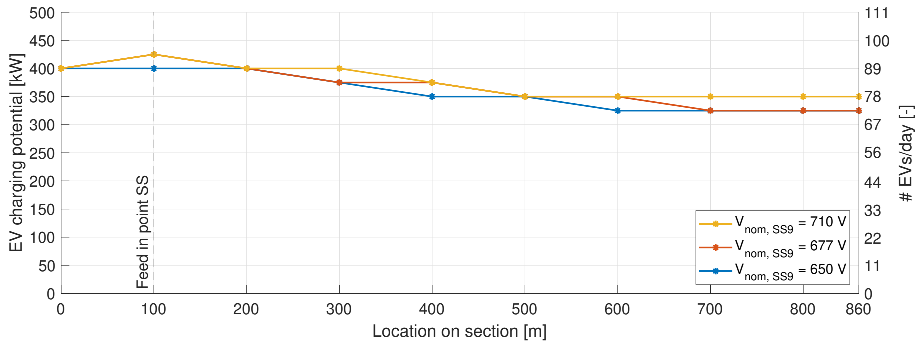

Figure 5.13: Section 25: maximum achievable EV charging potential for various $V_{\text{nom, SS9}}$ on, day 268. The EVs charging potential increases when $V_{\text{nom, SS9}}$ is higher.

Figure 5.14 shows the limiting factor for the various EV chargers on day 268. The Figures tells that for EV chargers above 350 kW, the substation power is a limiting factor. A 350 kW EV charger can be placed more than 500 meters from the feed-in point by increasing the voltage. Placing an EV charger of 450 kW is impossible on this section due to the power limitations of the substation. The minimum line voltage is not the limiting factor even when $V_{\text{nom, SS9}}$ is set to 650 V for any EV charger. The results are in line with the results found for section 23, but not found in the theoretical study. The difference is mainly due to the shorter section length and higher reference voltage.

Bus scheduling also influences the EV charging potential of section 25. Figure 5.15, shows the effect of varying the substations' nominal voltage on various days. On a quiet day (day 117), $V_{\text{nom, SS9}}$ can be set to 650 V to facilitate an EV charger of 450 kW at every location. Similar to section 23, the regular weekday in winter (day 268) and the high traffic and power demand in the summer required the highest $V_{\text{nom, SS9}}$, with the least charging potential possible.

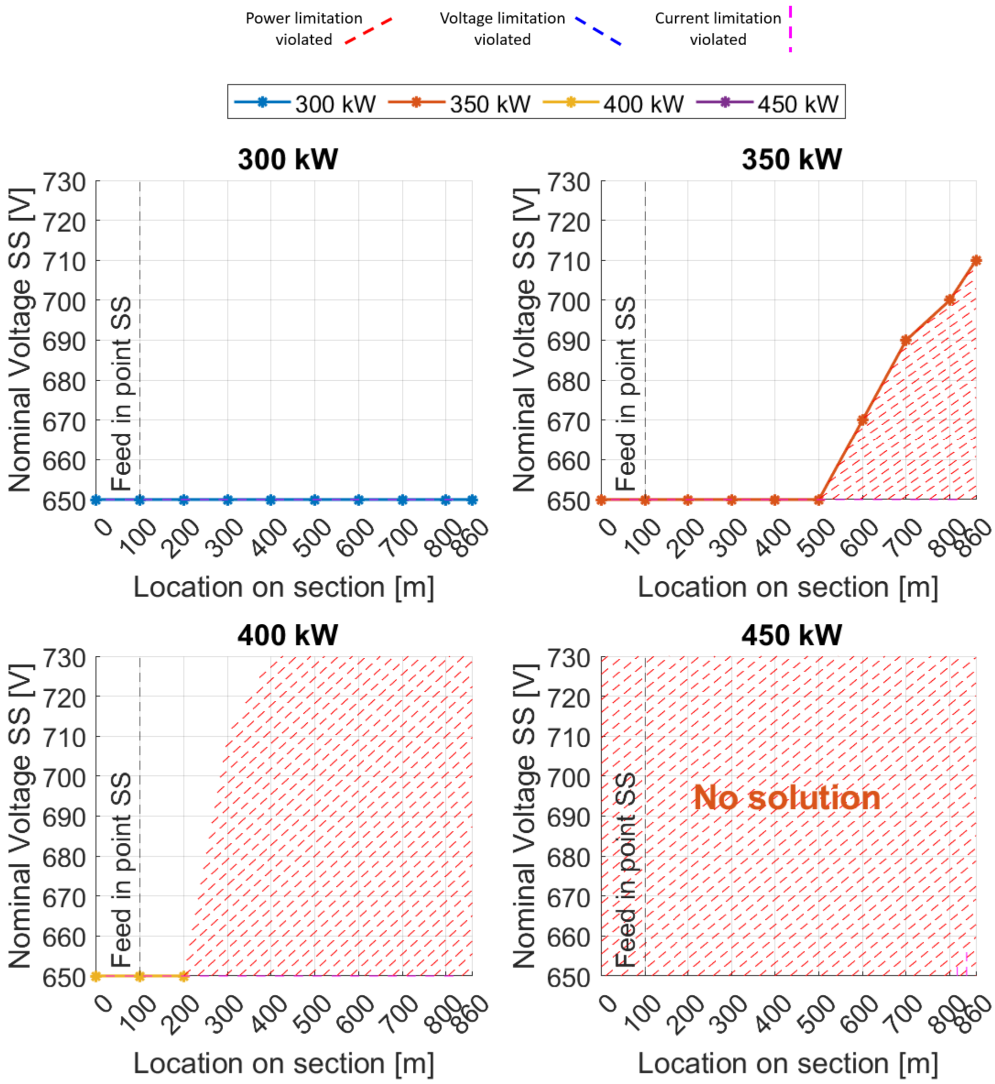

Figure 5.14: Section 25, the effect of varying substations nominal voltage on the maximum achievable EV charging potential on day 268. The colored area indicates the limiting factor for EV chargers' various sizes (title subplot). The power and voltage limitations are not violated with the addition of different-sized EV chargers.

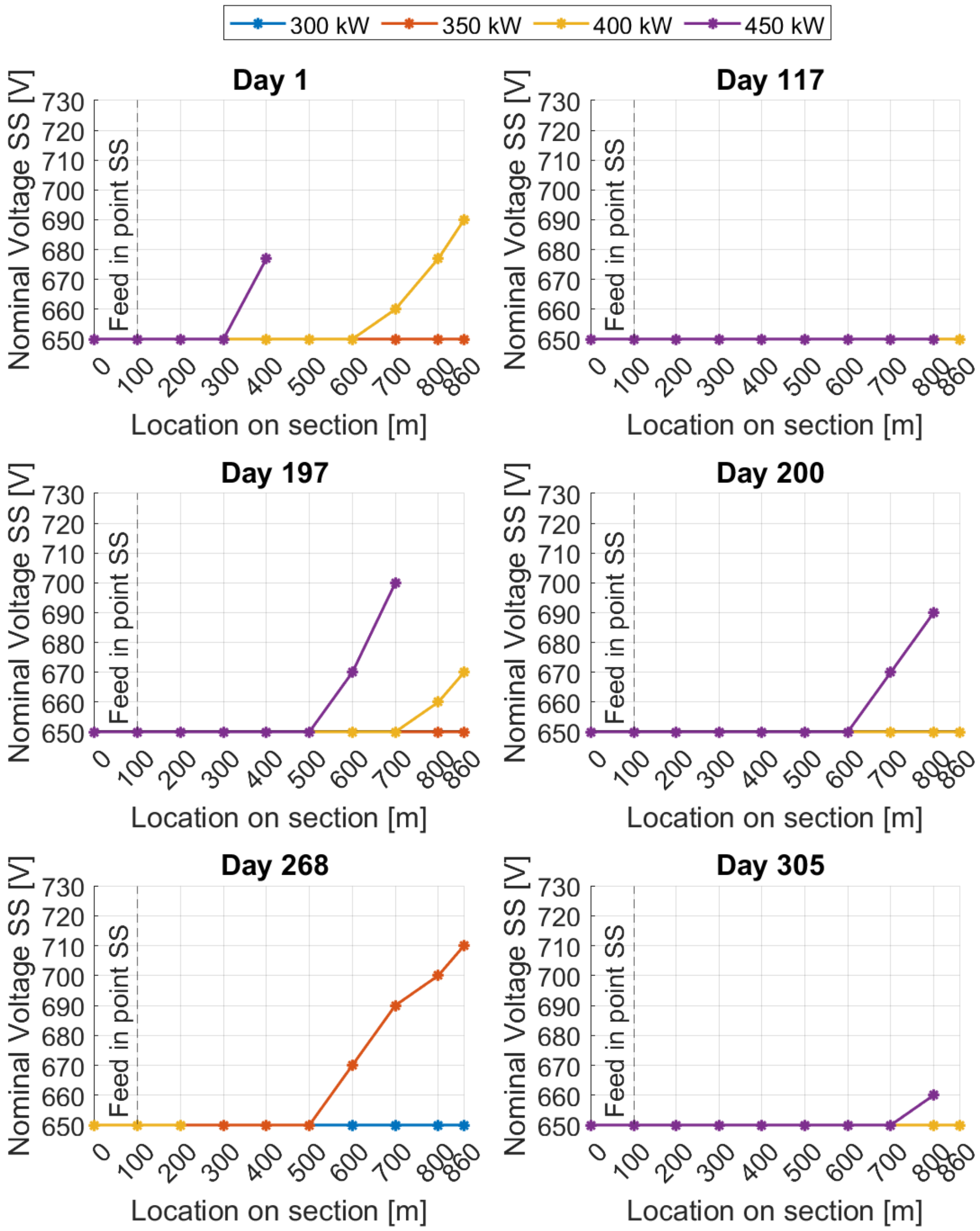

Figure 5.15: Effect of varying substations nominal voltage on the maximum achievable EV charging potential on section 25, for various days.

Energy consumption with various $V_{nom,\ SS}$

The effect of energy consumption with various $V_{\text{nom, SS9}}$ is analyzed for day 268. As mentioned earlier, the efficiency of the trolleygrid system could increase due to a reduction of transmission losses in the overhead lines.

In Figure 5.16, the maximum voltage at each second on the section is shown for various $V_{\text{nom, SS9}}$. The results for $V_{\text{nom, SS9}}$ of 720 V and 730 V are above V_{braking} and therefore threatened as invalid (see Chapter 1.1.1). Hence, only the results with a substation nominal voltage of 650 V to 710 V are analyzed for the energy consumption of the substation.

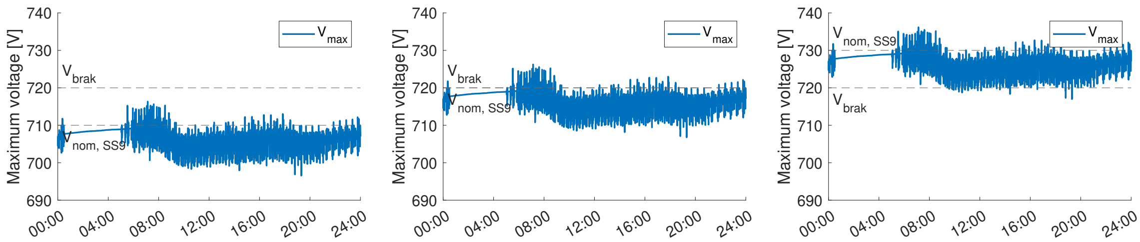

(a) $V_{\text{nom, SS9}} = 710$ V **(b)** $V_{\text{nom, SS9}} = 720$ V **(c)** $V_{\text{nom, SS9}} = 730$ V

Figure 5.16: Maximum voltage on section 25, day 268 with an EV charger of 350 kW at 500 meters. If the maximum voltage during the whole day is below 720 V, equation 3.1, is valid. That is not the case with a $V_{\text{nom, SS9}}$ of 720 V (Fig. 5.16b) & 730 V (Fig. 5.16c).

Figure 5.17 shows the effect of energy consumption of the substation relative to the default nominal substation voltage (677 V). A 350 kW EV charger is placed at four different locations on the section. As shown in the Figure, placing an EV charger close to the feed-in point (100 m) has little to no effect on the energy consumption of the substation. However, when the EV charger is placed further away from the feed-in point, increasing the voltage can save up to 0.98% (58 kWh/day $\approx$ 1 EV) of the substations' energy use.

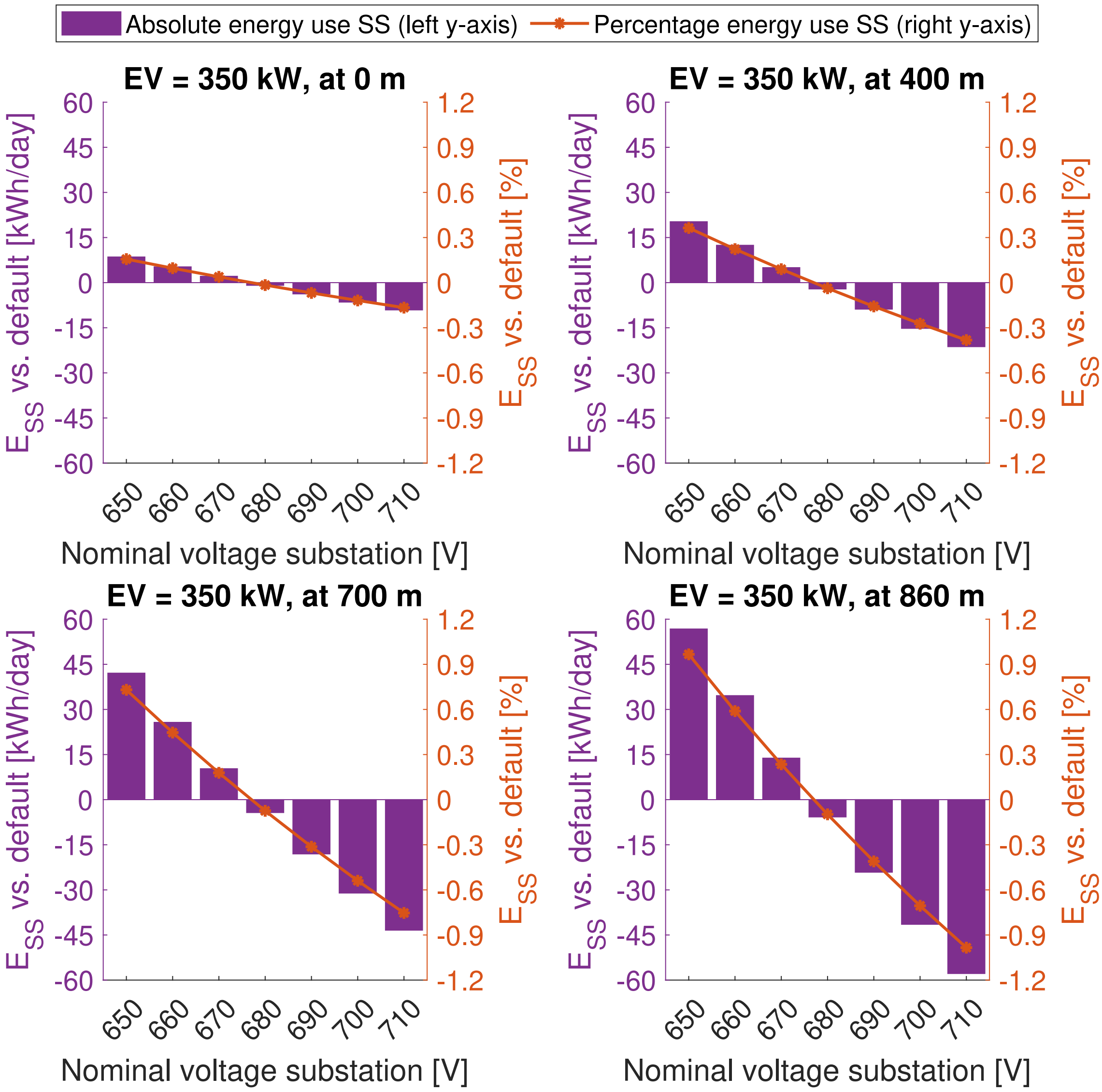

Figure 5.17: The energy use of the substation for the trolleybuses and a 350 kW EV charger at different locations on the section compared to the default voltage (677 V). The left axis shows the absolute energy use, whereas the right axis shows the percentage of energy savings.

5.3.2 Substation level - Increasing allowable substation's power tolerance

This part discusses, the effect of increasing the substations' power tolerance on the EV charging potential in the case study. As mentioned in Chapter 3.1, the substation power limitation is chosen very conservatively. Therefore, accepting a higher power tolerance within the IEEE standard could increase the EV charging potential. The substation's maximum power tolerance will be varied between 120% and 200% for 10 or 60 consecutive seconds. For example, with a tolerance of 200%, 60s, the substation's power can be between 100% and 200% of the rated capacity for 60 consecutive seconds, and the substation power can never be above 200%. Furthermore, the maximum size of the EV charger is 500 kW.

Supply zone A

Substation 12, with a present power rating of 800 kW, is powering sections 23 and 24. In the baseline simulation, one can see that the substations' power was the limiting factor for a further increase in the EV charging potential. Figure 5.18 demonstrates the effect of increasing the permissible substations' power tolerance on the EV charging potential. Increasing the duration that the substation power level can be between 100% and 120% does not affect the EV charging potential. The lack of difference can be explained that the peak power is the limiting factor, as shown in Figure 5.19. A significant increase in EV charging potential can be seen when the magnitude of the tolerance rises from 120% to 150%. For example, at the end of the line, the EV charging potential increases from 250 kW to 475 kW (+90%).

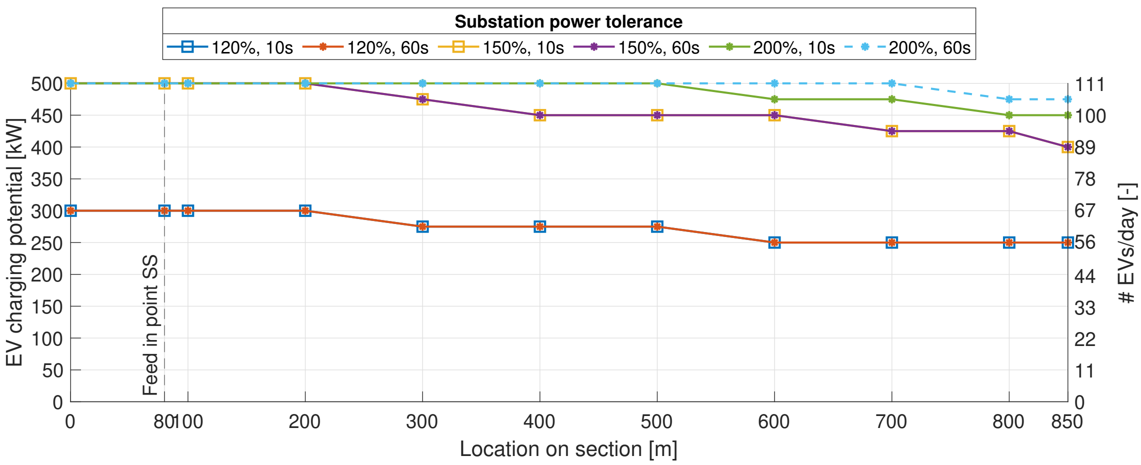

Figure 5.18: Section 23, day 268: effect of various substation power tolerances on the maximum achievable EV charging potential on section 23 for different locations. The first number gives the threshold value relative to the substation power rating. The second number is the consecutive duration between 100% and the threshold. The substation cannot be above the threshold for all the scenarios.

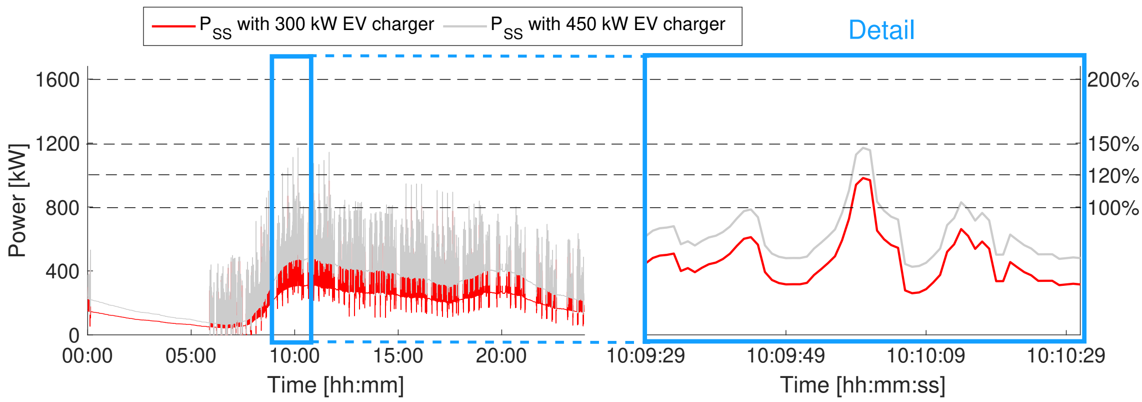

Figure 5.19: Section 23, day 268: effect of a 300 kW and 450 kW EV charger at 400 meters on the substations' power output. A detailed graph of the substations' power during peak time is on the right. The maximum duration of $P_{SS} > 100\%$ is three consecutive seconds for the 300 kW EV charger and eight seconds for the 450 kW EV charger.

Table 5.3 overviews the number of violations and maximum duration with different sized EV chargers and substation power tolerances. The most prolonged period above the substation power limit for all the given EV charger sizes with the baseline power tolerance is only eight consecutive seconds. On the other hand, the magnitude of the substation power output with a 500 kW EV charger can reach up to 155% of the rated capacity. As a result, it is more likely that the peak power will cause failures in the substations' components than the longest period above the limit. This study does not monitor the temperature in the substations' parts. Therefore the effect of increasing the substations' power tolerances in magnitude and duration needs to be further investigated.

Table 5.3: Frequency (#/day) and maximum duration (max dur) of substation power violations with different substation tolerances. Various sized EV chargers are located at 400 meters in section 23 on day 268.

P_{EV}	$P_{SS,max}$	$P_{SS,tol}$ = 100%-120%		$P_{SS,tol}$ = 120%-150%		$P_{SS,tol}$ = 150%-200%	
[kW]	[kW]	#/day	max dur [s]	#/day	max dur [s]	#/day	max dur [s]
300	981	29	3	3	2	0	0
350	1043	46	3	9	3	0	0
400	1106	67	4	20	3	0	0
450	1170	144	5	24	3	0	0
500	1236	322	8	37	4	3	2

Supply zone B

In Figure 5.20 one can see that in the busier section, the EV charging potential also increases with a higher substation power tolerance. Figure 5.21 shows that the duration between 100% and 120% is not the limiting factor in the power limitation of the substation, but the peak value is. An increment in the magnitude of the substations' power tolerance increases the EV charging potential from 375 kW to 475 kW (+27%) halfway through the section (400 meters).

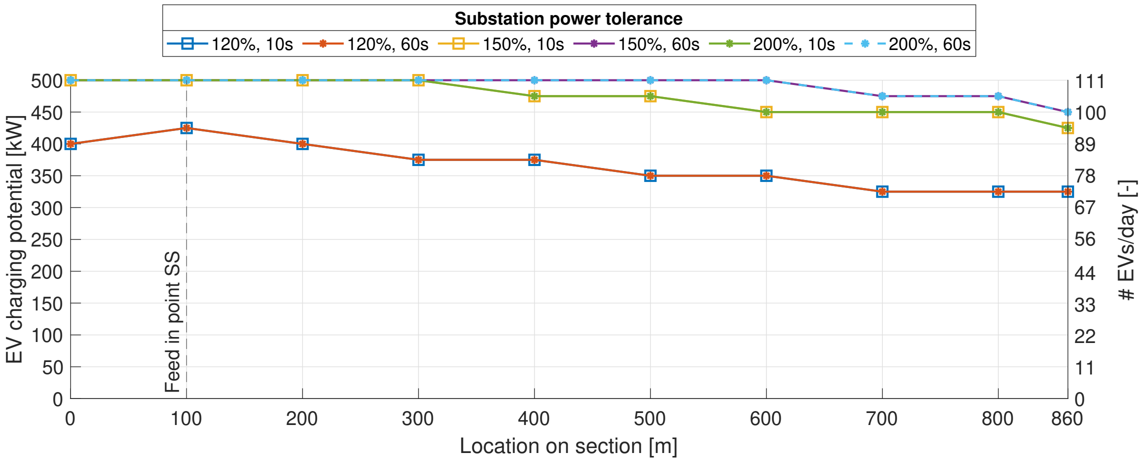

Figure 5.20: Section 25, day 268: effect of various substation power tolerances on the maximum achievable EV charging potential on section 25 for different locations. The feed-in point is at 100 meters on the section.

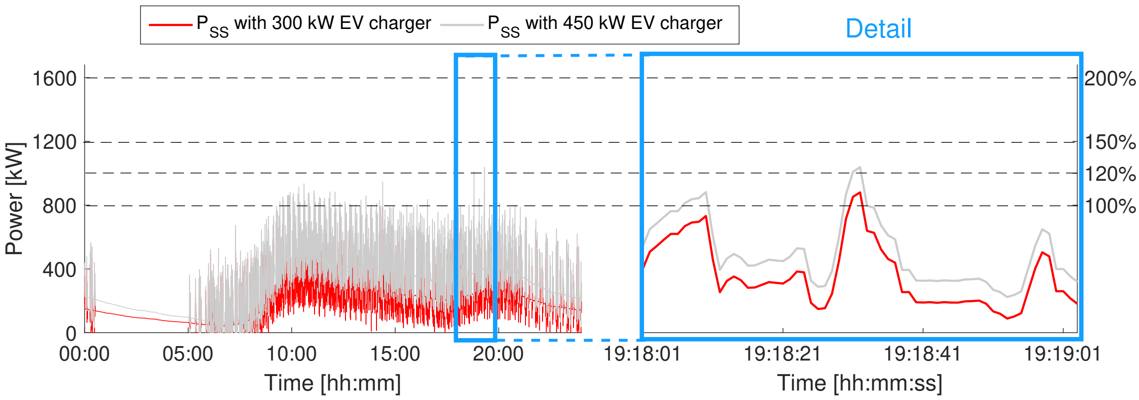

Figure 5.21: Section 25, day 268: effect of a 300 kW and 450 kW EV charger at 400 meters on the substations' power output. A detailed graph of the substations' power during peak time is on the right. The maximum duration of $P_{SS} > 100\%$ is two consecutive seconds for the 300 kW EV charger and ten seconds for the 450 kW EV charger.

An overview of the number of violations and maximum duration with different sized EV chargers and substation power tolerances for section 25 is given in Table 5.4. With a 500 kW EV charger, the maximum power output of the substation can reach up to 136% of the rated capacity. Because substation 9 in supply zone B only powers one section, the peak power is lower than substation 12 in supply zone A. The most extended period above the substation power limit for all the given EV charger sizes with the baseline power tolerance is ten consecutive seconds. As a result, it is most likely that the peak power will cause failures in the substations' components.

Table 5.4: Frequency (#/day) and maximum duration (max dur) of substation power violations with different substation tolerances. Various sized EV chargers are located at 400 meters in section 23 on day 268.

P_{EV}	$P_{SS,max}$	$P_{SS,tol}$ = 100%-120%		$P_{SS,tol}$ = 120%-150%		$P_{SS,tol}$ = 150%-200%	
[kW]	[kW]	#/day	max dur [s]	#/day	max dur [s]	#/day	max dur [s]
300	880	4	2	0	0	0	0
350	932	7	2	0	0	0	0
400	985	41	7	1	1	0	0
450	1039	188	8	4	2	0	0
500	1093	469	10	13	5	0	0

Instead of increasing the tolerance and taking the risk of overheating, installing additional substation capacity can be another solution with the same effect to increase the EV charging potential.

5.3.3 Grid infrastructure level - Extra parallel line

Adding an extra overhead line increases the maximum allowed current in the overhead wires by 50% and reduces the voltage drop due to a reduced impedance. On top of that, the transmission losses are reduced due to the lower resistance. For the simulation, the power of the EV charger varies between 50 kW and 500 kW, with intervals of 25 kW. Besides, the EV charger is placed at 100 meters intervals on the section, at the substation feed-in point, and at the end of the section. The extra parallel line is assumed to be installed over the whole length of the section where the EV charger is placed.

Supply zone A

Figure 5.22 shows the EV charging potential for two parallel overhead lines (baseline scenario) and three parallel overhead lines. One can see that the EV charging potential is 25 kW higher for most locations on section 23. The colored area above the orange line shows the limiting factors for the EV charger if there are three parallel overhead lines. With the introduction of an extra parallel line, the power rating of the substation is still the limiting factor. In contrast to the results found in the theoretical study, the substations' power tolerance is the limiting factor on this section and not the minimum line voltage, therefore, the effect is negligible. Adding an extra parallel reduces the substation power slightly and increases the EV charging potential. But the effect of the reduction on the voltage drop is more significant, as shown in the case study (Chap. 4.3.2).

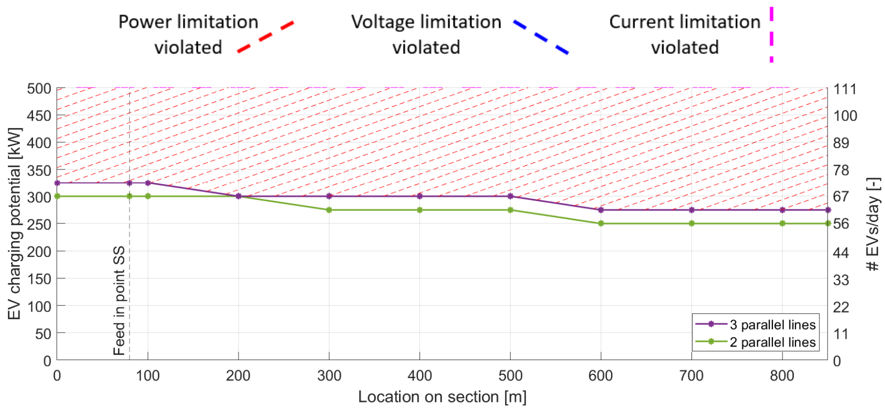

Figure 5.22: Effect of adding extra parallel overhead wire on the maximum achievable EV charging potential on section 23, day 268. The colored area indicates the limiting factor in the three parallel overhead wire scenario.

Additionally, installing an extra parallel overhead wire reduces the transmission losses in the traction grid. Table 5.5 summarizes the energy savings associated with introducing the additional parallel overhead line. Placing the EV charger further away from the feed-in point has a more significant effect on the reduction of the energy consumption of the substation. With a 250 kW EV charger, adding an extra parallel line reduces the energy use by 74 kWh/day (-1.67%).

Table 5.5: Section 23: comparison of energy consumption substation and transmission losses with an extra parallel line. The size of the EV charger is the maximum potential in that specific location for the two parallel line case.

Location [m]	EV charger [kW]	E_{SS} [kWh/day] 2 lines	E_{SS} [kWh/day] 3 lines	$E_{loss,trans}$ [%] 2 lines	$E_{loss,trans}$ [%] 3 lines
0	300	4970	4959 (-0.22%)	0.89	0.68 (-23.6%)
200	300	4987	4970 (-0.34%)	1.24	0.90 (-27.4%)
400	275	4686	4649 (-0.79%)	2.53	1.75 (-30.8%)
600	250	4365	4313 (-1.19%)	3.57	2.41 (-32.5%)
800	250	4424	4350 (-1.67%)	4.85	3.23 (-33.4%)

Supply zone B

Figure 5.23 shows the EV charging potential for two parallel overhead lines (baseline scenario) and the three parallel overhead lines scenario. Depending on the location of the EV charger, the potential increases between 25 and 50 kW. As shown in the colored area, the substation power rating is still the limiting factor. The minimum line voltage and the maximum line current are not violated. The addition of the extra parallel line has a similar effect on the EV charging potential found for supply zone A because the substation power limitation is the limiting factor on this section.

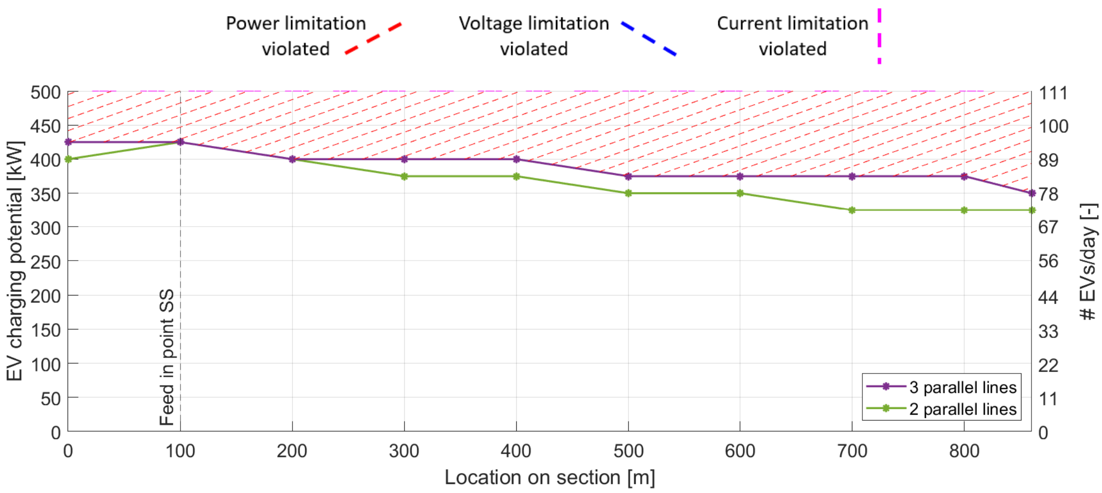

Figure 5.23: Effect of adding extra parallel overhead wire on the maximum achievable EV charging potential on section 25, day 268. The colored area indicates the limiting factor in the three parallel overhead wire scenarios.

Table 5.6 shows the energy-saving associated with adding an extra parallel overhead line on section 25. Placing the EV charger further away from the feed-in point has a more significant effect on the reduction of the energy consumption of the substation. The transmission losses can be reduced to 34.6%, with a total energy saving of 141 kWh/day (2.61%).

Table 5.6: Section 25: comparison of the energy consumption of the substation and transmission losses with an extra parallel line. The size of the EV charger is the maximum potential in that specific location for the two parallel line case.

Location [m]	EV charger [kW]	E_{SS} [kWh/day] 2 lines	E_{SS} [kWh/day] 3 lines	$E_{loss,trans}$ [%] 2 lines	$E_{loss,trans}$ [%] 3 lines
0	400	6186	6160 (-0.42%)	1.96	1.54 (-21.4%)
200	400	6191	6163 (-0.45%)	2.02	1.58 (-21.8%)
400	375	5953	5880 (-1.23%)	4.11	2.93 (-28.7%)
600	350	5691	5580 (-1.95%)	5.99	4.11 (-31.4%)
800	325	5401	5260 (-2.61%)	7.56	5.08 (-32.8%)

5.3.4 Grid infrastructure level - Introducing bilateral connection

Supply zone A

In supply zone A, a bilateral connection between sections 23 and 2 is possible, see Figure 3.13a. Substation 12 is powering sections 23 and 24, whereas substation 13 is powering sections 2 and 3. The substations' voltages are 686 V and 698 V, respectively. The effect of this smart grid method is shown in Figure 5.24. In the bilateral connected scenario, the maximum EV charging potential is between the connection point and substation 13. In this region, substation 13 supplies most of the power to the charger. The colored area indicates the limiting factor for the bilateral case.

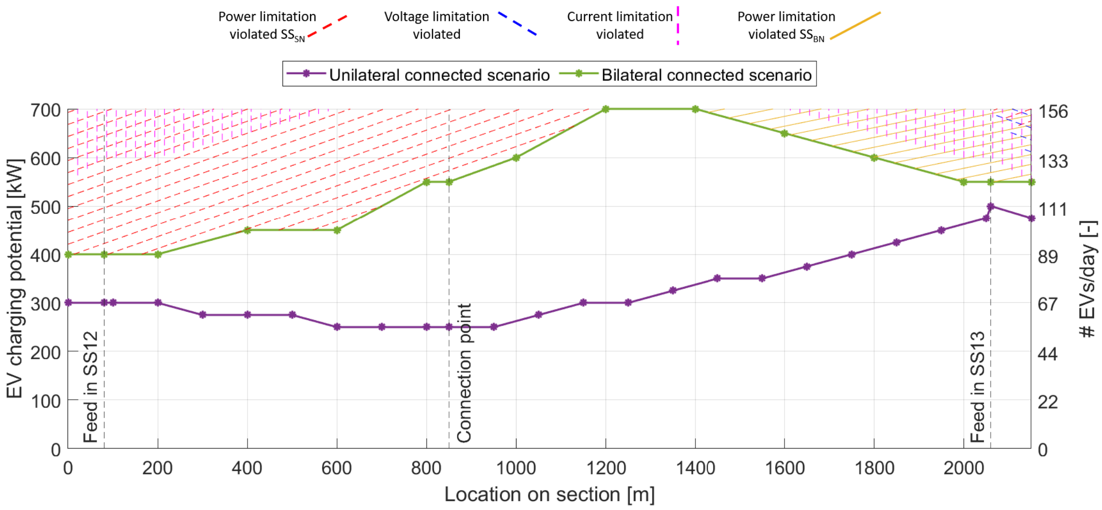

Figure 5.24: Effect of introducing bilateral connections between sections 23 (0-850 m) and 2 (850-2150 m) on the maximum achievable EV charging potential.

Figure 5.25 shows the energy share to power the trolleybuses and a 400 kW EV charger at different locations. If the EV charger is placed close to a substation, this substation delivers most of the energy to the trolleygrid. The energy share is more balanced when the EV charger is placed at the intersection point of the two sections. The transmission losses, indicated with the orange line, are higher when the EV charger is placed in the middle of the sections. The total energy use of both substations is the lowest when the EV charger is placed at the feed-in point on section 23, as shown with the blue line. This can be explained by the fact that the EV charger can use the recuperation energy of the trolleybuses on the relatively long section 24, which has a shared substation busbar.

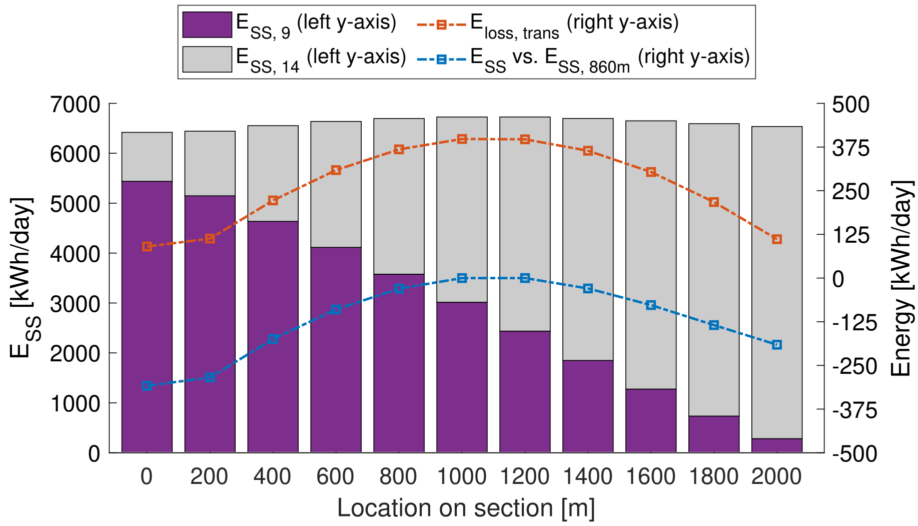

Figure 5.25: Energy share of the two substations in supply zone A (left axis). A 400 kW EV charger is placed at different locations on sections 23 and 2. The orange line (right axis) shows the cables' energy losses due to transmission losses. The blue line (right axis) indicated the total energy consumption of both the substations relative to a 200 kW EV charger placed at the intersection point of the two sections (850 meters).

Supply zone B

Due to the relatively significant difference of $V_{\text{nom, SS}}$, 677 V vs. 628 V, the introduction of the bilateral changes the power source for the trolleybuses and EV chargers in supply zone B. For the baseline simulation, the EV charging potential on section 26 is zero at every location, as seen in Figure 5.26. The zero potential at every location can be explained by the fact that substation 14 (Fig. 3.13b) is powering three different sections. With the bilateral connection between sections 25 and 26, substation 9 can power section 26, see Figure 3.13b. Therefore, the loads on section 26 can be served by substation 9. As downside, the EV charging potential decreases at some point on section 25. On the other hand, with the bilateral connection, the EV charging potential on section 26 increases significantly. The colored areas in Figure 5.26 indicate the limiting factor for the bilateral connection case.

Figure 5.27 shows the energy shared between the two substations on supply zone B when an EV charger of 100 kW is integrated on the sections. Due to the higher nominal voltage of substation 9 compared to substation 14, most of the supplied power is supplied by substation 9. As indicated with the orange line, moving away from the domination substation increases the transmission loss. For the least amount of energy consumption of all the loads on the supply zone, a 100 kW EV charger is best placed near substation 9 (100 meters). At this location, the transmission losses are minimized, and the total energy consumption of both substations is the lowest (orange line).

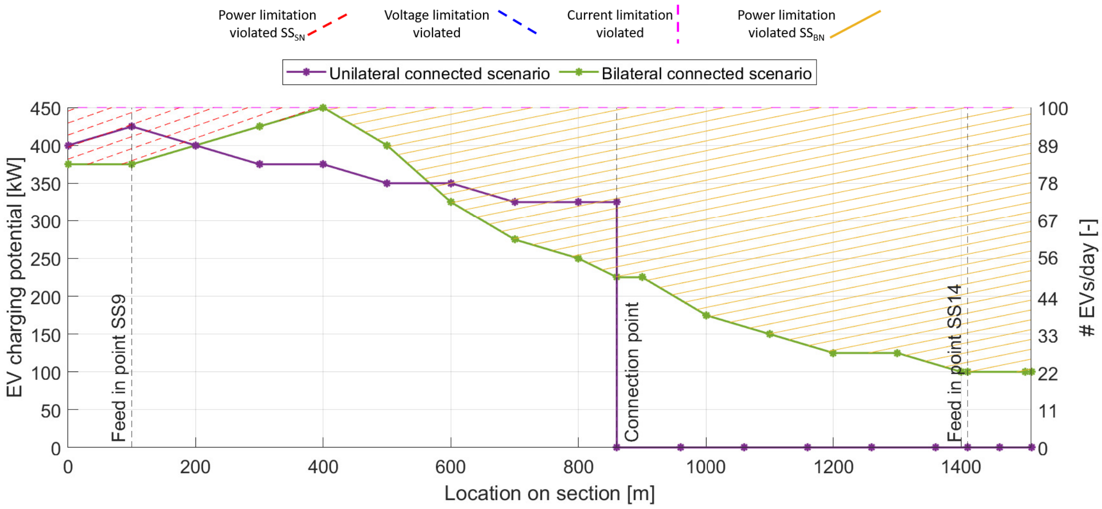

Figure 5.26: Effect of introducing bilateral connections between sections 25 (0-860m) and 26 (860-1510m).

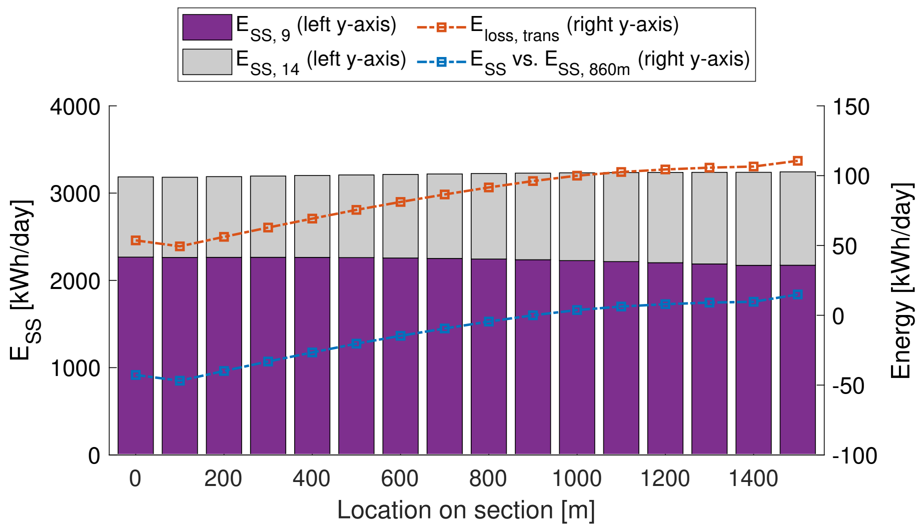

Figure 5.27: Energy share of the two substations in supply zone B (left axis). A 100 kW EV charger is placed at different locations on sections 25 and 26. The orange line (right axis) shows the cables' energy losses due to transmission losses. The blue line (right axis) indicated the total energy consumption of both the substations relative to an EV charger placed at the intersection point of the two sections (860 meters).

5.3.5 EV charging level - Introduction of smart charging

Figure 5.3 shows that during low bus demand instances, the EV charging potential increases significantly. In Chapter 4.3.5 a more detailed explanation of the effect of smart charging on the grids' substation power, line voltage, and line current with various ramp-up/down speeds. The same method will be applied in the case study. Different ramp-up/down rates for the EV chargers are considered with intervals of 3 kW/s.

Supply zone A

Figure 5.28 shows the average number of EVs charged daily with various converter specifications on a day where the traffic and power demand of the buses are low (day 117) and high (day 268). In line with the results found in the theoretical study, smart charging significantly increases the EV charging potential. The main difference is that the EV charger specification plays a role in the number of EVs charged per day. The effect is mainly due to the power limitation on this section. On day 268, the 9 kW/s ramp-up/down converter cannot get the full potential out of the traction grid. Additionally, with smart charging, the EV charging potential is not limited by the busiest type of day in the year.

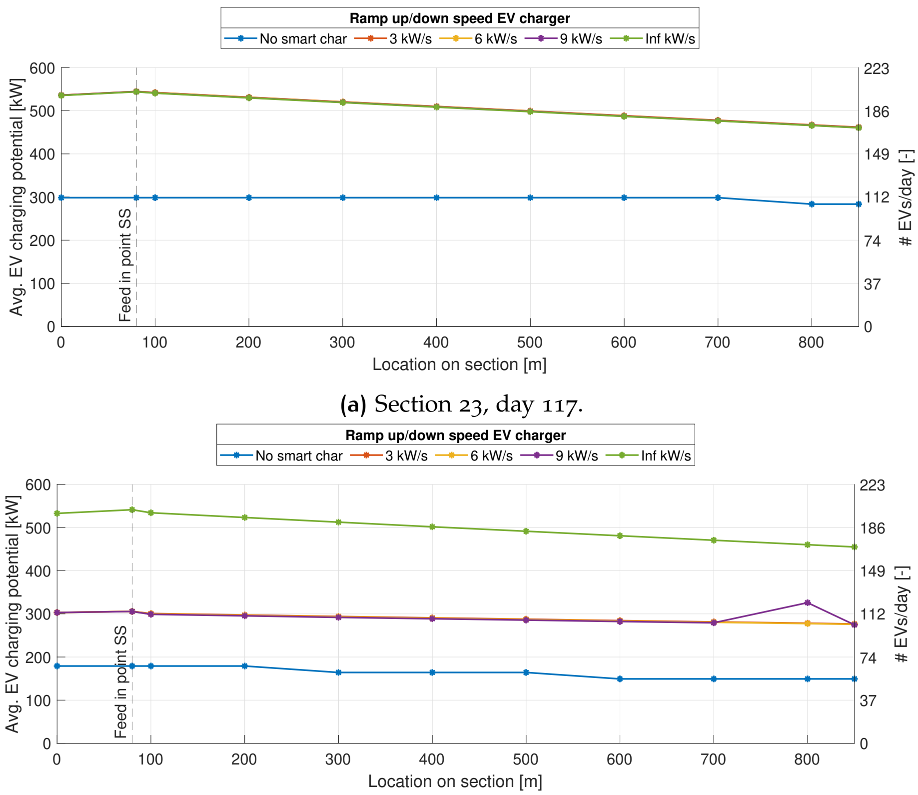

(a) Section 23, day 117.

(b) Section 23, day 268.

Figure 5.28: Maximum achievable EV charging potential with smart charging on two different days on section 23.

Supply zone B

Figure 5.29 shows the number of EVs charged daily with various converter specifications for two days on section 25. On a quiet day (117), the EV charging potential increases from 112 EVs/day to 186 EVs/day (+66%), and the converter specification does not play a role in the EV charging potential. However, on a busy day (268), the EV's higher ramp-up/down speed increases the EV charging potential up to 186 EVs/day. With a fast ramp-up/down speed EV charger, the charging potential is very similar on busy days compared to quiet days.

The dip at the feed-in point of the substation occurs by the slow response of the EV charger. The EV charger is within limits at the feed-in point, so the charging power will not be reduced. However, the next second, the load on the trolleygrid peaks, and the substation power limitation is violated. Before the peak, at a location next to the feed-in place, the charging power is already reduced due to the violation of one of the criteria. As a result, the peak load will not result in a breach of the trolleygrid parameters.

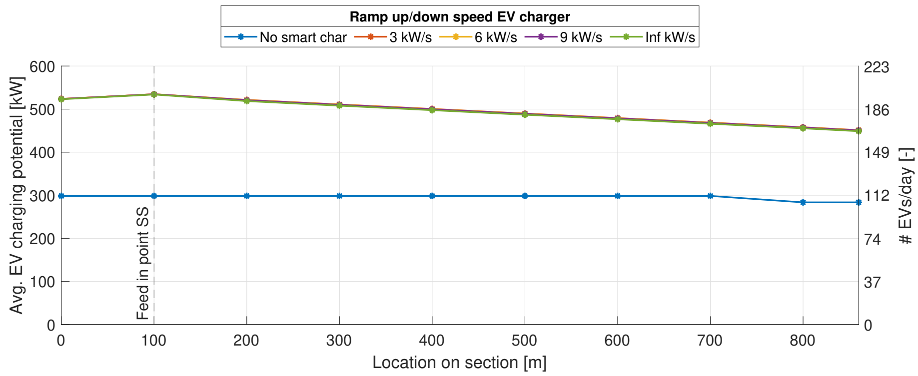

(a) Section 25, day 117.

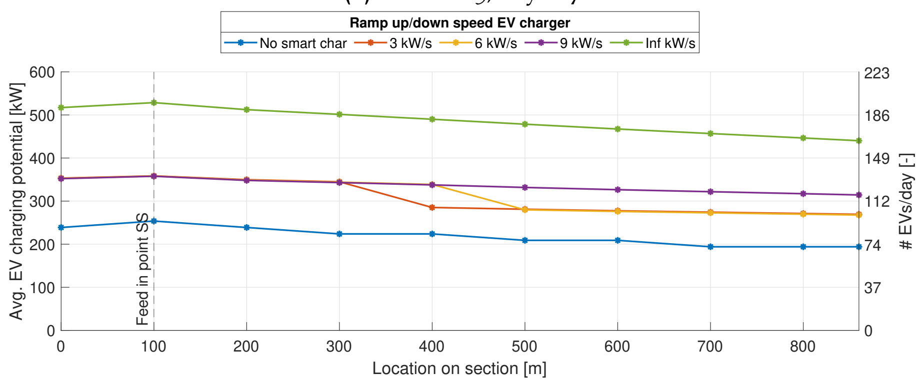

(b) Section 25, day 268.

Figure 5.29: Maximum achievable EV charging potential with smart charging on two different days on section 25.

Semi-smart charging could easily charge more EVs per year without the need for a complex communication method. By oversizing and controlling the EV charging capacity based on the type of day, the EV charging potential could increase over the year, as shown in Figures 5.5 & 5.7.

5.3.6 EV charging level - Multi-port EV charger

Supply zone A

In supply zone A, sections 23 and 2 are connected (Fig 3.13a), but power flow from one to another is impossible. With one multi-port converter, the EV charging potential of both the sections at the connection point can be utilized. Figure 5.30 shows the EV charging potential on section 2. At the connection point with section 23, the potential is 250 kW.

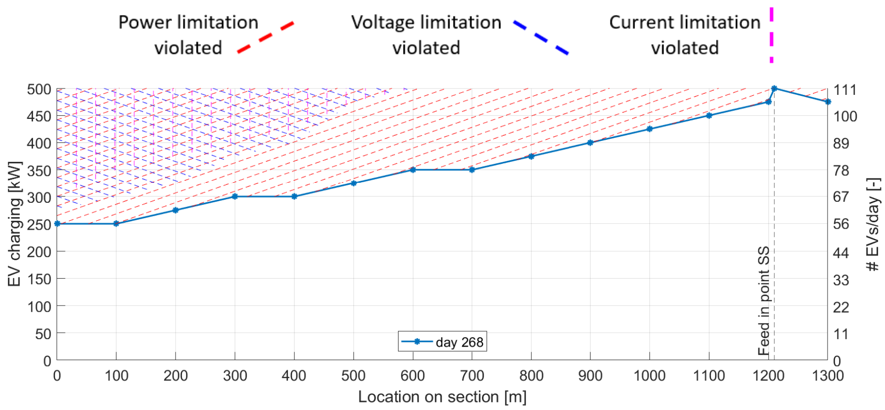

Figure 5.30: Section 2: maximum achievable EV charging potential at the end of the line is 250 kW on day 268. The colored area indicates the limiting factor which reduces the EV charging utilization.

As mentioned in Chapter 4.3.6, three different orientations are possible at the connection point of the sections:

1. Single-port converter with a maximum charging potential of 250 kW from section 23 (Fig. 5.5).

2. Single-port converter with a maximum charging potential of 250 kW from section 2.

3. Multi-port converter with a maximum charging potential of 250+250 kW from both the sections.

The substations' energy use for the same sized single-port converter and multi-port converter are shown in Table 5.7. Powering a 250 kW EV charger with the help of a multi-port converter can save 143 kWh (-2.89%). Interestingly, where the EV charger is entirely powered by section 2, the total energy produced by the substations is higher. This is mainly because the braking energy of the buses on sections 23 and 24 cannot be recuperated. Placing a multi-port converter saves energy, and on top of that, the EV charging potentials at the end of the line from both sections can be used, resulting in an EV charging potential of 500 kW with a single EV charger. The downside of this method is that the EV charger is limited by a location close to the connection point.

Table 5.7: Section 23 and 2: comparison of the energy use of the single-port vs. the multi-port converter.

$P_{\text{EV, 23}}$ [kW]	$P_{\text{EV, 2}}$ [kW]	E_{EV} [kWh]	$E_{\text{loss, trans}}$ [%]	$E_{\text{SS, 12+13}}$
250	0	3582	6.74	4948
125	125	3582	4.66 (-30.9%)	4805 (-2.89%)
0	250	3582	11.65 (+72.8%)	5079 (+5.54%)

Supply zone B

The EV charging potential on section 26 at the end of the line is 0 kW (Fig 5.31). As a result, switching from a single-port converter to a multi-power converter does not influence the EV charging potential in this supply zone. To increase the charging opportunities on this section, one should consider other methods such as increasing the substation power tolerance or introducing a bilateral connection with section 25.

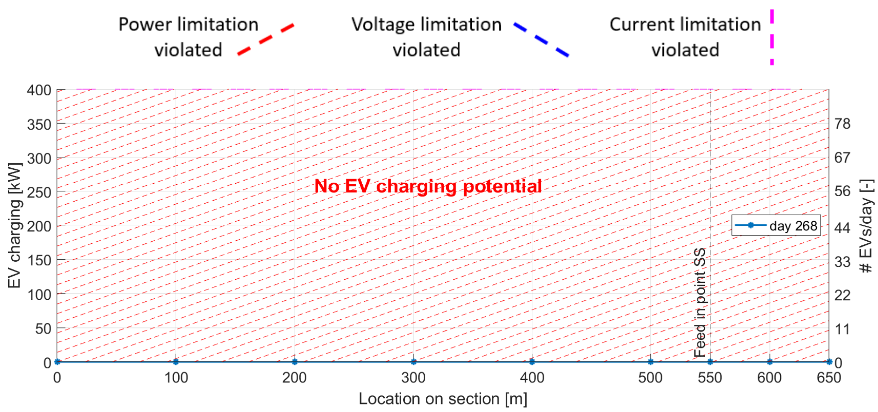

Figure 5.31: Section 26: the maximum achievable EV charging potential at every location is 0 kW on day 268. This is mainly due to the high bus traffic in combination with the low $V_{\text{nom,SS14}}$ of 628 V. The colored area indicates the limiting factor, which reduces the EV charging potential.

Placing EV chargers far away from the feed-in point of the substation is not recommended due to the lower charging potential and high transmission losses. Nevertheless, if one chooses to place an EV charger close to the connection point, a multi-port converter is recommended in areas where the EV charger can be powered from both sections. The EV charging potential can increase, and the transmission losses are reduced. However, in supply zones where the EV charging potential on one of the sections is zero, using a multi-port converter is useless, as demonstrated in supply zone B.

5.4 OVERVIEW OF THE SMART GRID METHODS – CASE STUDY

This section presents an overview of the influence of the different smart grid methods on the EV charging potential for both the supply zones. A combination of smart grid methods is also introduced.

5.4.1 Supply zone A

Figure 5.32 summarizes the results of implementing various smart grid methods on day 268. Because the minimum line voltage is not the main limitation in supply zone A, increasing the substation voltage does not have the same effect as obtained in the theoretical study. As discussed, the substation power is primarily the limiting factor in supply zone A. Therefore, increasing the substation power tolerance increases the EV charging potential by +44 EVs/day (+25%). Adding an extra parallel line to the catenary grid reduces the transmission losses in the overhead lines, and therefore, 5 extra EVs/day can be charged. Introducing a bilateral connection moves the maximum EV charging potential towards the region close to the connection point of the sections. The potential increases to 156 EV/day for a single EV charger. Furthermore, the introduction of smart charging with a ramp-up/down speed of 3 kW/s significantly affects the number of vehicles charged daily (+137). With the use of the multi-port converter, 111 EVs can be charged daily at the connection point with one charging facility.

A combination of smart grid methods (Case 1) is also presented. Here $V_{\text{nom, SS}}$ = 710 V, an extra parallel overhead line is added to the section, and the substation power tolerance is increased to 150% for 60 consecutive seconds. The combination of these smart grid methods increases the EV charging potential at every location up to 311 EVs/day (+75%). In Table 5.8 an overview of the effect of the smart grid methods in numbers is summarized. One EV charger can be added to each section in the unilateral scenarios, resulting in two EV chargers on sections 23 and 2. In the bilateral connection and the multi-port converter, only one EV charger is added to sections 23 and 2.

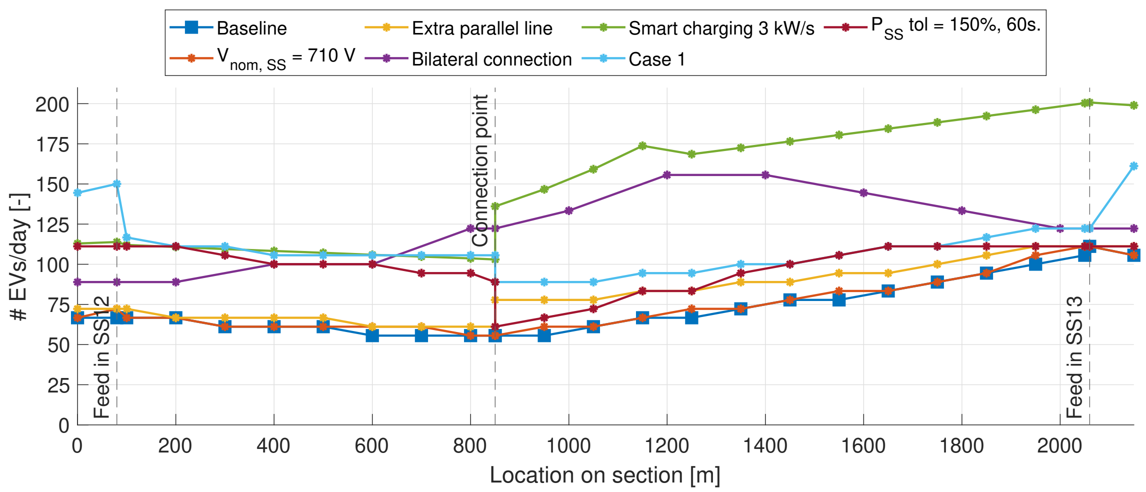

Figure 5.32: Summary of various smart grid methods on the maximum achievable EV charging potential in supply zone A sections 23 and 2 on day 268. Case 1: $V_{\text{nom, SS}}$ = 710 V, an extra parallel overhead line is added to the section, and the substation power rating is increased to 1100 kW.

Table 5.8: Supply zone A: effect of smart grid methods on the EV charging potential for the case study on day 268. *Achievable with one charging facility. **Achievable with one charging facility at the connection point of the sections.

Smart grid method	Section 23 [# of EV/day]		Section 2 [# of EV/day]		Section 23+2 [# of EV/day]
	Max.	Mean.	Max.	Mean.	Max.
0.1 Baseline	67	61	111	82	178
1.1 Increasing voltage	72 (+5)	63 (+2)	111 (0)	83 (+1)	183 (+5)
1.2 Substation power	111 (+44)	103 (+42)	111 (0)	96 (+14)	222 (+44)
2.1 Extra overhead line	72 (+5)	66 (+5)	111 (0)	94 (+12)	183 (+5)
2.2 Bilateral connection	122* (+55)	103* (+42)	156* (+45)	137* (+55)	156* (-22)
3.1 Smart charging	114 (+47)	108 (+47)	201 (+90)	178 (+96)	315 (+137)
3.2 Multi-port converter	56 (-11)	0	56 (-11)	0	111** (-67)
4.1 Case 1	150 (+83)	115 (+54)	161 (+50)	109 (+27)	311 (+133)

5.4.2 Supply zone B

Various smart grid methods influence the EV charging potential in supply zone B. The results are highlighted in Figure 5.33. Increasing the substation's voltages will slightly increase the daily charged EVs (+6). The substation power is the limiting factor for a further increase of the EV charging potential in supply zone B. Therefore, accepting a higher substation power tolerance significantly increases the EV charging potential to 156 EVs/day (+62). Because the minimum line voltage is not the limiting factor, adding an extra parallel line has little to no influence on the EV charging potential. Introducing smart charging with a ramp-up/down speed of 3 kW/s increases the number of vehicles charged per day on sections 25 up to 134. Because substation 14 is powering in total three sections, there is no room for additional charging from substation 14, even with smart charging. The bilateral connection increases supply zone B's maximum EV charging potential with a single charging facility by 6 EVs/day. Additionally, this method increases the possibility of charging on section 26 with 50 EVs/day. The multi-port converter (not visible in the graph) is not recommended in this section as the potential on section 26 is zero in the unilateral case.

A combination of smart grid methods (Case 1) is also presented. Here $V_{\text{nom, SS}} = 710$ V, an extra parallel overhead line is added to the section, and the substation power tolerance is increased to 150% for 60 consecutive seconds. The combination of smart methods increases the potential up to 250 EVs/day (156). The effect of the smart grid methods is summarized in Table 5.9. in this study, one EV charger can be added to each section in the unilateral scenarios, resulting in two EV chargers on sections 25 and 26. In the bilateral connection and the multi-port converter, only one EV charger is added to sections 25 and 26.

Table 5.9: Supply zone B: effect of smart grid methods on the EV charging potential for the case study. *Achievable with one charging facility. **Achievable with one charging facility at the connection point of the sections.

Smart grid method	Section 25 [# of EV/day]		Section 26 [# of EV/day]		Section 25+26 [# of EV/day]
	Max.	Mean.	Max.	Mean.	Max.
0.1 Baseline	94	81	0	0	94
1.1 Increasing voltage	94 (0)	83 (+2)	6 (+6)	6 (+6)	100 (+6)
1.2 Substation power	111 (+17)	109 (+28)	44 (+44)	44 (+44)	156 (+62)
2.1 Extra overhead line	94 (0)	87 (+6)	0 (0)	0 (0)	94 (0)
2.2 Bilateral connection	100* (+6)	78* (-3)	50* (+50)	30* (+30)	100* (+6)
3.1 Smart charging	134 (+40)	114 (+33)	0 (0)	0 (0)	134 (+40)
3.2 Multi-port converter	72 (-22)	0	0 (0)	0	72** (-22)
4.1 Case 1	128 (+34)	106 (+25)	122 (+122)	91 (+91)	250 (+156)

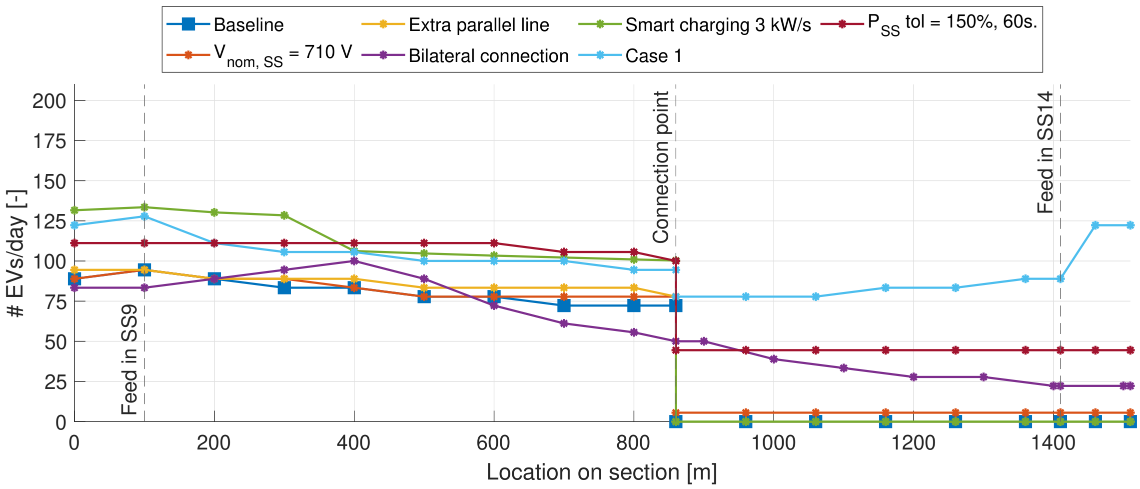

Figure 5.33: Summary of the effect of various smart grid methods on the EV charging potential in supply zone B sections 25 and 26. Case 1: $V_{\text{nom, SS}}$ = 710 V, an extra parallel overhead line is added to the section, and the substation power rating is increased to 1100 kW.

5.4.3 Comparison between the two supply zones

As discussed, the supply zones in the case study are limited by the maximum substation power. The main difference is the number of sections each substation supplies and the traffic intensity. We can draw the following conclusions by comparing the two supply zones based on the EV charging potential.

- Without any smart grid method, the average EV charging potential in supply zones A and B are 178 and 94 EV/day, respectively.
- Increasing the voltage of all the substations to 710 V in supply zone A and B has a limited effect. In both the supply zones, the maximum EV charging potential increases by less than 6 EVs/day.
- Both supply zones benefit from an increase in the substation's power tolerance. An additional 44 EVs can be charged daily in supply zone A and 62 in supply zone B.

- An increase of 5 EVs/day is achievable with an extra parallel line in supply zone A. In supply zone B, the maximum charging potential does not change, but on average, 6 additional EVs can be charged daily.

- Introducing the bilateral connection between the sections positively affects both supply zones. The maximum EV charging potential for a single EV charger in supply zone A increases from 111 EVs/day to 156 EVs/day. In supply zone B, this increases from 94 to 100 EVs daily. Additionally, the bilateral connection makes a high EV charging potential possible in the region close to the connection point.

- The best smart grid method to increase the charging utilization from a trolleygrid is smart charging. Smart charging can boost the number of EVs charged daily to 315 EVs/day and 134 EVs/day for zones A and B, respectively.

- With one multi-port converter, the EV charging potential at the connection point in supply zone A increases from 56 EVs/day to 111 EVs/day. The EV charging potential on section 26 at the connection point is zero. Therefore, adding a multi-port converter will not change the potential in supply zone B.

5.5 EFFECT ON THE PV UTILIZATION WITH THE INTEGRATION OF EV CHARGERS

The trolley2.0 project aims to convert a DC trolleygrid into a multi-functional traction grid with EV chargers, renewable energy sources (RES), energy storage systems, and in-motion-charging buses. Diab et al. [8] have studied the integration of PV and wind as RES directly into the trolleygrid of Arnhem. The challenge with solar and wind as RES is that the power output is weather dependent and hard to control. Figure 5.34 shows the mismatch between simulated PV generation and bus loads for two substations. Three methods are suggested to deal with this mismatch, a storage system, exchange with the LVAC grid, or curtailing the energy.

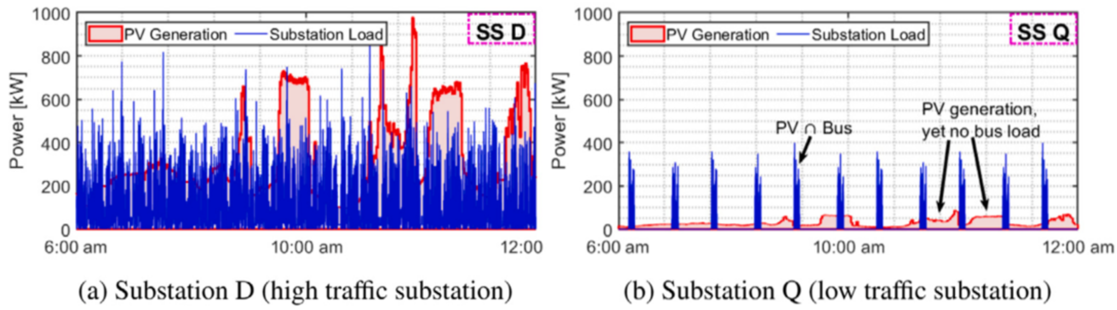

Figure 5.34: Mismatch of solar production and bus loads on two different substations in the trolleygrid of Arnhem[8].

To quantify the percentage of solar power that is directly used by the loads on a trolleygrid, the authors make use of the PV Utilization factor [8]:

$$U_{PV} \triangleq \frac{\int_{\text{year}} (P_{\text{load}} - P_{\text{grid}})\,\mathrm{d}t}{\int_{\text{year}} P_{\text{PV}}\mathrm{d}t} \tag{5.1}$$

The size of the PV system is scalable therefore, the following Energy-Neutrality Ratio, ζ, is introduced [8]:

$$\zeta \triangleq \frac{\int_{\text{year}} P_{\text{PV}}\mathrm{d}t}{\int_{\text{year}} P_{\text{load}}\,\mathrm{d}t} \tag{5.2}$$

When $\zeta = 1$, the sum of the generated power over a year equals the sum of all the loads over a year.

In the article's conclusion, the authors opt for a fourth method. Adding a base load, such as EV chargers, to the trolleygrid could increase the PV utilization factor. Figure 5.35 shows the effect of the integration of various-sized EV chargers on the PV utilization factor for two different supply zones with various Energy-Neutrality Ratios.

For substation 12 with a $\zeta = 1$, the PV utilization increases from 27% to 42% with a 150 kW EV charger at a location of 400 meters. For substation 9, the PV utilization increases from 19% to 41% for a $\zeta = 1$ and a 150 kW EV charger. To conclude, adding a base load such as EV chargers to the trolleybus grid, has a positive effect on PV utilization.

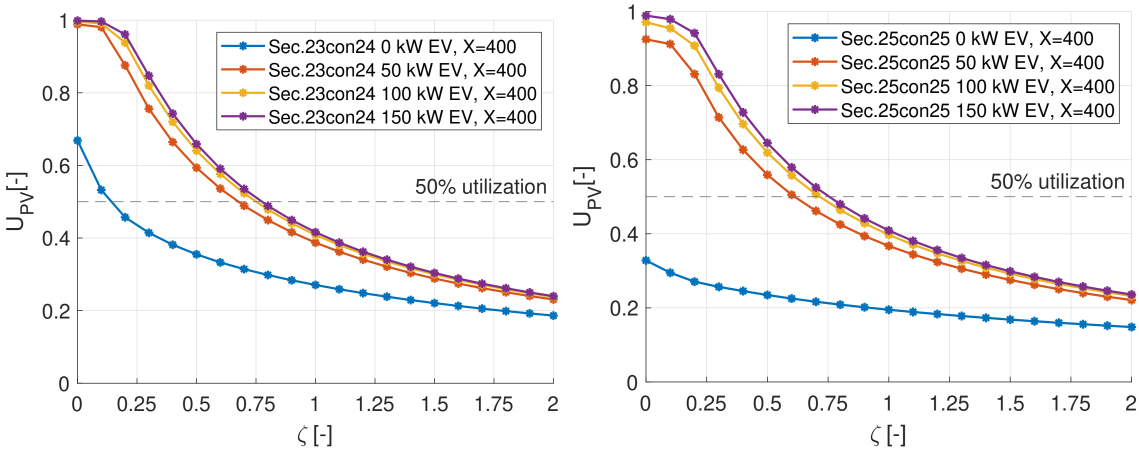

(a) Substation 12. (low bus traffic) **(b)** Substation 9. (high bus traffic)

Figure 5.35: PV utilization factor for two different substations with various size EV chargers.

6 DISCUSSION, CONCLUSIONS, AND RECOMMENDATIONS

6.1 DISCUSSION AND FUTURE WORK

For this thesis, three main limitations with its boundaries are chosen to determine the EV charging potential on trolleygrids. Chapter 5.3.2 discusses the effect of changing the boundaries of the power limitation. During the case study, it is found that the limits of the substation influence the EV charging potential significantly. Therefore, setting up the correct limits for the trolleygrid is one of the most critical steps in determining the potential size of the EV charger. For followings studies, it is recommended to get a better understanding of the temperature of the substations' components and the overhead wires.

This thesis investigated three supply zones, one artificial one and two real-world examples. The theoretical and case studies found the opposite limitations in the trolleygrid. Due to the relatively long section and lower nominal substation voltage, the minimum line voltage was the main limiting factor in the theoretical study. On top of that, the substation was only connected to section 111; therefore, the maximum substation power was not above the rated capacity. On the other hand, for both the supply zones in the case study, the maximum substation power was the limitation to increase the charging utilization. Consequently, the effect of the six smart grid methods on the EV charging potential strongly depends on the composition of a supply zone. The number of sections powered by a single substation, substations' power capacity, substations' voltage, section length, and the bus intensity are some parameters that influence the limits of the trolleygrid. The effect of the smart grid method, as listed in Table 3.2 can be used as a reference to solve the first limitation. In the following research, more supply zones should be evaluated to find a general trend in the boundaries of the trolleygrid.

The assumption was made that there only can be one EV charger per section with a maximum of two per supply zone. Spacial availability and other environmental limitations were not considered in the case study. As this can play a significant role in serving people's demand for EV charging, this should be included in the following study. In Appendix A.3 an introduction on the charging station location problem is given.

Additionally, the effect of placing two but smaller EV chargers on the same section could be an exciting idea, especially in the bilateral case. This can increase the charging utilization and give the EV owner more opportunities and flexibility to charge EVs via a traction network.

In this thesis, the assumption is made that the EV charging power of one transaction is constant. As described in [54], the charger's power demand changes based on the battery level of the EVs. This effect can influence the total EV charging profile (Fig. 3.3).

Furthermore, the same weekend and weekday EV charging profiles are used during various seasons. To better understand the EV charging demand over the year with day-to-day variations due to customer behavior, fluctuations and randomness needs to be considered.

This study is limited by six smart grid methods. However, there are many more methods that can strengthen a traction grid. In Appendix A.4, some smart grid methods are listen and can be used for future work. Adding a renewable energy source (PV, for example) to the traction grid as smart grid method, is shortly discussed in 5.5.

6.2 CONCLUSIONS

The main goal of this study is to explore the charging potential for electric vehicles directly from the trolleygrid of Arnhem. Therefore, three research questions have been formulated and answered in the following paragraphs.

RQ1: What is the EV charging potential in a trolleygrid network without violating the grids' substations' power, line voltage, and line current limitations?

The EV charging potential strongly depends on the location relative to the feed-in point of the substation. The highest EV charging potential can be found near the feed-in point in supply zones where the substation is powering a single section. Further away, the EV charging potential decreases significantly and depends on the grid limitations. In supply zones where the substation is powering two sections, the trolleygrid can serve at least 55 EVs/day. In cases where the substation is powering three or more sections, the EV charging potential is insignificant. Other grid parameters (seasonal effects, section length, bus intensity, etc.) also play a role in the EV charging potential.

For example, placing an EV charger close to the feed-in point section 111 could fully charge 111 EVs/day of 60 kWh each. At the end of the section, where the minimum voltage limits the EV charging potential, the number of EVs charged per day decreases to 22. As shown in Figure 6.1, both the maximum substations' power and the minimum line voltage play a limiting role in the EV charging potential. Hence, the focus should be on eliminating these two limiting factors to increase the EV charging potential.

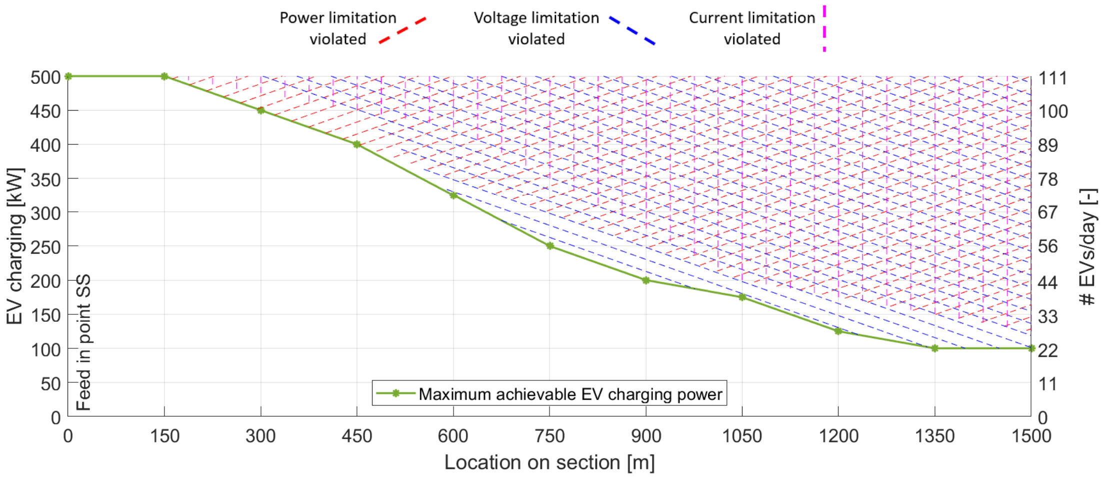

Figure 6.1: Maximum achievable EV charging power on the theoretical section without any smart grid methods implemented. The colored area indicates the limiting factor which reduces the EV charging utilization. Copy of Figure 4.4.

RQ2: What is the effect of smart grid methods on increasing the EV charging potential on a trolleygrid within the substation power, line voltage, and line current limitations?

The six smart grid methods affect the ability to charge EVs via a trolleygrid in various ways for the case study.

1. **Substation level**

   1.1 *Increasing substations' nominal voltage*
   When the section is long or if the minimum line voltage is the limiting factor, increasing the substations' nominal voltage positively affects the EV charging potentials. For example, the number of EVs served per day doubles at the end of the line in the theoretical study. In supply zones where the sections are shorter or the minimum line voltage does not limit the trolleybus behavior, increasing the substations' nominal voltage has a minor effect on the charging potential.

   1.2 *Increasing allowable substation's power tolerance*
   Theory shows that the substations' power tolerance is only a limiting factor close to the feed-in of the substation. Therefore, increasing the substation power has little to no effect on the EV charging potential when the substation is powering one section. However, the substation's maximum power is the limiting factor in areas where the substation is powering two or more sections (case study). Consequently, increasing the substation power capacity expands the EV charging potential in supply zones where the substation is powering two or more sections.

2. **Grid infrastructure level**

   2.1 *Adding extra parallel line*
   Reducing the impedance by adding an extra parallel line only benefits sections where the voltage reaches the grids' minimum voltage. For example, in the theoretical study, the extra parallel line reduces the voltage drops resulting in a higher minimum line voltage. On top of that, the third parallel line eliminates the maximum current. The EV charging potential halfway through the section increases by 39 EVs/day (+70%) and, at the end of the line by, 45 EVs/day (+200%). Because the minimum line voltage was not reaching its limits in the case study, the effect of adding an extra line was marginal.

   2.2 *Introduction of bilateral connection*
   A bilateral connection between connected sections is a cost-effective way to increase the EV charging potential. Bilateral links are recommended in supply zones where the need for an EV charger is high in the region around the connection point of the sections. A bilateral connection is not beneficial only in supply zones where one of the two substations is overloaded.

3. **EV charging level**

   3.1 *Introduction of smart charging*
   On average smart charging could charge an additional 56 more EVs/day and is, therefore, one of the best methods to increase the EV charging potential. The downside of this method its complexity and immaturity.

   3.2 *Introduction of multi-port converter*
   This smart grid method only affects the EV charging potential at the connection point when both sections have an EV charging potential at the end of the line. In many cases, the introduction of a bilateral connection is superior to the multi-port converter and therefore recommended.

RQ3: Case study: What is the available capacity for EV charging on the present trolleygrid network of Arnhem without violating the grids' substations' power, line voltage, and line current limitations?

In the case study, the placement of the EV charging stations relative to the feed-in point of the substation plays a role in the EV charging potential. The highest charging potential in the unilateral connected section is close to the feed-in. But in the bilateral connected case, the maximum EV charging potential shifts towards the connection point of the sections.

On average, without any smart grid method, the number of EVs charged on the busiest days in supply zones A and B are 178 and 94. The EV charging potential differs significantly from day to day. The difference is mainly due to the varying bus traffic intensity during weekdays and weekends and the load demand of the trolleybuses in multiple seasons. Also shown in these Figures is that the maximum power of the substation is the limiting factor for a further increase of the EV charging potential. Therefore, smart grid methods which eliminate this limitation will be most helpful.

Figures 5.32 & 5.33 show the effect of the various smart grid methods at different locations in the case study. Both smart charging and increasing the substation tolerance should be considered to reach the maximum EV charging potential. Within the smart charging method, a higher ramp-up/down speed increases the charging potential. The bilateral connection could be a solid solution if the EV charger is placed in the region close to the connection point of the substations. Both the EV charging potentials at the connection point of the sections in supply zone A are 56. With a single multi-port converter, the charging possibilities of both sections can be utilized (111 EVs/day). In supply zone B, the multi-port converter is not recommended due to the zero EV charging potential on section 26.

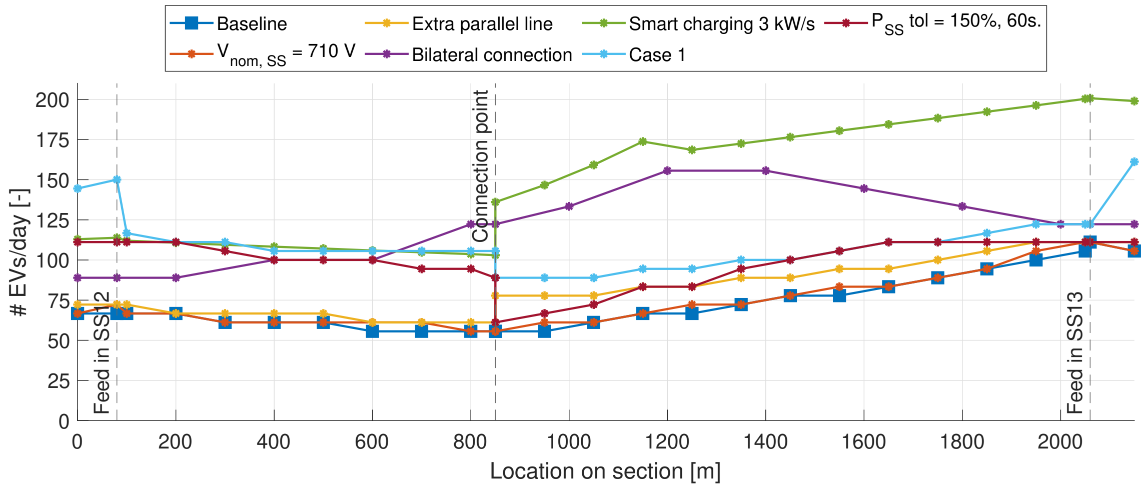

Figure 6.2: Summary of various smart grid methods on the maximum achievable EV charging potential in supply zone A sections 23 and 2 on day 268. Case 1: $V_{\text{nom, SS}}$ = 710 V, an extra parallel overhead line is added to the section, and the substation power rating is increased to 1100 kW. Copy of Figure 5.32.

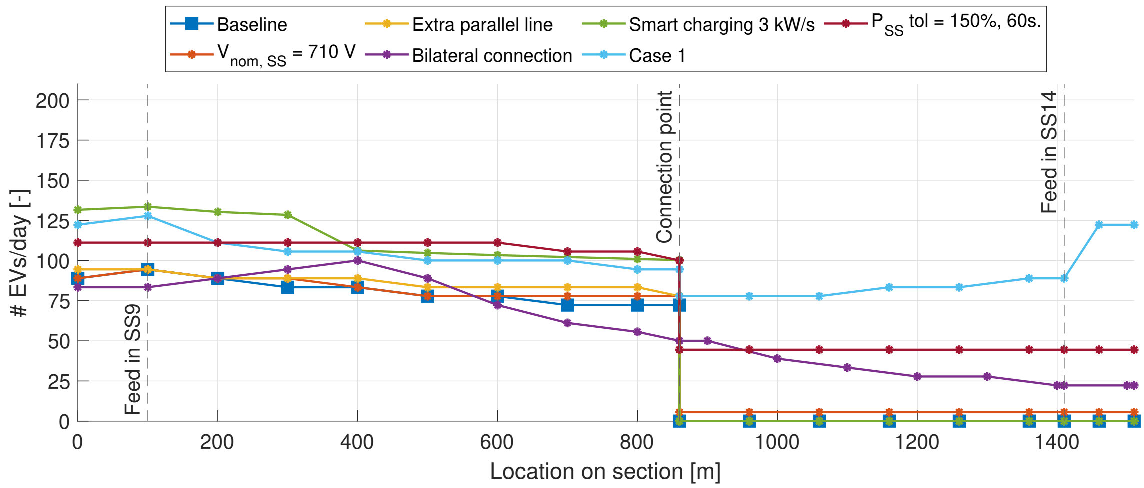

Figure 6.3: Summary of the effect of various smart grid methods on the EV charging potential in supply zone B sections 25 and 26. Case 1: $V_{\text{nom, SS}}$ = 710 V, an extra parallel overhead line is added to the section, and the substation power rating is increased to 1100 kW. Copy of Figure 5.33.

The EV charging potential can be maximized with a combination of the smart grid methods. For case 1, where the substation nominal voltage and power tolerance are increased, and with the addition of an extra parallel line, the maximum EV charging potential in supply zone A and B increases to 311 (+133) and 250 (+156) EVs/day.

Due to the lower bus traffic in supply zone A, the EV charging potential with three smart grid methods combined (case 1) is higher than in supply zone B (311 versus 250 EVs/day). Nevertheless, there is still EV charging potential on one of the busiest sections on the trolleygrid of Arnhem with various smart grid methods.

Without any implementation of smart grid methods, charging electric vehicles directly from a traction grid is technically feasible. Various smart grid methods can increase the charging potential. When the voltage is the limiting factor on the section, the smart grid methods, adding an extra parallel line or increasing the substations' nominal voltage, should be considered. If the substations' maximum power is the limiting factor, adding additional substation capacity or accepting a higher tolerance are suitable options. Smart charging with a high ramp-up/down speed is superior to other smart grid methods due to the volatile power demand of the trolleybuses.

6.3 RECOMMENDATIONS

The EV charging potential is based on various supply zone parameters such as the number of sections powered by a single substation, substations' power capacity, substations' voltage, section length, and the bus intensity. Analyzing these parameters can forecast the expected limits of a supply zone. For example, when the section length is long, or the substation's nominal voltage is low, the minimum voltage in the overhead lines will play a significant role in the EV charging potential. When the substation is powering two or more sections, the EV charging potential is limited by the substation's maximum power. Based on the predicted limits of the trolleygrid, the best smart grid method can be chosen, as shown in Table 3.2. The maximum continuous current in the overhead wires is never the only violated limitation and should not be prioritized using smart grid methods.

As demonstrated in the case study, there is room for charging electric vehicles on the trolleygrid of Arnhem. The substations' maximum power was the dominant limiting factor for the EV charging potential. Hence, smart grid technologies that counter these limitations should be considered to increase the number of vehicles charged daily. Two solutions can opt, 1. increase the tolerance of the substation power limitation, or 2. add extra substation capacity.

For maximum EV charging potential and minimum transmission losses, it is recommended to install the EV chargers close to the feed-in point of the substation. When this is not desirable due to other constraints, the introduction of a bilateral connection should be considered.

Smart charging is almost in every case the best smart grid method. However, the technology is a relatively immature technology. Therefore, semi-smart charging could be an easier way to charge more EVs per year without the need for a complex communication method. By oversizing and controlling the EV charging capacity based on the type of day, the EV charging potential could increase significantly over the year.

Lastly, the power demand for public EVs and trolleybuses is low at nighttime. To maximize the utilization of the traction grid for charging purposes, other charging applications such as battery-powered electric buses can be considered.

BIBLIOGRAPHY

[1] EV Monitor Team, "Electric Vehicles Statistics in the Netherlands," tech. rep., Netherlands Enterprise Agency, Ministry of Infrastructure and Water Management, The Hague, Mar. 2021.

[2] Liander, "Beschikbaarheid capaciteit per gebied — Liander." https://www.liander.nl/transportschaarste/beschikbaarheid-capaciteit.

[3] NOS, "Zorgen over vol elektriciteitsnet: netbeheerder en werkgevers willen actie." https://nos.nl/l/2398165.

[4] I. Diab, A. Saffirio, G. R. C. Mouli, A. S. Tomar, and P. Bauer, "A Complete DC Trolleybus Grid Model With Bilateral Connections, Feeder Cables, and Bus Auxiliaries," *IEEE Transactions on Intelligent Transportation Systems*, pp. 1–12, 2022.

[5] "Trolleybus." https://www.trolleybus.nl/.

[6] V. Calderaro, V. Galdi, G. Massa, and A. Piccolo, "Distributed Generation and local voltage regulation: An approach based on sensitivity analysis," in *2011 2nd IEEE PES International Conference and Exhibition on Innovative Smart Grid Technologies*, (Manchester, United Kingdom), pp. 1–8, IEEE, Dec. 2011.

[7] M. Bartłomiejczyk, "Smart Grid Technologies in Electric Power Supply Systems of Public Transport," *Transport*, vol. 33, pp. 1144–1154, Dec. 2018.

[8] I. Diab, B. Scheurwater, A. Saffirio, G. R. Chandra-Mouli, and P. Bauer, "Placement and sizing of solar PV and Wind systems in trolleybus grids," *Journal of Cleaner Production*, vol. 352, p. 131533, June 2022.

[9] T. Brand, "Arnhems Trolleybusnet Onderzoek Bovenleidingnet," Oct. 2012.

[10] N. Openbaar Vervoer Wereldwijd, "Arnhem Breng Trolleybus 2.0 en andere bussen." https://www.youtube.com/watch?v=mPqtcgYQKsE.

[11] A. S. Tomar, B. P. A. Veenhuizen, L. Buning, and B. Pyman, "Viability of traction battery for battery-hybrid trolleybus," in *Electric Vehicle Symposium*, (Lyon), p. 13, June 2019.

[12] A. Shekhar, G. C. R. Mouli, S. Bandyopadhyay, and P. Bauer, "Electric Vehicle Charging with Multi-Port Converter based Integration in DC Trolley-Bus Network," in *2021 IEEE 19th International Power Electronics and Motion Control Conference (PEMC)*, (Gliwice, Poland), pp. 250–255, IEEE, Apr. 2021.

[13] V. R. Vuchic, *Urban Transit Systems and Technology*. Hoboken, N.J: John Wiley & Sons, 2007.

[14] M. Brenna, M. Longo, and W. Yaïci, "Modelling and Simulation of Electric Vehicle Fast Charging Stations Driven by High Speed Railway Systems," *Energies*, vol. 10, p. 1268, Aug. 2017.

[15] H. Douglas, C. Roberts, S. Hillmansen, and F. Schmid, "An assessment of available measures to reduce traction energy use in railway networks," *Energy Conversion and Management*, vol. 106, pp. 1149–1165, Dec. 2015.

[16] M. Bartłomiejczyk and M. Połom, "The impact of the overhead line's powersupply system spatial differentiation on the energy consumption of trolleybustransport: Planning and economic aspects," *Transport*, vol. 32, pp. 1–12, Oct. 2015.

[17] K. Smith, S. Galloway, and G. Burt, "A review of design criteria for low voltage DC distribution stability," in *2016 51st International Universities Power Engineering Conference (UPEC)*, (Coimbra), pp. 1–6, IEEE, Sept. 2016.

[18] M. Ahmadi, H. Jafari Kaleybar, M. Brenna, F. Castelli-Dezza, and M. S. Carmeli, "Integration of Distributed Energy Resources and EV Fast-Charging Infrastructure in High-Speed Railway Systems," *Electronics*, vol. 10, no. 20, p. 2555, 2021.

[19] Rail Baltica, "Design guidelines Railway Energy," Mar. 2018.

[20] M. Wazifehdust, D. Baumeister, M. Salih, P. Steinbusch, M. Zdrallek, C. von Kalben, and J. O. Schumacher, "Predictive flexibility calculation for battery-trolleybuses," in *ETG-Kongress 2021 - Von Komponenten Bis Zum Gesamtsystem Fur Die Energiewende*, vol. 9, pp. 191–196, 2021.

[21] D. Baumeister, M. Salih, M. Wazifehdust, P. Steinbusch, M. Zdrallek, S. Mour, L. Lenuweit, P. Deskovic, and H. B. Zid, "Modelling and Simulation of a Public Transport System with Battery-Trolleybuses for an Efficient E-Mobility Integration," p. 7, 2017.

[22] M. Wazifehdust, D. Baumeister, M. Salih, M. Koch, P. Steinbusch, M. Zdrallek, S. Mour, and C. Troullier, "Potential Analysis for the Integration of Renewables and EV Charging Stations Within a Novel LVDC Smart-Trolleybus Grid," in *International Conference on Electricitiy Distribution*, p. 5, 2019.

[23] M. Weisbach, U. Spaeth, B. Schmuelling, and C. Troullier, "Flexible EV Charging Strategy for a DC Catenary Grid," in *2020 Fifteenth International Conference on Ecological Vehicles and Renewable Energies (EVER)*, (Monte-Carlo, Monaco), pp. 1–6, IEEE, Sept. 2020.

[24] M. Salih, D. Baumeister, M. Wazifehdust, P. Steinbusch, M. Zdrallek, S. Mour, P. Deskovic, T. Küll, and C. Troullier, "Impact Assessment of Integrating Novel Battery-Trolleybuses, PV Units and EV Charging Stations in a DC Trolleybus Network," p. 6, 2018.

[25] M. Salih, M. Koch, D. Baumeister, M. Wazifehdust, P. Steinbusch, and M. Zdrallek, "Adapted Newton-Raphson Power Flow Method for a DC Traction Network including Non-receptive Power Sources and Photovoltaic Systems," in *2019 IEEE PES Innovative Smart Grid Technologies Europe (ISGT-Europe)*, (Bucharest, Romania), pp. 1–5, IEEE, Sept. 2019.

[26] M. Bartłomiejczyk, L. Jarzebowicz, and R. Hrbáč, "Application of Traction Supply System for Charging Electric Cars," *Energies*, vol. 15, p. 1448, Feb. 2022.

[27] M. Bartłomiejczyk and M. Połom, "Multiaspect measurement analysis of breaking energy recovery," *Energy Conversion and Management*, vol. 127, pp. 35–42, Nov. 2016.

[28] M. Bartłomiejczyk, "Bilateral power supply of the traction network as a first stage of Smart Grid technology implementation in electric traction," *MATEC Web of Conferences*, vol. 180, p. 02003, 2018.

[29] K. Smith, L. Hunter, S. Galloway, C. Booth, C. Kerr, and M. Kellett, "Integrated Charging of EVs Using Existing LVDC Light Rail Infrastructure: A Case Study," in *2019 IEEE Third International Conference on DC Microgrids (ICDCM)*, (Matsue, Japan), pp. 1–7, IEEE, May 2019.

[30] T. Dragicevic, J. M. Guerrero, and J. C. Vasquez, "A Distributed Control Strategy for Coordination of an Autonomous LVDC Microgrid Based on Power-Line Signaling," *IEEE Transactions on Industrial Electronics*, vol. 61, pp. 3313–3326, July 2014.

[31] P. Santos, P. Fonte, and R. Luis, "Improvement of DC Microgrid Voltage Regulation Based on Bidirectional Intelligent Charging Systems," in *2018 15th International Conference on the European Energy Market (EEM)*, (Lodz), pp. 1–6, IEEE, June 2018.

[32] T. Zhang, R. Zhao, E. E. Ballantyne, and D. Stone, "Increasing urban tram system efficiency, with battery storage and electric vehicle charging," *Transportation Research Part D: Transport and Environment*, vol. 80, p. 102254, Mar. 2020.

[33] T. Zhang, E. E. Ballantyne, R. Zhao, and D. A. Stone, "Technical and economic feasibility of increasing tram system efficiency with EV batteries," *Transportation Research Part D: Transport and Environment*, vol. 91, p. 102681, Feb. 2021.

[34] H. Lin, C. Bian, Y. Wang, H. Li, Q. Sun, and F. Wallin, "Optimal planning of intracity public charging stations," *Energy*, vol. 238, p. 121948, Jan. 2022.

[35] J. Smart and S. Schey, "Battery Electric Vehicle Driving and Charging Behavior Observed Early in The EV Project," *SAE International Journal of Alternative Powertrains*, vol. 1, pp. 27–33, Apr. 2012.

[36] J. Schäuble, T. Kaschub, A. Ensslen, P. Jochem, and W. Fichtner, "Generating electric vehicle load profiles from empirical data of three EV fleets in Southwest Germany," *Journal of Cleaner Production*, vol. 150, pp. 253–266, May 2017.

[37] G. Pasaoglu, D. Fiorello, L. Zani, A. Martino, A. Zubaryeva, and C. Thiel, "Projections for Electric Vehicle Load Profiles in Europe Based on Travel Survey Data. European Commission," tech. rep., DG JRC. Institute for Energy and Transport., 2013.

[38] G. R. C. Mouli, J. Kaptein, P. Bauer, and M. Zeman, "Implementation of dynamic charging and V2G using Chademo and CCS/Combo DC charging standard," in *2016 IEEE Transportation Electrification Conference and Expo (ITEC)*, (Dearborn, MI, USA), pp. 1–6, IEEE, June 2016.

[39] G. R. C. Mouli, P. Venugopal, and P. Bauer, "Future of electric vehicle charging," in *2017 International Symposium on Power Electronics (Ee)*, (Novi Sad), pp. 1–7, IEEE, Oct. 2017.

[40] B. V. E. Bakolas, P. Bauer, and D. Prins, "Testing of Smart Charging Controller for dynamic charging from solar panels," in *2014 IEEE Transportation Electrification Conference and Expo (ITEC)*, (Dearborn, MI), pp. 1–4, IEEE, June 2014.

[41] Â. Casaleiro, R. Amaro e Silva, and J. Serra, "Plug-in Electric Vehicles for Grid Services Provision: Proposing an Operational Characterization Procedure for V2G Systems," *Energies*, vol. 13, p. 1240, Mar. 2020.

[42] A. Zecchino, A. Thingvad, P. B. Andersen, and M. Marinelli, "Test and Modelling of Commercial V2G CHAdeMO Chargers to Assess the Suitability for Grid Services," *World Electric Vehicle Journal*, vol. 10, p. 21, Apr. 2019.

[43] S. Martinenas, M. Marinelli, P. B. Andersen, and C. Troholt, "Evaluation of electric vehicle charging controllability for provision of time critical grid services," in *2016 51st International Universities Power Engineering Conference (UPEC)*, (Coimbra), pp. 1–5, IEEE, Sept. 2016.

[44] "IEEE Standard Practices and Requirements for Semiconductor Power Rectifier Transformers," Nov. 2021.

[45] Z. Tian, T. Kamel, and P. Tricoli, "A study to design the locations of reversible traction substations for minimizing power losses of DC railways," in *2019 21st European Conference on Power Electronics and Applications (EPE '19 ECCE Europe)*, (Genova, Italy), pp. P.1–P.9, IEEE, Sept. 2019.

[46] CENELEC, "EN 50163 - Railway applications - Supply voltages of traction systems," Nov. 2004.

[47] R. Barbone, R. Mandrioli, M. Ricco, R. F. Paternost, V. Cirimele, and G. Grandi, "Novel Multi-Vehicle Motion-Based Model of Trolleybus Grids towards Smarter Urban Mobility," *Electronics*, vol. 11, p. 915, Mar. 2022.

[48] Z. Wang, F. Chen, and J. Li, "Implementing Transformer Nodal Admittance Matrices Into Backward/Forward Sweep-Based Power Flow Analysis for Unbalanced Radial Distribution Systems," *IEEE Transactions on Power Systems*, vol. 19, pp. 1831–1836, Nov. 2004.

[49] ELAAD, "ElaadNL Open Datasets for Electric Mobility Research." https://platform.elaad.io/analyses/ElaadNL_opendata.php.

[50] G. Chandra Mouli, P. Bauer, and M. Zeman, "System design for a solar powered electric vehicle charging station for workplaces," *Applied Energy*, vol. 168, pp. 434–443, Apr. 2016.

[51] A. Łebkowski, "Studies of Energy Consumption by a City Bus Powered by a Hybrid Energy Storage System in Variable Road Conditions," *Energies*, vol. 12, p. 951, Mar. 2019.

[52] International Association of Public Transport, "SORT - Standardised On-Road Tests Cycles," May 2004.

[53] Z. Tian, N. Zhao, S. Hillmansen, S. Su, and C. Wen, "Traction Power Substation Load Analysis with Various Train Operating Styles and Substation Fault Modes," *Energies*, vol. 13, p. 2788, June 2020.

[54] J. Mies, J. Helmus, and R. van den Hoed, "Estimating the Charging Profile of Individual Charge Sessions of Electric Vehicles in The Netherlands," *World Electric Vehicle Journal*, vol. 9, p. 17, June 2018.

[55] M. Kchaou-Boujelben, "Charging station location problem: A comprehensive review on models and solution approaches," *Transportation Research Part C: Emerging Technologies*, vol. 132, p. 103376, Nov. 2021.

[56] M. J. Hodgson, "A Flow-Capturing Location-Allocation Model," *Geographical Analysis*, vol. 22, pp. 270–279, Sept. 2010.

[57] C. Upchurch, M. Kuby, and S. Lim, "A Model for Location of Capacitated Alternative-Fuel Stations," *Geographical Analysis*, vol. 41, pp. 85–106, Jan. 2009.

[58] H. Zheng and S. Peeta, "Routing and charging locations for electric vehicles for intercity trips," *Transportation Planning and Technology*, vol. 40, pp. 393–419, May 2017.

[59] S. A. MirHassani and R. Ebrazi, "A Flexible Reformulation of the Refueling Station Location Problem," *Transportation Science*, vol. 47, pp. 617–628, Nov. 2013.

[60] Y. Xiang, J. Liu, R. Li, F. Li, C. Gu, and S. Tang, "Economic planning of electric vehicle charging stations considering traffic constraints and load profile templates," *Applied Energy*, vol. 178, pp. 647–659, Sept. 2016.

[61] M. Islam, H. Shareef, and A. Mohamed, "Optimal siting and sizing of rapid charging station for electric vehicles considering Bangi city road network in Malaysia," *Turkish Journal of Electrical Engineering & Computer Sciences*, vol. 24, no. 5, pp. 3933–3948, 2016.

[62] M. Islam, H. Shareef, and A. Mohamed, "Optimal location and sizing of fast charging stations for electric vehicles by incorporating traffic and power networks," *IET Intelligent Transport Systems*, vol. 12, pp. 947–957, Oct. 2018.

[63] M. Bartłomiejczyk and M. Połom, "Sustainable Use of the Catenary by Trolleybuses with Auxiliary Power Sources on the Example of Gdynia," *Infrastructures*, vol. 6, p. 61, Apr. 2021.

[64] M. Brenna, F. Foiadelli, and H. J. Kaleybar, "The Evolution of Railway Power Supply Systems Toward Smart Microgrids: The concept of the energy hub and integration of distributed energy resources," *IEEE Electrification Magazine*, vol. 8, pp. 12–23, Mar. 2020.

[65] M. Ahmadi, H. J. Kaleybar, M. Brenna, F. Castelli-Dezza, and M. S. Carmeli, "DC Railway Micro Grid Adopting Renewable Energy and EV Fast Charging Station,"

in *2021 IEEE International Conference on Environment and Electrical Engineering and 2021 IEEE Industrial and Commercial Power Systems Europe (EEEIC / I&CPS Europe)*, (Bari, Italy), pp. 1–6, IEEE, Sept. 2021.

A APPENDIX

A.1 EXAMPLE BUS MODEL CALCULATION

In Figure A.1, an example at time-step t is shown. Here the bus power demand is 100 kW, located at 300 meters on the section. Furthermore, the substation is connected via the feed-in cable with the overhead wires at 1310 meters. The connection point of the substation to the overhead wires is called the slack node (SN). The example section has a total length of 1400 meters.

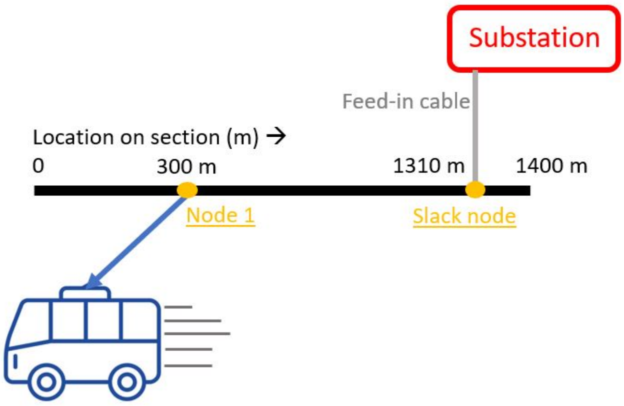

Figure A.1: Example of one bus on the section at time t. The section length is 1400 meters.

On the left side of Figure A.2, the equivalent circuit of the example is shown. As most of the sections in Arnhem are parallel connected, the resistance can be divided by two (Chapter 1.1.2). As a result, the resistance in the return path is compensated by the parallel connection and, therefore, not shown in the simplified equivalent circuit as shown on the right of Figure A.2.

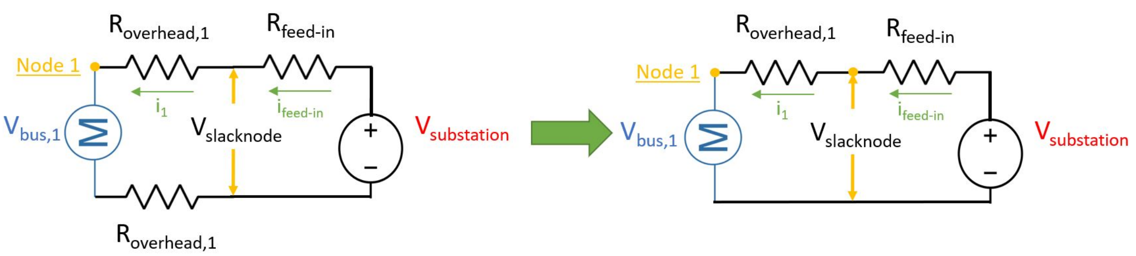

Figure A.2: The equivalent circuit is shown for one bus on a section on the left side. On the right side, the equivalent circuit whereby the parallel connected overhead wires compensates for the resistance of the return path.

The impedance of the overhead and feed-in cables is calculated with the following formula:

$$R_{\text{cable}} = \frac{\rho_{\text{Cu}} L_{\text{cable}}}{A_{\text{cable}}} [\Omega] \tag{A.1}$$

Where:
ρ_{Cu} is the resistivity of copper ($1.72 * 10^{-8} \Omega$ m);
L_{cable} the length of the cable (in m);
A_{cable} is the cross-sectional area of the cable (in m^2).

The voltage at the feed-in point is calculated with the following formula:

$$V_{\text{SN}} = R_{\text{feed-in}} \cdot i_{\text{feed-in}} [\text{V}] \tag{A.2}$$

General solution

A more general equivalent circuit that is used in the model is shown in Figure A.3.

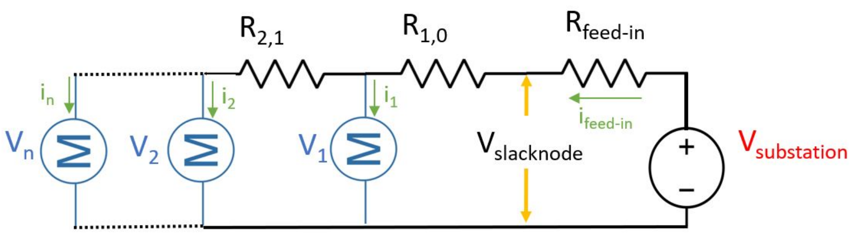

Figure A.3: Equivalent circuit with n buses on the section.

The buses are now represented as loads that require the following current demand:

$$i_{\text{k}}(t) = \frac{P_{\text{k}}(t)}{V_{\text{k}}(t)} \tag{A.3}$$

Hereby the power $P_{\text{k}}(t)$ is the power demand of the load at time-step t. With the use of the backward-forward sweep method [48], the voltage and current at each node are calculated via an iterative process with the use of the following formula:

$$V_{\text{k}}(t) = V_{\text{k}-1}(t) - \left(\sum_{k}^{n} i_{\text{k}}(t) \cdot \frac{\rho_{\text{Cu}}}{A_{\text{cable}}} \cdot (X_{\text{k}}(t) - X_{\text{k-1}}(t)) \right) [\text{V}] \tag{A.4}$$

Where:
k is the node number;
n is the total number of nodes on the section;
i_{k} is the current for load k;
X_{k} the location of node k on the section.
$V_0 = V_{\text{SN}}$

A.2 FORCES ACTING ON MOVING BUS

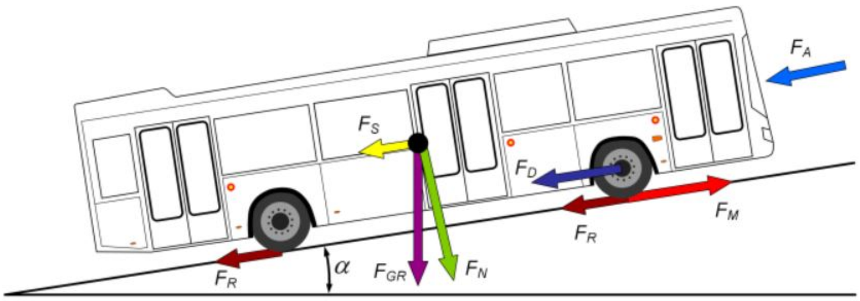

Figure A.4: Forces acting on moving bus [51].

The required traction force to overcome the resistance forces is described as follows:

$$F_{tr} = F_A + F_{rr} + F_{in} + F_S \tag{A.5}$$

Where:

$$F_A = \frac{1}{2} \cdot C_d \cdot A_f \cdot \rho \cdot v^2; \text{the aerodynamic resistance} \tag{A.6}$$

$$F_{rr} = m_{bus} \cdot g \cdot C_{rr} \cdot \cos(\alpha); \text{rolling resistance} \tag{A.7}$$

$$F_{in} = m_{bus} \cdot a; \text{Resistance associated with inertia forces} \tag{A.8}$$

$$F_S = m_{bus} \cdot g \cdot \sin(\alpha); \text{sliding force} \tag{A.9}$$

With the use of the SORT 2 driving cycle and the forces acting on the bus, the power demand of the bus is calculated:

$$P_{bus} = \frac{F_{tr} \cdot v_{bus}}{\eta} + HVAC \tag{A.10}$$

Table A.1: Parameters used for the theoretical study [51]

Bus parameters	Quantity	Unit
A_f	8.42	$[m^2]$
m_{bus}	20 000	$[kg]$
C_{rr}	0.01	-
C_d	0.7	-
$\eta_{traction}$	0.75	-
$\eta_{recuperation}$	0.75	-
P_{aux}	40	$[kW]$
General Parameters		
ρ	1.25	$[kg/m^3]$
g	9.81	$[m/s^2]$

A.3 SELECTION OF SUITABLE LOCATIONS FOR EV CHARGERS

This appendix gives an introduction to the charging station location problem. M. Kchaou-Boujelben [55] has recently done a large literature review on the charging station location problem. The author discusses and categorizes 179 papers published in journals in this survey. Firstly, different ways of representing the recharging demand and coverage are discussed. Then different decision variables are considered. Furthermore, different solving methods are mentioned with the associated benefits and downsides.

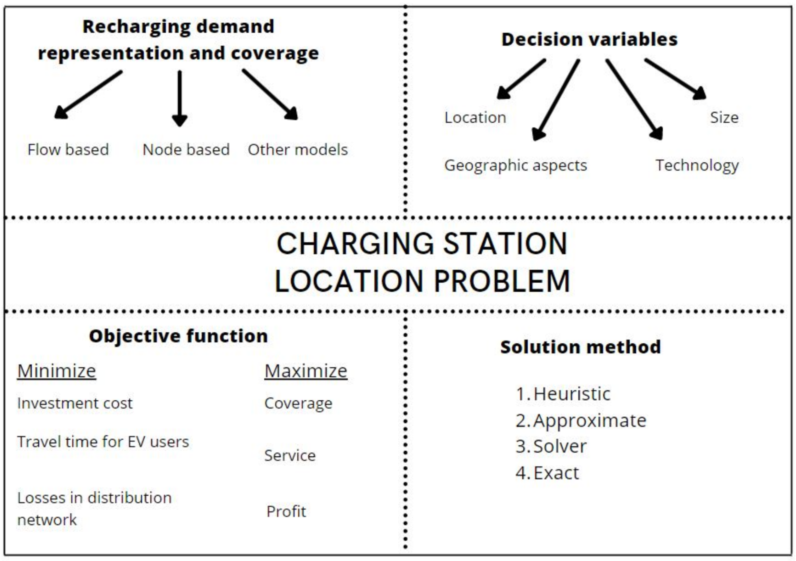

Figure A.5: Overview of charging station location problem based on the categories described in [55].

A.3.1 Recharging demand representation and coverage models

Demand representation for charging stations is an important aspect of the charging location problem. In the literature, two main methods are used: flow-based and node-based models. Furthermore, the game theory approach is categorized under the "other models" group.

Flow-Based Models

In the flow-based models, the trips (flow) of EV drivers are simulated. In flow-based modeling, often the goal is to place EV chargers at locations where they cover as many trips as possible (e.g., where the most flow in the network is). An example of the recharging demand can be modeled as four nodes on an origin-destination(OD) trip, as shown in Figure A.6. On long trips, and due to the limited driving range of an EV, the battery needs to be recharged at adequately placed EV charging stations. In this example, an EV has a driving range of 100 km; the maximum distance between two charging stations is 100 km. As a result, a charging station must be placed on node B. In theory, there does not have to be a charging facility on node C if the EV can be fully discharged at the destination (node D). However, the authors also looked into a round trip, so the EV must drive from D to C. This means, that placing a charging station at node C might be preferred over node D. The authors expanded the model with multiple driving ranges and different OD trips and optimized the solution using a flexible mixed-integer linear programming model. Most flow-based modeling is used to determine the location for (ultra)fast charging facilities. More examples of this type of modeling are described in [56, 57, 58].

Figure A.6: Simple path for flow-based modeling [59]. The maximum driving distance of the EV in this example is 100 km.

Node base Models

For EV modeling in urban environments, the chance that the EV battery is out of charge before reaching the destination is less likely. For this reason, another method is introduced, the node-based model. Here, the demand for EV charging stations is based on the housing of EV drivers who prefer charging close-by home or work. An example is shown in Figure A.7. This paper categorizes the urban environment into residential (villa and apartment), commercial (e.g., shops), and working. An EV charging profile is determined for these different categories, as shown in Figure 2.7. With this data, the paper aims to provide the optimal location and size of public charging stations, maximizing the benefit of the investment cost. The optimal solution is found by mixed-integer linear programming (MILP). Node-based modeling is mainly used for slow charging facilities within an urban environment.

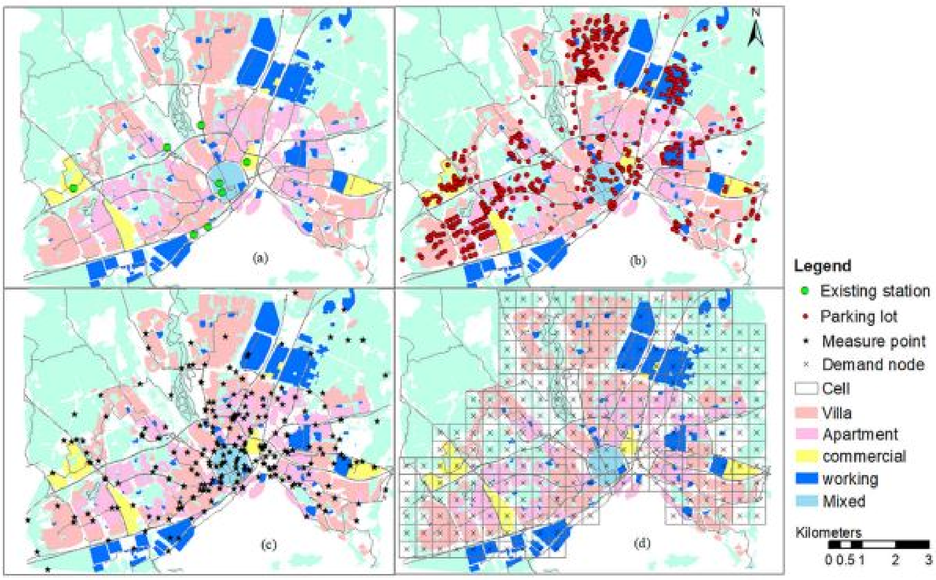

Figure A.7: Geographic information system (GIS) on transportation demand in Västerås, Sweden [34].

Other models

A completely different modeling technique is the Game Theory approach. In this type of modeling, multiple actors interact with each other limited by a set of rules. However, this is an interesting research field; it is not the focus of this thesis and will not be further discussed.

A.3.2 Decision variables

The location of charging stations is important, but other decision variables such as the number of chargers, technology choice, geographic deviation, investment costs, and routing limitation play a role in finding the optimal location of EV charging stations. One of the papers that cover these aspects is [60] (OD flow based). This paper uses transport load profiles from the UK and traffic constraints to simulate the electric car transportation network. Combined with the distribution network state, an economic decision for EV chargers is obtained, see Figure A.8. The objective function of the authors is to minimize the economic cost of the EV chargers.

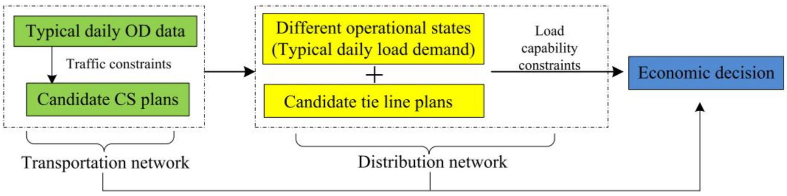

Figure A.8: Flow diagram to optimize for the economic decision variable [60].

A.3.3 Objective functions

In the charging station location problem literature, objective functions are often used to optimize the charging location. A few examples of objectives to be minimized are investment cost, travel time to the charging station, and/or losses in the distribution network. Or maximizing the coverage (e.g., the number EV charged), service, and/or profit. A multi-objective (a combination of objective functions) could also be used to optimize the size and location of EV chargers. The case study performed by Islam et al. [61, 62] is such a multi-objective function where they optimize for three objectives: EV transportation energy loss, station build-up cost, and sub-station energy loss. To find the optimal solution, different solving methods are used. These are described in the next section.

A.3.4 Solution methods

The charging station location problems are often complex, with multiple variables and constraints. Therefore different solving methods have opted in literature to find a good balance between accuracy and computational effort. In [55], the solving methods are categorized as follows: heuristic, approximate, exact, and solvers.

Heuristic solving methods are used to find the local optimal solution. The benefit of this type of solving leads to a good quality solution with a short computation time. This type of solving could be used as a baseline to find the global optimal solution. The heuristic solving method is often used in the literature (43% of the papers analyzed in [55]). The approximate method is used where the problem leads to a non-convex solution. This occurs most often in non-linear problems and considers the randomness of certain parameters. Monte Carlo is an approximate method. Exact methods are used to find the global optimum for the problem. As this solving method is computationally demanding with the increase of problem parameters, this method is not used often in realistic problems. The solver class is a collection where the researchers use off-the-shelf solvers to solve the problem to the desired accuracy. This is a broad field of different methods. This type of solving is used in 38% of the papers analyzed in [55].

A.4 LIST OF POTENTIAL SMART GRID METHODS

Table A.2: Smart grid methods for increasing EV charging potential on a traction grid.

Investigated during this study
1.1 Increasing substation voltage [30]
1.2 Increasing substation tolerance/capacity
2.1 Adding extra parallel line
2.2 Introduction of bilateral connection [27, 28]
3.1 Smart power charging [23, 29, 38, 40]
3.2 Multi-port converter [12]

High priority
In-depth Smart power charging [23, 29, 38, 40]
Stationary energy storage system [32, 27]
Energy storage system on bus [63]

Medium priority
Voltage variation between substations, part of bilateral connection [4]
Peak load shaving buses (e.g., intelligent heating) [27]
Splitting the neighboring supply sections [27]

Low priority
Distributed generators on grid (e.g., PV panels) [18, 22, 24, 25, 64, 65]
Vehicle for grid (V4G), voltage stability [31, 42]
Rescheduling buses
Connection of EV charger to multiple sections of different substations

A.5 TECHNICAL SPECIFICATIONS OF DC/DC CONVERTER

25kW DC/DC Charger Module

Based on years of experience PRE has developed a standard 25kW Modular Isolated Power Concept designed for multiple charge posts. The Output of the Charger Module can be switched in parallel and in series for systems up to 1000V. The Charger Module is based on the latest resonant technology which results in high efficiency and excellent overall performance. Output Voltage and Current can be controlled by a CAN-bus Interface. Other controls and configurations are optional.

Features

- CCS / CHAdeMO compatible
- High Efficient Resonant Topology (>98%)
- Easy parallelable, CAN-bus Control Interface
- Output switchable between 500V/1000V

Applications

- EV Charger Parks
- Modular EV Fast Chargers
- Industrial Battery Chargers
- Industrial Current Source

CHAdeMO

Key Specifications

Model		EVDC500V63A
Output (Battery)	Voltage range (series option)	150 - 500Vdc (300 - 1000Vdc)
	Current Range (series option)	0 - 64Adc (0 - 32Adc)
	Rated Power (5)	25.000W
	Voltage Ripple + Noise (2)	500mVp-p
	Voltage & Current Tolerance (3)	0.5% (typ.) 1% max.
	Load Regulation	1%
	Current Ripple	<1Arms @ Rated Power (measured on a resistive Load)
	Hold up Time	N/A
Input (DC bus)	DC Voltage Range (nom.) (5)	600 - 800Vdc
	DC Voltage Range (Max.)	400 - 900V (No defects up to 1400Vdc for 5 Sec.)
	DC Current (Max.)	43A @ 600Vdc
	Efficiency (Max.)	98%
	Off / Stand-by consumption	<1.5W / <8W @ 700Vdc
	Inrush Current	No inrush Current (≤43A Cold Start @ 700Vdc)
	Leakage Current	<3.5mA @ 700Vdc
Protection	Input UVP/ OVP & (OCP)	400Vdc / 900Vdc (50V hys.) (50A 700Vdc Fuse 14x51mm)
	Output OVP (OCP)	550V (2x40A 700Vdc Fuse 14x51mm)
	Output RCP	Reverse Current Protection by 1200V Internal Diode
	Over Temperature	70°C at main Heatsink. Output Power derating at >50 °C temperature
Control	Control	CAN-bus with hardware Interlock (Charge Enable) (CANopen protocol / 500kbps)
	Auxiliary supply (Input)	9V - 30V 100mA max. (for Control side circuits)
General	Charge Interface	CHAdeMO & CCS compatible
	Isolation	4kV Input - Output / 2kV PE - Input & PE-Output / 4kV Output - Controls
	Cooling	Air cooled.
	IP protection class	IP20
	Working (Storage) Temp. & Humid.	-20 .. 50°C (-20 .. 70°C) / 20 .. 90% Non Condensing
	Dimension & Weight	Approx. 500x300x140mm / 20kg
	Lifetime (MTBF)	>100.000 hours @ 25 °C (Designed to meet <0.1% / Year)
Safety & EMC(4)	Safety	EN60950
CE	Emission (Industrial)	EN55011, class A (optional B)
	Immunity (Industrial)	EN61000-4-2, EN61000-4-3, EN61000-4-4, EN61000-4-5, EN61000-4-6, EN61000-4-11.

1. All parameters NOT specially mentioned are measured at 700Vdc input, rated load and 20°C ambient temperature.
2. Ripple & noise are measured at 20MHz bandwidth by using a standard probe.
3. Tolerance : includes set up tolerance, line regulation and load regulation.
4. The Charger Module is considered a component which will be installed into a final equipment. The final equipment must be re-confirmed that it still meets EMC directives.
5. Derating may be needed under low input voltage and higher ambient temperature.
6.

Power Research Electronics B.V.
Minervum 7073, 4817ZK, Breda (NL)
T: +31(0)76-5811077
F: +31(0)76-5811237
info@pr-electronics.nl
www.pr-electronics.nl